Greener Starch Oxidation:

Exploring challenges in designing catalytic processes for polydisperse feedstocks

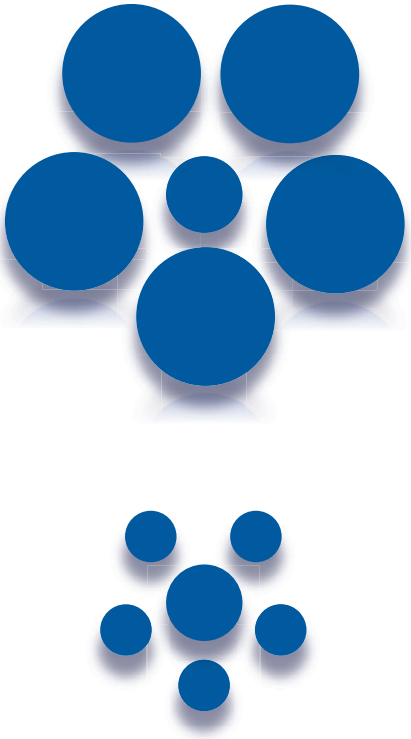

T.M. Hoogstad

Propositions

1. Empirically determined values for kinetic parameters in models for polydisperse feedstocks are irrelevant to publish.
   (this thesis)

2. The timing of optimization in catalyst design is as important as the optimization itself.
   (this thesis)

3. Scientific peer review is a necessary but flawed and inefficient process in its current form.

4. Differences in requirements between universities on propositions reduce the relevance of propositions.

5. The profit margins of scientific journals are detrimental to the credibility of science

6. Fact-checking and recognition of misinformation should be included in the middle school educational curriculum.

Propositions belonging to the thesis, entitled

Greener starch oxidation: exploring challenges in designing catalytic processes for polydisperse feedstocks

Tim Martinus Hoogstad
Wageningen, 23 October 2023

Greener starch oxidation: exploring challenges in designing catalytic processes for polydisperse feedstocks

Tim M. Hoogstad

Thesis committee

Promotor

Prof. Dr J.H. Bitter
Professor of Biobased Chemistry and Technology
Wageningen University & Research

Other members:

Prof. Dr A. ter Heijne, Wageningen University & Research
Dr M. Laus, Koninklijke Avebe, Veendam, the Netherlands
Prof. Dr L.C.P.M. de Smet, Wageningen University & Research
Prof. Dr S.R.A. Kersten, University of Twente, Enschede

This research was conducted under the auspices of VLAG Graduate School
(Biobased, Biomolecular, Chemical, Food, and Nutrition Sciences)

Greener starch oxidation: exploring challenges in designing catalytic processes for polydisperse feedstocks

Tim M. Hoogstad

Thesis

submitted in fulfilment of the requirements for the degree of doctor
at Wageningen University
by the authority of the Rector Magnificus,
Prof. Dr A.P.J. Mol,
in the presence of the
Thesis Committee appointed by the Academic Board
to be defended in public
on Monday 23 October 2023
at 4 p.m. in the Omnia Auditorium.

Tim M. Hoogstad
Greener starch oxidation: exploring challenges in designing catalytic processes for polydisperse feedstocks,

160 pages.

PhD thesis, Wageningen University, Wageningen, The Netherlands (2023)
With references, with summary in English

ISBN 978-94-6447-813-6
DOI https://doi.org/10.18174/635254

Table of Contents

1.

1. General introduction

1.1 Biobased feedstocks, their potential, modification, and challenges

A transition towards less fossil dependent materials and production processes is needed to attenuate detrimental effects of current production processes on the environment (Henrich, Dahmen, Dinjus, & Sauer, 2015; Rama et al., 2022). Biobased materials and chemicals provide a renewable, and more sustainable alternative to fossil based materials and chemicals as indicated by several life cycle assessment studies and reviews (Dahiya, Katakojwala, Ramakrishna, & Mohan, 2020; Vinod, Sanjay, Suchart, & Jyotishkumar, 2020; Weiss et al., 2012). Weiss et al. (2012) showed that on average, one metric ton of biobased materials relative to conventional materials reduces primary energy input by 55 ±34 GJ and reduces carbon dioxide emissions by 3 ± 1 ton. Although not all impact categories see a reduction, eutrophication and ozone depletion on average increase by 5 ± 7 kg Phosphate equivalent and 1.9 ± 1.8 kg nitrous oxide equivalent. Weiss et al. (2012) and Dahiya et al. (2020) both note that a reliable and consistent measurement framework is still a key challenge in life cycle assessments for, and that variability in results between LCAs hamper drawing generalised conclusions.

Biobased materials and chemicals (e.g. paper, bioplastics, bioethanol) are products made by processing biobased feedstocks like wood, roots, leaves and agricultural by-products. These feedstocks are often lumped under the term lignocellulosic biomass. Lignocellulosic biomass is a potent source for production of biobased materials and chemicals (García, González Alriols, & Labidi, 2014; Machineni & Rao Anupoju, 2022) and one of the most abundantly available raw materials on earth (Wyman et al., 2005), with an estimated availability of over 1 billion dry tons in the USA and Canada alone (Gronowska, Joshi, & MacLeana, 2009; Nanda, Azargohar, Dalai, & Kozinski, 2015). Comparatively, the estimated production of chemicals from the organic chemical sector is approximately 600 million tons (Levi & Cullen, 2018; Popp, Kovács, Oláh, Divéki, & Balázs, 2021).

Lignocellulosic biomass comprises three biopolymers: cellulose (40-50%), hemicellulose (25-35%), and lignin (15-20%) (Holtzapple, 1993). In addition to these biopolymers, several others biopolymers are potent feedstocks for biobased materials and chemicals e.g. chitin, alginate, inulin, and starch (Patel (Patel et al., 2022; Shamshina & Berton, 2020). Although these biopolymers substantially different from each other in terms of molecular structure, monomer composition and physical properties, two properties that are shared between them is that the molecular size is high i.e. they are macromolecular (here defined as hydrodynamic radius >5nm) and that they are often inhomogeneous in their composition and size. Meaning that substrates can contain more than one type of biopolymer (e.g. hemicellulose mixed with cellulose, or amylose with amylopectin) and that a wide distribution of molecular sizes is present within one type of biopolymer. The width of such a distribution is expressed with the polydispersity index (PI) which is defined as the weight average molecular weight of a sample divided

by the number average molecular weight of the sample. The larger the polydispersity index, the wider the distribution of the biopolymer. Table 1 provides an overview of some biopolymers, their average size and their polydispersity index.

Table 1 Estimated molecular sizes, expressed in hydrodynamic radius, of some biobased feedstocks and their polydispersity index (PI)

	Hydrodynamic radius (nm)	***PI***
Cellulose	20-50 (Chang et al., 2016)	2-7 (Emsley, Ali, & Heywood, 2000)
hemicellulose	34–57 (Shen et al., 2021)	1.37-1.61 (Xie et al., 2020)
lignin	8.4 – 33.5 (Gidh, Decker, See, Himmel, & Williford, 2006) 2-50 (Li, Cui, Wang, & Long, 2023)	1.65 – 8.8 (Tolbert, Akinosho, Khunsupat, Naskar, & Ragauskas, 2014)
Amylopectin	110 – 267 (Rolland-Sabaté, Guilois, Jaillais, & Colonna, 2011) 76 – 97 (Zou, Xu, Wen, & Yang, 2020)	1.04 – 1.27 (Mua & Jackson, 1997) >100 (Stacy & Foster, 1957) ~34 (Bertoft, 2017) 2.22-3.39 (Zou et al., 2020)
Amylose	46 to 73nm (Roger, Tran, Lesec, & Colonna, 1996)	1.29 - 6.9 (Bertoft & Blennow, 2016)

These biopolymers, also known as biomacromolecules, often require modification to introduce or remove desired functional properties for their respective applications (Nakagawa, Tamura, & Tomishige, 2013). A common approach is to break the polymeric structures down to monomers, and convert them to platform molecules, which can then be used as building blocks to produce biobased materials and chemicals (Aeschelmann & Carus, 2015; Attard, Clark, & McElroy, 2020; Kohli, Prajapati, & Sharma, 2019; Laurichesse & Avérous, 2014; Paone, Tabanelli, & Mauriello, 2020). However, for specific applications, it is beneficial to retain the original polymeric structure and functionalities of the original biopolymer with minor modifications. Examples of this are found in the modification of inulin fibers for colon drug targeting (Giri, Dutta, & Giri, 2021), modification of barley fibers for dietary functionality (Park, Lee, & Lee, 2013), production of aerogel nanofibers from cellulose for insulating materials (Tafreshi et al., 2022), carboxymethylcellulose from cellulose for production of edible coatings

(Panahirad et al., 2021; Pinto et al., 2022), and oxidation of starch (Grommers & van der Krogt, 2009).

To introduce modifications to a biopolymer, a form of catalysis is often employed (Ventura, Marinas, & Domine, 2020, 2021). In general, it is estimated that approximately 90% of all industrial processes are catalytic (Bravo-Suárez, Chaudhari, & Subramaniam, 2013; Hegedus et al., 1987). Catalysis can be classified as homogenous catalysis where the catalyst and substrates are present in the same state of matter e.g. both substrate and catalyst are in a solution, and heterogeneous catalysis where the catalyst and substrates are present in a different state of matter e.g. solid catalyst particles and a substrate in a liquid or gaseous phase. Further subdivision of catalysis based on their origin or working mechanism can be made e.g. bio-catalysis, (noble)metal catalysis, photocatalysis, electrocatalysis, or a combination thereof, although these generally still fall under homo- or heterogeneous catalysis based on the respective phases of catalyst and substrate. Currently, it is estimated that heterogeneous catalysis is applied in approximately 80- 90% of the industrial catalytic processes since the different phases of the catalyst and the substrate/product simplify the separation and re-use of the catalyst from the reaction mixture (Bravo-Suárez et al., 2013; Copéret, Chabanas, Petroff Saint-Arroman, & Basset, 2003). Additionally, heterogeneous catalysts are generally more stable at high temperatures (Simonneaux, Le Maux, Ferrand, & Rault-Berthelot, 2006). For these reasons, heterogeneous catalysts are the workhorse of catalysis (De Clercq, Dusselier, & Sels, 2017; Hulea, 2018; Pelckmans, Renders, Van de Vyver, & Sels, 2017; Serrano, Melero, Morales, Iglesias, & Pizarro, 2018; Timofeev & Vodyankina, 2021).

In a typical heterogeneous catalyst, catalytically active sites are bound on a solid, porous matrix of a catalyst support material. The catalyst (support plus active sites e.g. metal nanoparticles) can be used in fixed bed (flow) reactors where a reaction mixture moving through the catalyst or in batch reactors where the catalyst is suspended in the reaction mixture. At the molecular scale, different steps at the catalyst level can be discriminated (figure 1). A substrate molecule first has to diffuse through a stagnant layer of medium, also referred to as a boundary layer (figure 1 point 1). The thickness of the stagnant layer depends on the viscosity, and turbulence of the medium caused by mixing or other forms of agitation. After diffusion through the stagnant boundary layer, a molecule has to come in contact with an active site. Some of these active sites are on the surface of a catalyst particle, however, considering the ratio of external versus internal surface area of a catalyst particle, it is more likely that the substrate first has to diffuse into a pore (figure 1 point 2). Diffusion into a pore is generally slower than diffusion through the stagnant boundary layer, since the pore walls can impose friction and may limit the mobility of the molecule. The extra hinderance imposed by a pore increases as the size of the molecule approaches the size of the pore. This concept is called hindered diffusion. After the substrate molecule diffused into the pore, it has to adsorb (figure 1 point 3) to interact with an active site (figure 1 point 4), which, depending on the size of

the substrate can mean adsorption on the active site and/or on the catalyst support material. For adsorption, functional groups on the catalyst support material may influence adsorption and conformation of a substrate molecule when it is adsorbed. Here, the substrate is converted into a product. The product then has to desorb (figure 1 point 5), and follow the previously mentioned steps of diffusion in reverse order.

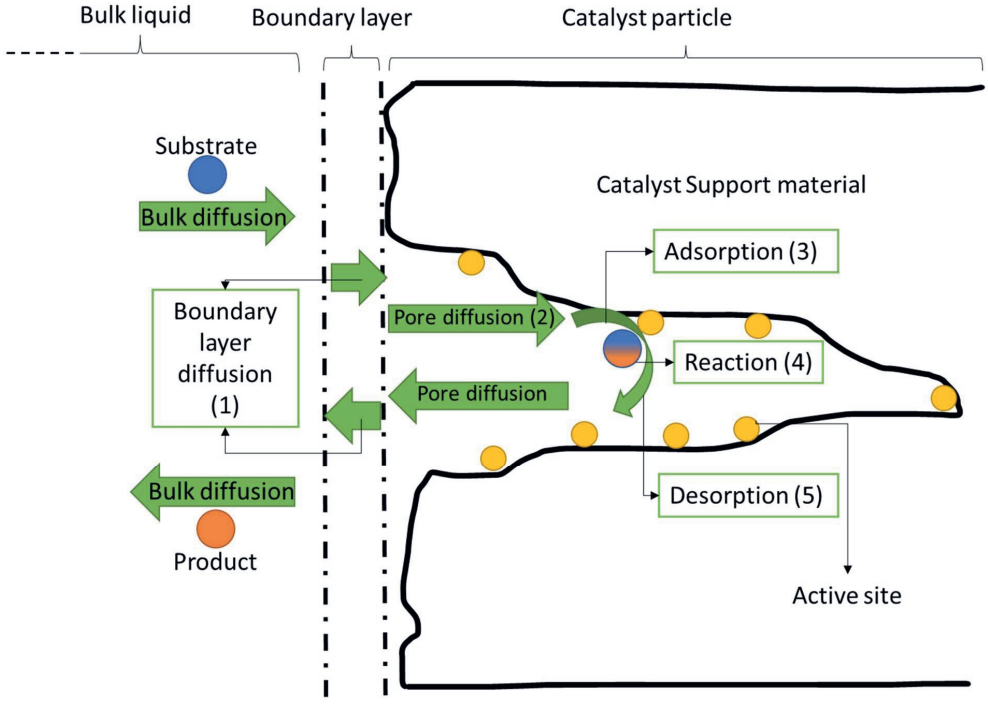

Figure 1 catalytic cycle in heterogeneous catalysis. A substrate (blue) is converted into a product (orange) inside a catalyst particle (black) with active sites (yellow). The conversion from substrate to product via the catalyst particle can be divided into steps (green): bulk diffusion, boundary layer diffusion, pore diffusion, adsorption, reaction, and desorption, whereafter the diffusion steps are repeated in reverse order. Depending on the reaction type, a second substrate or product may be present, but are not shown in the figure.

The largest fields of application of heterogeneous catalysis are chemical processing (e.g. oxidation, hydrogenation, ammonia production), automotive emission control, and petroleum refining e.g. hydroprocessing, cracking, alkylation (Bravo-Suárez et al., 2013). Among the largest substrates in these application fields are asphaltenes with a molecular weight ranging between 500 – 10000 Dalton (Groenzin & Mullins, 2000; Speight, Wernick, Gould, Overfield, & Rao, 1985) and molecular radius ranging between 1.5 and 20 nm (Durand et al., 2010; Eyssautier, Frot, & Barré, 2012; Groenzin & Mullins, 2000) 2000). However, biopolymers from biobased feedstocks can be several times that size, ranging from ~10 to ~250 nm (table 1). As a result of the different size scale of the substrate, catalytic modification of biopolymers through heterogeneous catalysis faces additional challenges in the form of mass transfer limitation though hindered diffusion

and size exclusion, and substrate the influence of molecule size (distribution) thereupon (Li et al., 2023; Sudarsanam, Peeters, Makshina, Parvulescu, & Sels, 2019). This is especially relevant for depolymerisation reactions of the substrate where the substrate is processed from its native form, or conversions that aim to retain some of the original structure of the biopolymer intact, which use biobased feedstocks as substrate that have undergone minimal depolymerisation.

An increase in molecular size is known to reduce bulk and boundary layer diffusion rates (figure 1 step 1) as described by the Stokes-Einstein law, where if the molecular radius is doubled, the bulk diffusion rate is halved. Additionally an increase in molecular size reduces pore diffusion rates if the size of the substrate is in the same order of magnitude as the size of the pore as described by equations for hindered diffusion (figure 1 step 2) (Dechadilok & Deen, 2006; Deen, 1987; Renkin, 1956). The pore sizes in a heterogeneous catalyst are subdivided in micropores (pore radius <2 nm), mesopores (2 nm< pore radius < 50 nm), or macropores (pore radius >50 nm). Table 1 shows that many biopolymers are in the same size range as meso- and macropores, thus, hindered diffusion is expected to play a significant role. Additionally, molecular size has been shown to influence adsorption and desorption of various polymers on various adsorbents (figure 1 steps 3 and 5) (Bessaies-Bey et al., 2019; El'tekov, El'tekova, & Roldughin, 2007; Fu & Santore, 1998; Lee, Kwon, & Moon, 2004; Shirazi, van de Ven, & Garnier, 2003a, 2003b; Yamaguchi, Endo, Takagi, & Hukao, 1977).

In the aforementioned studies, it has been shown that at least steps 1, 2, 3, and 5 in the catalytic cycle as defined in figure 1 are influenced by molecular size. As a result, molecules of different sizes from a size distribution will diffuse, adsorb, and desorb at different rates. Since biopolymers often have wide distributions in their molecular sizes (Table 1), differences in diffusion, adsorption and desorption rates between the different molecules in the substrate are expected. If molecules of a certain size undergo the catalytic cycle at a higher rate due to these influences of size, a subset of the original distribution will be converted at a higher rate than the other molecules in the distribution. As a result, the size distribution of converted molecules (product) may deviate from the size distribution of the substrate. However, the magnitude of the degree to which the size dependent effects play a role in the conversion of these biopolymers is not known, and methods to evaluate and quantify these effects are lacking. Additionally, the cumulative effects multiple size dependent steps throughout the catalytic cycle is not known.

Studies that focus on the conversion of (bio)macromolecules often do not include substrate polydispersity, by omission, or simply working with an average rather than a distribution, where it is implicitly assumed that all molecular sizes in a distribution behave like their average. To illustrate: a search on Scopus for biomacromolecule OR macromolecule OR biopolymer AND NOT protein (since these are inherently

monodisperse) yields 116,506 results at the time of writing. Within these 115,916 results, only 9,998 (8.6%) contain the terms polydispersity, dispersity, or distribution. However, neglecting the molecular weight distribution introduces an error since the influence of molecular size on the process is neglected. If there is an influence of size on a molecular process then the further a molecule in a distribution is from the average molecule size of the distribution, the larger the error will be. As a result, the wider the distribution of the feedstock, the larger the potential error of neglecting the influence of size on a process. Some recent studies recognise this problem like (Li et al., 2023) on the potential of heterogeneously catalysed depolymerisation of lignin, and some studies try to address this challenge like (Khaleel, Sisco, Tavakkoli, & Vargas, 2022), who took substrate polydispersity into account in modelling the precipitation behaviour of asphaltenes. However, studies that integrate the knowledge on size dependency in multiple processing steps and quantitatively evaluate the cumulative size dependent effects are lacking. This thesis aims to lay some groundwork on the investigation of these size selective effects and provide some modelling tools to include substrate polydispersity in kinetic models.

To achieve this goal, the oxidation of potato starch was chosen as a model reaction. The motivation to use this the oxidation of starch as a model reaction is two-fold: First, starch is an example of a renewable biobased feedstock that has a high molecular size (hydrodynamic radius up to 267 nm), and a wide size distribution (polydispersity index up to ~33) (Table 1), making it a representative substrate for the class of biobased feedstocks. Second, the development of a heterogenous catalyst for the oxidation of starch with molecular oxygen is potentially beneficial over the current industrial processes for the production of oxidised starches with sodium hypochlorite.

1.2 Starch oxidation

Chemical oxidation of potato starch introduces carboxylic acid moieties into the starch molecule, thereby producing oxidised starch (figure 2). Due to the negative molecular charge of oxidised starch (at pH>pKa) oxidised potato starch has better pasting and adhesive properties and better shelf life than unmodified potato starch (Sangseethong, Termvejsayanon, & Sriroth, 2010; Zhou, Zhang, Chen, & Chen, 2017). These properties make oxidised starches suitable as a biobased replacement for polyacrylates for applications in the food and feed sector as thickeners, in the paper and textile industry as surface sizing agents, and in various adhesive industries (Masina et al., 2017; Vanier, El Halal, Dias, & da Rosa Zavareze, 2017).

Three oxidation methods are discussed in this thesis: Oxidation with sodium hypochlorite (NaOCl), oxidation with hydrogen peroxide (H_2O_2), and oxidation with molecular oxygen (O_2). Figure 2 shows a schematic representation of these reactions. Oxidation with sodium hypochlorite is currently the industrial standard for the industrial production of anionic starch (Masina et al., 2017; Vanier et al., 2017).

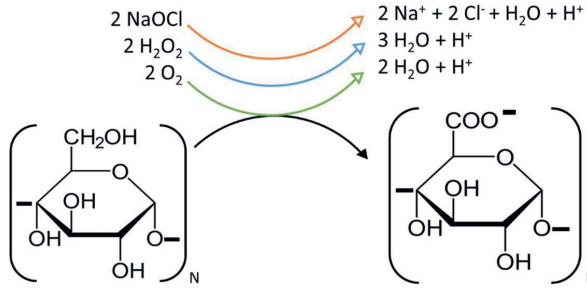

Figure 2 The overall reactions for C6 oxidation of starch with sodium hypochlorite (orange), hydrogen peroxide (blue), and oxygen (green), at pH>pKa. Intermediate steps are not shown.

Although oxidation with hypochlorite is the current industrial standard, this process has two unfavourable characteristics: unwanted by-products, and unwanted side reactions. The use of hypochlorite for the oxidation of starch produces stoichiometric amounts of salt (NaCl) during the oxidation process (figure 2), and small amounts of chlorates are formed that remain in the product (Rutenberg & Solarek, 1984). These by-products are undesired from an environmental and a food safety perspective. As an unwanted side-reaction, some chloride is built into the backbone of the oxidised starch (<1%) during hypochlorite oxidation. Additionally, the oxidation of starch with hypochlorite is not a selective reaction, leading to oxidative depolymerisation of the starch through oxidation of C2-C3 carbons (Rutenberg & Solarek, 1984; Whistler & Schweiger, 1957). Depolymerisation of the starch during oxidation is an unwanted process, since excessive depolymerisation alters the physiochemical properties, i.e., decreases viscosity, pasting properties, and retrogradation enthalpy, and thereby reduces the functionality as an adhesive (Fiedorowicz, Tomasik, You, & Lim, 1999; Jane et al., 1999; Masina et al., 2017; Salemis & Rinaudo, 1984; Sangseethong et al., 2010). These undesired side reactions reduce the applicability of oxidised starches for food and adhesive applications.

A proposed alternative to hypochlorite oxidation is the oxidation of starch with hydrogen peroxide and a homogenous catalyst like copper sulphate, iron complexes, or vanadium complexes (Ketola, 2003; Masina et al., 2017; Tolvanen, Mäki-Arvela, Sorokin, Salmi, & Murzin, 2009; Vanier et al., 2017; Wang et al., 2015). However, the downside of the hydrogen peroxide oxidation, is that residues of the catalyst remain in the product, resulting in substantial purification costs or contaminated products, which has thus far hindered the industrial scale application of this process (Vanier et al., 2017).

A potential solution to the undesired side effects is the use of molecular oxygen and heterogeneous catalysts for the oxidation of starch. Heterogeneously catalysed oxidation of dissolved polysaccharides with molecular oxygen has been achieved on the lab scale with supported Au and Pt nanoparticles (Heyns & Paulsen, 1963; Verraest, Peters, & van Bekkum, 1998) and vanadium complexes (Chen et al., 2015). With heterogeneous catalysis, the catalyst can be separated easily. Additionally, the reaction can be more

selective towards oxidation of the C6 primary hydroxyl group (Chen et al., 2015; Verraest et al., 1998), thereby reducing oxidative depolymerisation through C2-C3 diol cleavage associated with hypochlorite and hydrogen peroxide oxidation (Bragd, Besemer, & van Bekkum, 2002; Rutenberg & Solarek, 1984; Sangseethong et al., 2010; Whistler & Schweiger, 1957). As a result, oxidation of dissolved starch using molecular oxygen and a solid heterogeneous catalyst could potentially alleviate many of the undesired traits of both sodium hypochlorite and hydrogen peroxide oxidation.

1.3 Problem statement

However, the universal challenges regarding the conversion of a large and polydisperse biopolymer (large molecular size, mass transfer limitations, and unknown influence of size distributions) need to be addressed in the development of a heterogenous catalyst for the molecular oxygen oxidation of starch. Figure 3 depicts the overall problem statement covered in this thesis. Starch (indicated in blue) is the biobased feedstock (substrate) to be modified by oxidation in a heterogenous catalyst consisting of a porous catalyst support material (indicated in black) with catalytically active sites attached (indicated in yellow). The oxidation will introduce negatively charged carboxylic acid moieties into the starch, resulting in a negatively charged product (indicated in orange). The green boxes indicate the different steps in the catalytic cycle, similar to figure 1. Diffusion of the substrate into the catalyst (bulk diffusion, stagnant layer diffusion (1), and pore diffusion (2)), adsorption of the substrate to the catalyst support and active sites (3), oxidation of the adsorbed substrate (4), desorption of the oxidised product (5), and diffusion of the product out of the catalyst. Molecular oxygen is dissolved in the medium and not shown in the figure. Throughout this thesis oxygen is assumed to be a non-limiting variable since the diffusivity of molecular oxygen in water (2.1×10^{-9} $m^2 s^{-1}$) is several orders of magnitude higher than the bulk diffusivity of a generic macromolecule of 5 nm (4.3×10^{-14} $m^2 s^{-1}$) as described by the Stokes-Einstein relation. For the bulk diffusion, pore diffusion, adsorption, and reaction, the influence of molecular size, size distribution, and how these effects affect the product distribution and yield is not well understood. In this thesis, the goal is to elucidate the effects of substrate size and size distribution on the oxidation, adsorption, and diffusion steps in the catalytic cycle and investigate the effect of substrate polydispersity on the obtained product distribution and yield. This goal is achieved by a mixed approach including experiments and modelling. By taking the oxidation of starch as a model reaction, some groundwork is laid for the development of heterogeneously catalysed starch oxidation as a more sustainable alternative to hypochlorite oxidation, although some of the results and the developed modelling tools are generalisable to any heterogeneously catalysed conversion of biopolymers.

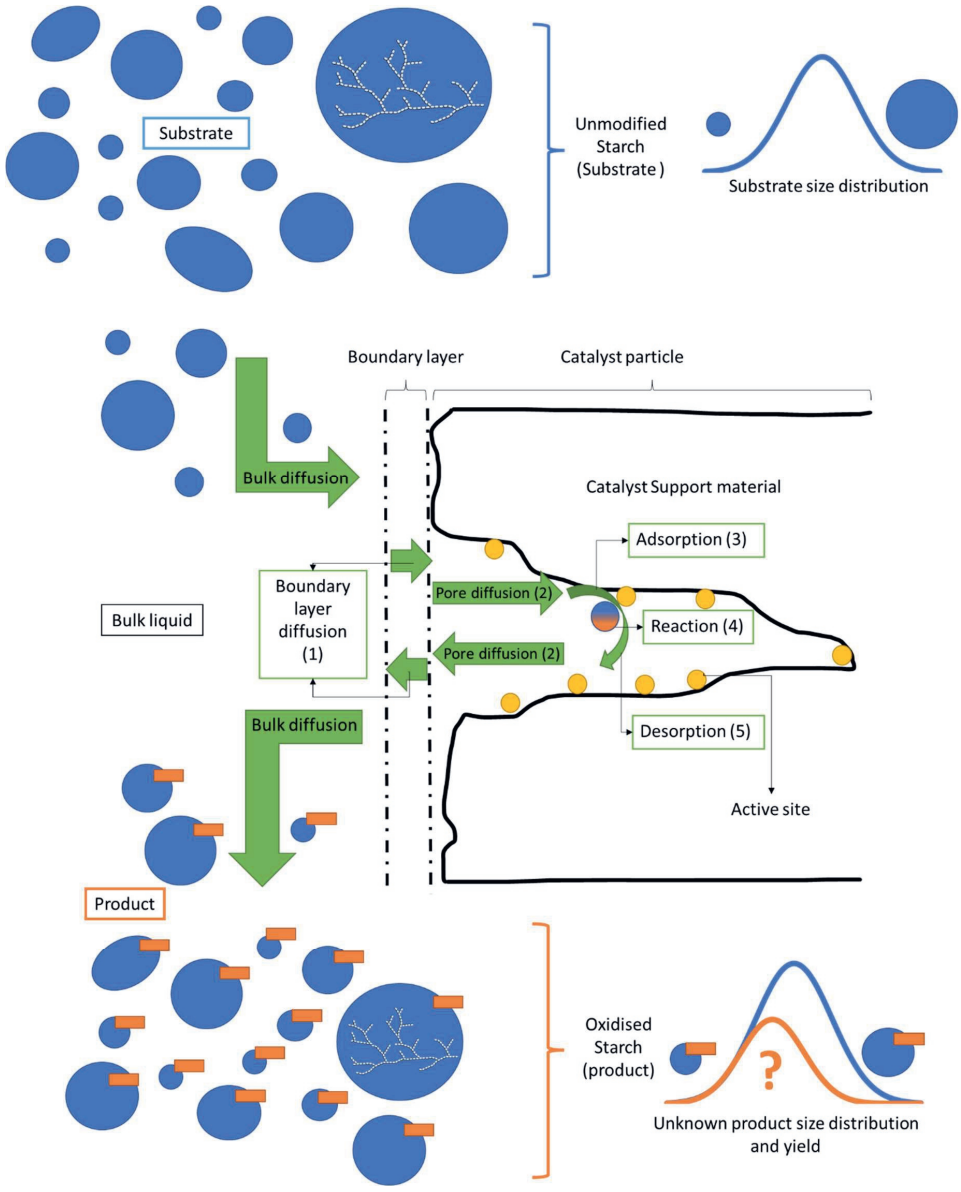

Figure 3 schematic overview of the problem statement. Starch (blue) is oxidised to anionic starch (blue + orange) by undergoing the catalytic cycle (green) a heterogeneous catalyst (black + yellow). The effect of different steps in the catalytic cycle on the difference between the substrate distribution and product distribution, as well as overall reaction yield is to be investigated. Numbers 1-5 refer to the different steps in the catalytic cycle, similar to figure 1.

1.4 Roadmap

In the second chapter of this thesis the environmental impact of starch oxidation with sodium hypochlorite (not catalysed), hydrogen peroxide (homogenously catalysed), and oxygen oxidation (heterogeneously catalysed) are compared. This chapter will show that both hydrogen peroxide oxidation and oxygen oxidation can reduce the environmental impact compared to hypochlorite oxidation. Heterogeneously catalysed oxygen oxidation reduces environmental impact more than hydrogen peroxide oxidation, but is technologically more difficult to develop.

In the third chapter of this thesis, the effect of molecular weight and polydispersity of starch on the TEMPO-catalysed hypochlorite oxidation of starch is investigated. A kinetic model that includes the molecular size dependency of oxidation and depolymerisation is presented that allows tracking of the molecular weight and degree of oxidation in the starch distribution throughout the conversion.

In the fourth chapter, the adsorption of starches on activated carbon is shown to depend on size and degree of branching of the substrate, confirming that polydispersity is a relevant parameter to include in adsorption studies. A 3-point kinetic model that, in addition to the average adsorption rate, includes the adsorption rate of the 20^{th} and 80^{th} percentile molecular weights is presented. With this model, it was demonstrated that, in addition to the molecular size and degree of branching, internal competition within a substrate distribution played a relevant role in the adsorption of polydisperse starches.

In the fifth chapter, the molecular size-dependent diffusion of polydisperse macromolecules in a porous catalyst support materials is modelled. The effects of mass-transfer limitations and the effect of polydispersity on the difference between substrate and product distribution are quantified. An optimum pore size in the trade-off between mass transfer limitations and specific surface area is determined for substrates of different distributions. Challenges as a result of large molecular size and polydispersity of a substrate in the design of catalysts are discussed.

Lastly, in the sixth chapter, the results of chapters two through five are integrated and perspectives on the heterogeneously catalysed conversion of polydisperse macromolecular substrates is discussed.

1.5 References

Aeschelmann, F., & Carus, M. (2015). Biobased Building Blocks and Polymers in the World: Capacities, Production, and Applications–Status Quo and Trends Towards 2020. *Industrial biotechnology, 11*(3), 154-159. doi:10.1089/ind.2015.28999.fae

Attard, T. M., Clark, J. H., & McElroy, C. R. (2020). Recent developments in key biorefinery areas. *Current Opinion in Green and Sustainable Chemistry, 21*, 64-74. doi:https://doi.org/10.1016/j.cogsc.2019.12.002

Bertoft, E. (2017). Understanding Starch Structure: Recent Progress. *Agronomy, 7*(3). doi:10.3390/agronomy7030056

Bertoft, E., & Blennow, A. (2016). Chapter 3 - Structure of Potato Starch. In J. Singh & L. Kaur (Eds.), *Advances in Potato Chemistry and Technology (Second Edition)* (pp. 57-73). San Diego: Academic Press.

Bessaies-Bey, H., Fusier, J., Hanafi, M., Zhang, S., Destarac, M., Jouenne, S., . . . Sanson, N. (2019). Competitive adsorption of PAM and HPAM on siliceous material. *Colloids and Surfaces A: Physicochemical and Engineering Aspects, 579*, 123673. doi:https://doi.org/10.1016/j.colsurfa.2019.123673

Bragd, P. L., Besemer, A. C., & van Bekkum, H. (2002). Selective oxidation of carbohydrates by 4-AcNH-TEMPO/peracid systems. *Carbohydrate Polymers, 49*(4), 397-406. doi:https://doi.org/10.1016/S0144-8617(01)00344-7

Bravo-Suárez, J. J., Chaudhari, R. V., & Subramaniam, B. (2013). Design of Heterogeneous Catalysts for Fuels and Chemicals Processing: An Overview. In *Novel Materials for Catalysis and Fuels Processing* (Vol. 1132, pp. 3-68): American Chemical Society.

Chang, H., Luo, J., Bakhtiary Davijani, A. A., Chien, A.-T., Wang, P.-H., Liu, H. C., & Kumar, S. (2016). Individually Dispersed Wood-Based Cellulose Nanocrystals. *ACS Applied Materials & Interfaces, 8*(9), 5768-5771. doi:10.1021/acsami.6b00094

Chen, X., Yan, S., Wang, H., Hu, Z., Wang, X., & Huo, M. (2015). Aerobic oxidation of starch catalyzed by isopolyoxovanadate Na4Co(H2O)6V10O28. *Carbohydrate Polymers, 117*, 673-680. doi:https://doi.org/10.1016/j.carbpol.2014.10.066

Copéret, C., Chabanas, M., Petroff Saint-Arroman, R., & Basset, J.-M. (2003). Homogeneous and Heterogeneous Catalysis: Bridging the Gap through Surface Organometallic Chemistry. *Angewandte Chemie International Edition, 42*(2), 156-181. doi:https://doi.org/10.1002/anie.200390072

Dahiya, S., Katakojwala, R., Ramakrishna, S., & Mohan, S. V. (2020). Biobased Products and Life Cycle Assessment in the Context of Circular Economy and Sustainability. *Materials Circular Economy, 2*(1), 7. doi:10.1007/s42824-020-00007-x

De Clercq, R., Dusselier, M., & Sels, B. F. (2017). Heterogeneous catalysis for bio-based polyester monomers from cellulosic biomass: advances, challenges and prospects. *Green Chemistry, 19*(21), 5012-5040. doi:10.1039/C7GC02040F

Dechadilok, P., & Deen, W. M. (2006). Hindrance Factors for Diffusion and Convection in Pores. *Industrial & Engineering Chemistry Research, 45*(21), 6953-6959. doi:10.1021/ie051387n

Deen, W. M. (1987). Hindered transport of large molecules in liquid-filled pores. *AIChE Journal, 33*(9), 1409-1425. doi:https://doi.org/10.1002/aic.690330902

Durand, E., Clemancey, M., Lancelin, J.-M., Verstraete, J., Espinat, D., & Quoineaud, A.-A. (2010). Effect of Chemical Composition on Asphaltenes Aggregation. *Energy & Fuels, 24*(2), 1051-1062. doi:10.1021/ef900599v

El'tekov, A. Y., El'tekova, N. A., & Roldughin, V. I. (2007). Kinetic coefficients of the adsorption of polysaccharides from aqueous solutions by Sibunit. *Colloid Journal, 69*(2), 248. doi:10.1134/S1061933X07020160

Emsley, A. M., Ali, M., & Heywood, R. J. (2000). A size exclusion chromatography study of cellulose degradation. *Polymer, 41*(24), 8513-8521. doi:https://doi.org/10.1016/S0032-3861(00)00243-3

Eyssautier, J., Frot, D., & Barré, L. (2012). Structure and Dynamic Properties of Colloidal Asphaltene Aggregates. *Langmuir, 28*(33), 11997-12004. doi:10.1021/la301707h

Fiedorowicz, M., Tomasik, P., You, S., & Lim, S.-T. (1999). Molecular Distribution and Pasting Properties of UV-Irradiated Corn Starches. *Starch - Stärke, 51*(4), 126-131. doi:10.1002/(SICI)1521-379X(199904)51:4<126::AID-STAR126>3.0.CO;2-N

Fu, Z., & Santore, M. M. (1998). Kinetics of Competitive Adsorption of PEO Chains with Different Molecular Weights. *Macromolecules, 31*(20), 7014-7022. doi:10.1021/ma980042w

García, A., González Alriols, M., & Labidi, J. (2014). Evaluation of different lignocellulosic raw materials as potential alternative feedstocks in biorefinery processes. *Industrial Crops and Products, 53*, 102-110. doi:https://doi.org/10.1016/j.indcrop.2013.12.019

Gidh, A. V., Decker, S. R., See, C. H., Himmel, M. E., & Williford, C. W. (2006). Characterization of lignin using multi-angle laser light scattering and atomic force microscopy. *Analytica Chimica Acta, 555*(2), 250-258. doi:https://doi.org/10.1016/j.aca.2005.09.023

Giri, S., Dutta, P., & Giri, T. K. (2021). Inulin-based carriers for colon drug targeting. *Journal of Drug Delivery Science and Technology, 64*, 102595. doi:https://doi.org/10.1016/j.jddst.2021.102595

Groenzin, H., & Mullins, O. C. (2000). Molecular Size and Structure of Asphaltenes from Various Sources. *Energy & Fuels, 14*(3), 677-684. doi:10.1021/ef990225z

Grommers, H. E., & van der Krogt, D. A. (2009). Chapter 11 - Potato Starch: Production, Modifications and Uses. In J. BeMiller & R. Whistler (Eds.), *Starch (Third Edition)* (pp. 511-539). San Diego: Academic Press.

Gronowska, M., Joshi, S., & MacLeana, H. L. (2009). A review of US and Canadian biomass supply studies. *BioResources, 4*(1).

Hegedus, L. L., Aris, R., Bell, A. T., Boudart, M., Chen, N. Y., Gates, B. C., . . . Wei, J. (1987). Catalyst design: progress and perspectives.

Henrich, E., Dahmen, N., Dinjus, E., & Sauer, J. (2015). The Role of Biomass in a Future World without Fossil Fuels. *Chemie Ingenieur Technik, 87*(12), 1667-1685. doi:https://doi.org/10.1002/cite.201500056

Heyns, K., & Paulsen, H. (1963). Selective Catalytic Oxidation of Carbohydrates, Employing Platinum Catalysts. In M. L. Wolfrom & R. S. Tipson (Eds.), *Advances in Carbohydrate Chemistry* (Vol. 17, pp. 169-221): Academic Press.

Holtzapple, M. (1993). Chapters cellulose, hemicelluloses, and lignin. *Macrae R., Robinson RK, SadlerM. J.(Eds.), Encyclopedia of Food Science, Food Technology, and Nutrition. Academic Press, London*, 758-768.

Hulea, V. (2018). Toward Platform Chemicals from Bio-Based Ethylene: Heterogeneous Catalysts and Processes. *ACS Catalysis, 8*(4), 3263-3279. doi:10.1021/acscatal.7b04294

Jane, J., Chen, Y. Y., Lee, L. F., McPherson, A. E., Wong, K. S., Radosavljevic, M., & Kasemsuwan, T. (1999). Effects of Amylopectin Branch Chain Length and Amylose Content on the Gelatinization and Pasting Properties of Starch. *Cereal Chemistry, 76*(5), 629-637. doi:10.1094/CCHEM.1999.76.5.629

Ketola, H. H., FI), Hagberg, Peggy (Maidstone, GB). (2003). United States Patent No.

Khaleel, A. T., Sisco, C. J., Tavakkoli, M., & Vargas, F. M. (2022). An Investigation of the Effect of Asphaltene Polydispersity on Asphaltene Precipitation and Deposition Tendencies. *Energy & Fuels, 36*(16), 8799-8808. doi:10.1021/acs.energyfuels.2c01064

Kohli, K., Prajapati, R., & Sharma, B. K. (2019). Bio-Based Chemicals from Renewable Biomass for Integrated Biorefineries. *Energies, 12*(2). doi:10.3390/en12020233

Laurichesse, S., & Avérous, L. (2014). Chemical modification of lignins: Towards biobased polymers. *Progress in Polymer Science, 39*(7), 1266-1290. doi:https://doi.org/10.1016/j.progpolymsci.2013.11.004

Lee, J.-W., Kwon, T.-O., & Moon, I.-S. (2004). Adsorption of monosaccharides, disaccharides, and maltooligosaccharides on activated carbon for separation of maltopentaose. *Carbon, 42*(2), 371-380. doi:https://doi.org/10.1016/j.carbon.2003.11.008

Levi, P. G., & Cullen, J. M. (2018). Mapping Global Flows of Chemicals: From Fossil Fuel Feedstocks to Chemical Products. *Environmental Science & Technology, 52*(4), 1725-1734. doi:10.1021/acs.est.7b04573

Li, L., Cui, M., Wang, X., & Long, J. (2023). Critical Techniques for Overcoming the Diffusion Limitations in Heterogeneously Catalytic Depolymerization of Lignin. *ChemSusChem, n/a*(n/a). doi:https://doi.org/10.1002/cssc.202202325

Machineni, L., & Rao Anupoju, G. (2022). Review on valorization of lignocellulosic biomass for green plastics production: Sustainable and cleaner approaches. *Sustainable Energy Technologies and Assessments, 53*, 102698. doi:https://doi.org/10.1016/j.seta.2022.102698

Masina, N., Choonara, Y. E., Kumar, P., du Toit, L. C., Govender, M., Indermun, S., & Pillay, V. (2017). A review of the chemical modification techniques of starch. *Carbohydrate Polymers, 157*, 1226-1236. doi:https://doi.org/10.1016/j.carbpol.2016.09.094

Mua, J. P., & Jackson, D. S. (1997). Fine Structure of Corn Amylose and Amylopectin Fractions with Various Molecular Weights. *Journal of Agricultural and Food Chemistry, 45*(10), 3840-3847. doi:10.1021/jf960877a

Nakagawa, Y., Tamura, M., & Tomishige, K. (2013). Catalytic Reduction of Biomass-Derived Furanic Compounds with Hydrogen. *ACS Catalysis, 3*(12), 2655-2668. doi:10.1021/cs400616p

Nanda, S., Azargohar, R., Dalai, A. K., & Kozinski, J. A. (2015). An assessment on the sustainability of lignocellulosic biomass for biorefining. *Renewable and Sustainable Energy Reviews, 50*, 925-941. doi:https://doi.org/10.1016/j.rser.2015.05.058

Panahirad, S., Dadpour, M., Peighambardoust, S. H., Soltanzadeh, M., Gullón, B., Alirezalu, K., & Lorenzo, J. M. (2021). Applications of carboxymethyl cellulose- and pectin-based active edible coatings in preservation of fruits and vegetables: A review. *Trends in Food Science & Technology, 110*, 663-673. doi:https://doi.org/10.1016/j.tifs.2021.02.025

Paone, E., Tabanelli, T., & Mauriello, F. (2020). The rise of lignin biorefinery. *Current Opinion in Green and Sustainable Chemistry, 24*, 1-6. doi:https://doi.org/10.1016/j.cogsc.2019.11.004

Park, K. H., Lee, K. Y., & Lee, H. G. (2013). Chemical composition and physicochemical properties of barley dietary fiber by chemical modification. *International Journal of Biological Macromolecules, 60*, 360-365. doi:https://doi.org/10.1016/j.ijbiomac.2013.06.024

Patel, A. K., Vadrale, A. P., Singhania, R. R., Michaud, P., Pandey, A., Chen, S.-J., . . . Dong, C.-D. (2022). Algal polysaccharides: current status and future prospects. *Phytochemistry Reviews*. doi:10.1007/s11101-021-09799-5

Pelckmans, M., Renders, T., Van de Vyver, S., & Sels, B. F. (2017). Bio-based amines through sustainable heterogeneous catalysis. *Green Chemistry, 19*(22), 5303-5331. doi:10.1039/C7GC02299A

Pinto, E., Aggrey, W. N., Boakye, P., Amenuvor, G., Sokama-Neuyam, Y. A., Fokuo, M. K., . . . Rockson, M. A. D. (2022). Cellulose processing from biomass and its derivatization into carboxymethylcellulose: A review. *Scientific African, 15*, e01078. doi:https://doi.org/10.1016/j.sciaf.2021.e01078

Popp, J., Kovács, S., Oláh, J., Divéki, Z., & Balázs, E. (2021). Bioeconomy: Biomass and biomass-based energy supply and demand. *New Biotechnology, 60*, 76-84. doi:https://doi.org/10.1016/j.nbt.2020.10.004

Rama, H. O., Roberts, D., Tignor, M., Poloczanska, E. S., Mintenbeck, K., Alegría, A., . . . Ayanlade, S. (2022). *Climate Change 2022: Impacts, Adaptation and Vulnerability Working Group II Contribution to the Sixth Assessment Report of the Intergovernmental Panel on Climate Change*.

Renkin, E. M. (1956). FILTRATION, DIFFUSION, AND MOLECULAR SIEVING THROUGH POROUS CELLULOSE MEMBRANES. *Journal of General Physiology, 39*(5), 820-820. doi:10.1085/jgp.39.5.820

Roger, P., Tran, V., Lesec, J., & Colonna, P. (1996). Isolation and Characterisation of Single Chain Amylose. *Journal of Cereal Science, 24*(3), 247-262. doi:https://doi.org/10.1006/jcrs.1996.0057

Rolland-Sabaté, A., Guilois, S., Jaillais, B., & Colonna, P. (2011). Molecular size and mass distributions of native starches using complementary separation methods: Asymmetrical Flow Field Flow Fractionation (A4F) and Hydrodynamic and Size Exclusion Chromatography (HDC-SEC). *Analytical and Bioanalytical Chemistry, 399*(4), 1493-1505. doi:10.1007/s00216-010-4208-4

Rutenberg, M. W., & Solarek, D. (1984). CHAPTER X - STARCH DERIVATIVES: PRODUCTION AND USES. In R. L. Whistler, J. N. Bemiller, & E. F. Paschall (Eds.), *Starch: Chemistry and Technology (Second Edition)* (pp. 311-388). San Diego: Academic Press.

Salemis, P., & Rinaudo, M. (1984). Molecular weight-viscosity relationship for amylopectin, a highly branched polymer. *Polymer Bulletin, 12*(4), 283-285. doi:10.1007/BF00263139

Sangseethong, K., Termvejsayanon, N., & Sriroth, K. (2010). Characterization of physicochemical properties of hypochlorite- and peroxide-oxidized cassava starches. *Carbohydrate Polymers, 82*(2), 446-453. doi:https://doi.org/10.1016/j.carbpol.2010.05.003

Serrano, D. P., Melero, J. A., Morales, G., Iglesias, J., & Pizarro, P. (2018). Progress in the design of zeolite catalysts for biomass conversion into biofuels and bio-based chemicals. *Catalysis Reviews, 60*(1), 1-70. doi:10.1080/01614940.2017.1389109

Shamshina, J. L., & Berton, P. (2020). Use of Ionic Liquids in Chitin Biorefinery: A Systematic Review. *Frontiers in Bioengineering and Biotechnology, 8*. Retrieved from https://www.frontiersin.org/articles/10.3389/fbioe.2020.00011

Shen, F., Ling, H., Ge, W., Yang, Y., Wang, X., Ren, J., & Wang, X. (2021). Self-assembly behavior and conformation of amphiphilic hemicellulose-graft-fatty acid micelles. *Carbohydrate Polymers, 261*, 117886. doi:https://doi.org/10.1016/j.carbpol.2021.117886

Shirazi, M., van de Ven, T. G. M., & Garnier, G. (2003a). Adsorption of Modified Starches on Porous Glass. *Langmuir, 19*(26), 10829-10834. doi:10.1021/la0350655

Shirazi, M., van de Ven, T. G. M., & Garnier, G. (2003b). Adsorption of Modified Starches on Pulp Fibers. *Langmuir, 19*(26), 10835-10842. doi:10.1021/la035064c

Simonneaux, G., Le Maux, P., Ferrand, Y., & Rault-Berthelot, J. (2006). Asymmetric heterogeneous catalysis by metalloporphyrins. *Coordination Chemistry Reviews, 250*(17), 2212-2221. doi:https://doi.org/10.1016/j.ccr.2006.01.014

Speight, J. G., Wernick, D. L., Gould, K. A., Overfield, R. E., & Rao, B. M. L. (1985). Molecular Weight and Association of Asphaltenes: a Critical Review. *Rev. Inst. Fr. Pét., 40*(1), 51-61. Retrieved from https://doi.org/10.2516/ogst:1985004

Stacy, C. J., & Foster, J. F. (1957). Molecular weight heterogeneity in starch amylopectins. *Journal of Polymer Science, 25*(108), 39-50. doi:https://doi.org/10.1002/pol.1957.1202510804

Sudarsanam, P., Peeters, E., Makshina, E. V., Parvulescu, V. I., & Sels, B. F. (2019). Advances in porous and nanoscale catalysts for viable biomass conversion. *Chemical Society Reviews, 48*(8), 2366-2421. doi:10.1039/C8CS00452H

Tafreshi, O. A., Mosanenzadeh, S. G., Karamikamkar, S., Saadatnia, Z., Park, C. B., & Naguib, H. E. (2022). A review on multifunctional aerogel fibers: processing, fabrication, functionalization, and applications. *Materials Today Chemistry, 23*, 100736. doi:https://doi.org/10.1016/j.mtchem.2021.100736

Timofeev, K. L., & Vodyankina, O. V. (2021). Selective oxidation of bio-based platform molecules and their conversion products over metal nanoparticle catalysts: a review. *Reaction Chemistry & Engineering, 6*(3), 418-440. doi:10.1039/D0RE00352B

Tolbert, A., Akinosho, H., Khunsupat, R., Naskar, A. K., & Ragauskas, A. J. (2014). Characterization and analysis of the molecular weight of lignin for biorefining studies. *Biofuels, Bioproducts and Biorefining, 8*(6), 836-856. doi:https://doi.org/10.1002/bbb.1500

Tolvanen, P., Mäki-Arvela, P., Sorokin, A. B., Salmi, T., & Murzin, D. Y. (2009). Kinetics of starch oxidation using hydrogen peroxide as an environmentally friendly oxidant and an iron complex as a

catalyst. *Chemical Engineering Journal, 154*(1), 52-59. doi:https://doi.org/10.1016/j.cej.2009.02.001

Vanier, N. L., El Halal, S. L. M., Dias, A. R. G., & da Rosa Zavareze, E. (2017). Molecular structure, functionality and applications of oxidized starches: A review. *Food Chemistry, 221*, 1546-1559. doi:https://doi.org/10.1016/j.foodchem.2016.10.138

Ventura, M., Marinas, A., & Domine, M. E. (2020). Catalytic Processes for Biomass-Derived Platform Molecules Valorisation. *Topics in Catalysis, 63*(9), 846-865. doi:10.1007/s11244-020-01309-9

Ventura, M., Marinas, A., & Domine, M. E. (2021). Correction to: Catalytic Processes for Biomass-Derived Platform Molecules Valorisation. *Topics in Catalysis, 64*(5), 467-467. doi:10.1007/s11244-021-01438-9

Verraest, D. L., Peters, J. A., & van Bekkum, H. (1998). The platinum-catalyzed oxidation of inulin. *Carbohydrate Research, 306*(1), 197-203. doi:https://doi.org/10.1016/S0008-6215(97)10055-6

Vinod, A., Sanjay, M. R., Suchart, S., & Jyotishkumar, P. (2020). Renewable and sustainable biobased materials: An assessment on biofibers, biofilms, biopolymers and biocomposites. *Journal of Cleaner Production, 258*, 120978. doi:https://doi.org/10.1016/j.jclepro.2020.120978

Wang, H., Poya, Y., Chen, X., Jia, T., Wang, X., & Shi, J. (2015). Hydrogen peroxide as an oxidant in starch oxidation using molybdovanadophosphate for producing a high carboxylic content. *RSC Advances, 5*(57), 45725-45730. doi:10.1039/C5RA07747H

Weiss, M., Haufe, J., Carus, M., Brandão, M., Bringezu, S., Hermann, B., & Patel, M. K. (2012). A Review of the Environmental Impacts of Biobased Materials. *Journal of Industrial Ecology, 16*(s1), S169-S181. doi:https://doi.org/10.1111/j.1530-9290.2012.00468.x

Whistler, R. L., & Schweiger, R. (1957). Oxidation of Amylopectin with Hypochlorite at Different Hydrogen Ion Concentrations1,2. *Journal of the American Chemical Society, 79*(24), 6460-6464. doi:10.1021/ja01581a027

Wyman, C. E., Dale, B. E., Elander, R. T., Holtzapple, M., Ladisch, M. R., & Lee, Y. Y. (2005). Coordinated development of leading biomass pretreatment technologies. *Bioresource Technology, 96*(18), 1959-1966. doi:https://doi.org/10.1016/j.biortech.2005.01.010

Xie, Y., Guo, X., Ma, Z., Gong, J., Wang, H., & Lv, Y. (2020). Efficient Extraction and Structural Characterization of Hemicellulose from Sugarcane Bagasse Pith. *Polymers, 12*(3). doi:10.3390/polym12030608

Yamaguchi, T., Endo, K., Takagi, Y., & Hukao, K. (1977). Influence of Pore-size Distribution of Activated Carbons on the Correlation between Adsorptivities of Oligosaccharides and Their Degree of Polymerization. *NIPPON KAGAKU KAISHI, 11*. doi:10.1246/nikkashi.1977.1577

Zhou, D.-N., Zhang, B., Chen, B., & Chen, H.-Q. (2017). Effects of oligosaccharides on pasting, thermal and rheological properties of sweet potato starch. *Food Chemistry, 230*, 516-523. doi:https://doi.org/10.1016/j.foodchem.2017.03.088

Zou, J., Xu, M., Wen, L., & Yang, B. (2020). Structure and physicochemical properties of native starch and resistant starch in Chinese yam (Dioscorea opposita Thunb.). *Carbohydrate Polymers, 237*, 116188. doi:https://doi.org/10.1016/j.carbpol.2020.116188

2.

2. Environmental impact evaluation for heterogeneously catalysed starch oxidation

This chapter is published as: Hoogstad, T. M., Timmer, S. M., van Boxtel, A. J. B., Buwalda, P. L., Bitter, J. H., & Kiewidt, L. (2022). Environmental Impact Evaluation for Heterogeneously Catalysed Starch Oxidation. ChemistryOpen, 11(10)

Abstract

Oxidised starch is currently produced from native starch using sodium hypochlorite as oxidising agent. The use of hypochlorite has undesired side reactions and produces stoichiometric amounts of waste (salt), thus alternative oxidation methods are desired. In this study, the potential of two catalysed starch oxidation methods to reduce the environmental impact (EI) of oxidised starch production are assessed. We compared the EI of oxidation with molecular oxygen (heterogeneously catalysed) and hydrogen peroxide (homogeneously catalysed) to hypochlorite oxidation through life cycle assessment. The results confirm that hypochlorite oxidation is the main environmental hotspot in the current process of oxidised starch production, and that both hydroperoxide oxidation and molecular oxygen oxidation can significantly lower the EI of the process. The impact reduction is most significant in the categories of freshwater eutrophication (~67%), ozone depletion (~66%), climate change (35-60%) and resource use (40%-78%) for peroxide and molecular oxygen oxidation respectively.

Keywords: Starch Oxidation; Comparative Life Cycle Assessment; Green Chemistry; Anionic Starch; Heterogeneous Catalysis; Environmental Impact

2.1 Introduction

Chemical oxidation of potato starch, whereby negatively charged carboxylic acid moieties are introduced, produces anionic starch. Anionic starches are a renewable bio-based alternative for polyacrylates in the paper, textile, and food industry. Anionic potato starch has better pasting and adhesive properties and better shelf life than unmodified potato starch (Sangseethong, Termvejsayanon, & Sriroth, 2010; Zhou, Zhang, Chen, & Chen, 2017). These properties make anionic starch suitable for applications in the paper and textile industry as surface sizing agents, in the food and feed sector as thickeners, and in various adhesive industries (Masina et al., 2017; Vanier, El Halal, Dias, & da Rosa Zavareze, 2017). Worldwide, around 100 kilotons of anionic starch are produced annually.

Various oxidation methods are available to produce anionic starches. Oxidation with sodium hypochlorite (NaOCl) is an established process (Rutenberg & Solarek, 1984), but is currently still the standard for the industrial production of anionic starch (Vanier et al., 2017). Although application of new techniques like ultrasonication show potential to improve this process (Wei et al., 2020), the use of hypochlorite as oxidant has several fundamentally unfavourable characteristics. During hypochlorite oxidation, small amounts of chlorates are formed and some chloride is built into the backbone of the oxidised starch (<1%) (Rutenberg & Solarek, 1984). These undesired side reactions reduce the applicability of oxidised starches depending on legislation, e.g., for food applications.

Next to the formation of chlorates, depolymerisation of starch is another side reaction during hypochlorite oxidation. Using hypochlorite, depolymerisation occurs via oxidation at the C2-C3 carbons (Rutenberg & Solarek, 1984; Whistler & Schweiger, 1957), which induces oxidative depolymerisation. The link between the molecular weight of starch and its physiochemical properties, e.g., pasting properties and viscosity, has been well established (Fiedorowicz, Tomasik, You, & Lim, 1999; Jane et al., 1999; Salemis & Rinaudo, 1984). Excessive depolymerisation during the oxidation alters the physiochemical properties, i.e., decreases viscosity and retrogradation enthalpy of the product, and thereby reduces suitability of the starch for applications like adhesives (Masina et al., 2017; Sangseethong et al., 2010). Furthermore, excessive depolymerisation of the starch reduces reaction yield if small maltodextrins (degree of polymerisation, DP<6) are formed, which do not contribute to gelling properties of a starch mixture (Forssell, Hamunen, Autio, Suortti, & Poutanen, 1995; Parovuori, Hamunen, Forssell, Autio, & Poutanen, 1995).

In addition to depolymerisation, the use of hypochlorite produces stoichiometric amounts of salt (NaCl) during the oxidation process. Moreover, the production of the sodium hypochlorite for starch oxidation raises concerns of a high environmental impact of the overall process. Homogeneously catalysed hydrogen peroxide oxidation

with copper sulphate, iron complexes, or vanadium complexes has been proposed as a more environmentally friendly alternative to hypochlorite oxidation (Ketola, 2003; Masina et al., 2017; Tolvanen, Mäki-Arvela, Sorokin, Salmi, & Murzin, 2009; Vanier et al., 2017; Wang et al., 2015). The downside of the hydrogen peroxide oxidation, however, is that residues of the catalyst remain in the product, resulting in impurities in the product or higher purification costs. This challenge has thus far hindered the industrial scale application of this process (Vanier et al., 2017).

The combination of a potentially high environmental impact (chemicals and salts), undesired side reactions (chlorate formation), catalyst residues, and depolymerisation during oxidation, leads to the need for a new method of oxidising starch (Collinson & Thielemans, 2010; de Nooy, Besemer, & van Bekkum, 1994). A potential solution to phase out the chlorine chemistry in starch oxidation is the use of molecular oxygen and heterogeneous catalysts. Heterogeneously catalysed oxidation of dissolved polysaccharides with molecular oxygen has been achieved on the lab scale with supported Au and Pt nanoparticles (Heyns & Paulsen, 1963; Verraest, Peters, & van Bekkum, 1998) and vanadium complexes (Chen et al., 2015). With heterogeneous catalysis, no chemically produced oxidant is required since molecular oxygen from air can be used, the catalyst can be separated easily, and the reaction can be more selective towards C6 oxidation (Verraest et al., 1998), resulting in less depolymerisation in the process. We, therefore, hypothesise that oxidation of dissolved starch using molecular oxygen and a solid heterogeneous catalyst could alleviate many of the undesired traits of both hypochlorite and peroxide oxidation, and reduce the environmental impact of the process. However, a quantitative analysis comparing the environmental impact of these oxidation methods is not available yet (Holman, Shonnard, & Holles, 2009).

Comparative LCAs of new methods in an early stage of development provide valuable insights into the requirements that these new methods need to meet to be viable and can thereby guide further catalysis research (Holman et al., 2009). In this work, we therefore quantify the environmental impact of the current production of anionic potato starch with sodium hypochlorite through life cycle assessment (LCA), and investigate potential changes in environmental impact by applying three catalysed oxidation scenarios: two heterogeneously catalysed oxidations with molecular oxygen and one homogenously catalysed oxidation with hydrogen peroxide. With this analysis, we assess the requirements that a heterogeneous catalyst needs to meet to reduce the environmental impact of anionic starch production in order to guide research and development of this catalyst.

2.2 Materials and methods

2.2.1 Environmental impact analysis

Goal and scope

The goal of the assessment is to identify hotspots in the current production chain of anionic potato starch, and to estimate potential environmental impact reduction of alternative methods of starch oxidation compared to the current industrial standard, for the production of 1 tonne of anionic potato starch. To this end, a gate-to-gate LCA is applied. The production system was divided into 6 modules to assess pre-processing and side-stream processing steps (modules A and B) in combination with four different oxidation methods (modules OCl^-, H_2O_2, O_2, and O_2DA). Figure 1 gives an overview of the production system.

Mass and energy balances for each unit operation in all modules (see Supplementary Information: Process description) are linked to the life cycle assessment (LCA) to compare the different processing options.

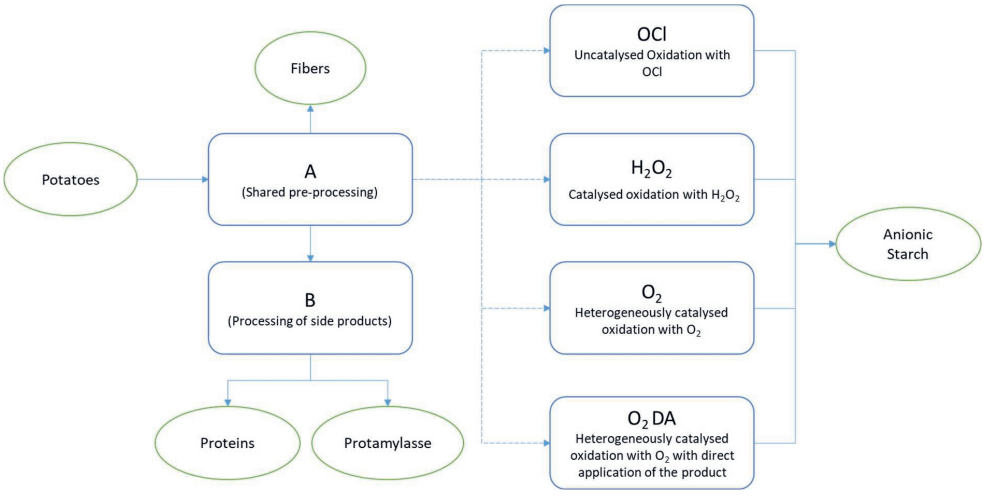

Figure 1. Flowsheet of the overall process to produce anionic starch from potatoes. The dashed lines indicate the four evaluated options for starch oxidation.

System boundaries

In this gate-to-gate LCA the first gate is at the delivery of fresh potatoes at the processing facility and the end gate for all processing options, with the exception of the O_2DA scenario, is dried anionic starch. In these scenarios, the starch has to be transported and gelatinised before application. For the option with module O_2DA the end gate is the oxidised starch solution from the oxidation step ready for direct application. Transportation of the dry anionic starch powder and gelatinisation are beyond the system boundaries for options OCl^-, H_2O_2 and O_2 and have equal impact for all options.

Therefore, transportation and gelatinisation of the dry anionic starch are omitted from the evaluation of the O_2DA module for an equal comparison. With these system boundaries, the oxidation methods are compared as they would integrate into the current production chain. By doing so, different processing requirements between oxidation and application of the starch are included in the comparison. The LCA is focussed on the unit operations only, other factors like heating and lighting for the facilities, and transport of raw materials to the facilities are excluded.

LCA methods

Since the LCA is used to compare different processing options for the same product, i.e. anionic starch suitable for application, internal normalisation (i.e. relative impact) is used as the main tool for comparison (equations 1 and 2).

Internal normalisation in comparative LCA studies helps avoid macroscopic mistakes e.g. use of datasets that are not scale-calibrated, while providing easily interpretable results (Norris, 2001; Pizzol et al., 2017). No subsequent weighing step is applied as this can distort the results (Laurent & Hauschild, 2015; Norris, 2001). Because the quality and quantity of the side streams remain equal for all processing options, allocation of impact to side products is not required. All quantities are expressed per tonne of produced anionic potato starch.

The LCA calculations have been performed with openLCA 1.10.2 (Ciroth, 2007). The Life Cycle Inventory (LCI) was based on the Product Environmental Footprints (PEF) database, and impact and category choice follow the International Reference Life Cycle Data System (ILCD 2011 midpoint) method in accordance with the guidelines of the European platform on life cycle assessment made by the Joint Research Centre of the European commission (European Commission, 2012; Recchioni, Mathieux, Goralczyk, & Schau, 2013). The categories on ionising radiation and the category water use were omitted from the LCI and ILCD 2011 midpoint method due to limited data availability for some flows, which would result in an incomplete analysis in these categories. Water use was instead evaluated based on total amount of clean water required within the different processes. The list of indicators and their units is given in Table 1. The LCI is given in appendix A.

Table 1. Summary of analysed impact categories and units.

Impact categories	**Units**
Acidification	mol H^+eq
Climate change	kg CO_2 eq
Ecotoxicity freshwater	CTUe
eutrophication freshwater	kg P eq
Human tox - cancer	CTUh
Human tox. Non-cancer	CTUh
Land use	kg C deficit
eutrophication marine	kg N eq
resource use mineral and metals	kg Sb eq
ozone depletion	kg CFC11 eq
particulate matter	kg PM2.5 eq
photochemical ozone formation	kg NMVOC eq
eutrophication terrestrial	mol N eq

From all mass and energy streams of each operation (see Supplementary Information), the total environmental impact per unit operation for each impact category is calculated (Equation 1). This results in a matrix with the impact from each unit operation in each impact category:

$$EI_{k,i} = \sum_j \mathrm{F}_{k,j} \cdot \mathrm{EIF}_{j,i} \quad (1)$$

Where $EI_{k,i}$ is the Environmental Impact of unit operation k in impact category i, $F_{k,j}$ is a quantity of mass or energy j going into unit operation k, and $EIF_{j,i}$ is the environmental impact factor associated with F_j in impact category i.

To compare the different oxidation scenarios, internal normalisation is applied. Hereby, the total impact in a category is calculated by summation of all the impacts across the unit operations. Then, the impact per category for each unit is expressed as a percentage of the total impact (equation 2).

$$\mathrm{NEI}_{k,i} = \frac{EI_{k,i}}{\sum_k EI_{k,i}} \cdot 100\% \quad (2)$$

Where $NEI_{k,i}$ is the normalised environmental impact of unit operation k in impact category i expressed as a percentage of the total impact of all unit operations in category i.

2.2.2 Process description

For the environmental impact analysis, the production process of anionic starch described by Grommers and van der Krogt, and Rutenberg and Solarek (Grommers & van der Krogt, 2009; Rutenberg & Solarek, 1984) was used as a case study as it closely resembles the current process used in industry. Flowsheets and process description of modules A and B are shown in the supplementary information (SI). Flowsheets of the different oxidation modules are shown in Figures 2 and 3. The corresponding mass and energy balances of the different unit operations, as well as the implemented efficiencies are given in the Supplementary Information (SI). The mass and energy balances of all modules were scaled to relevant industrial scale to evaluate their potential as a large scale replacement for the current industrial process.

The process steps for oxidation with hypochlorite (NaOCl) or hydrogen peroxide (H_2O_2) are given in Figure 2. First, dry native starch is dispersed in water to make a slurry of 39% (w/w) starch. Then either NaOCl (a) or H_2O_2 plus a catalyst (b) is added in a stirred tank batch reactor. During the oxidation acidic compounds are formed and the pH decreases. To avoid depolymerisation due to acidification, which would result in decreased pasting properties, NaOH is added to keep the pH>6 (Grommers & van der Krogt, 2009; Parovuori et al., 1995; Vanier et al., 2017). The mixture from the hypochlorite oxidation has a high NaCl concentration, which is produced in stoichiometric amounts. The NaCl is washed out in hydro-cyclones after oxidation (starch refining step). A sieving centrifuge recovers the starch loss from the hydro-cyclones. The anionic starch is dewatered by a drum filter and dried in a pneumatic dryer. Finally, the dry anionic starch powder is separated with cyclones. The anionic starch has a dry matter content of 80% (w/w).

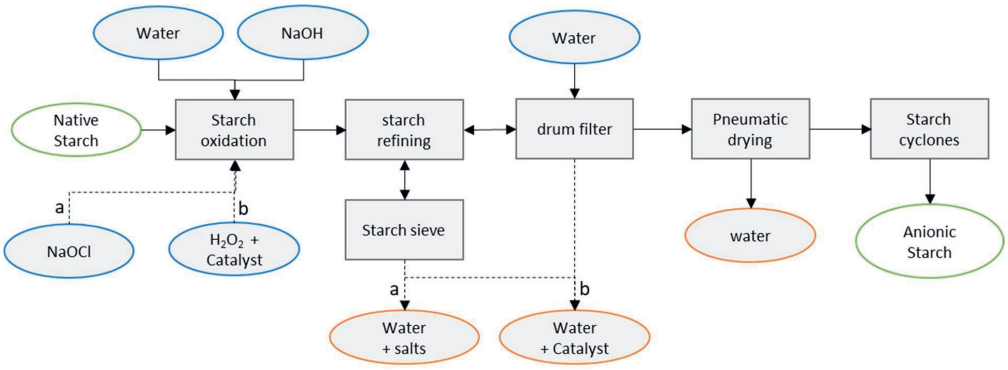

Figure 2. Flowsheet of modules OCl^- (a) and H_2O_2 (b) from figure 1 for the oxidation of native potato starch to anionic starch with sodium hypochlorite (a) and hydrogen peroxide (b), respectively.

Hydrogen peroxide oxidation (Figure 2 route b) proceeds similar to hypochlorite oxidation, but H_2O_2 is added as oxidant instead of NaOCl. Because of the lower oxidation strength of H_2O_2 compared to NaOCl, a catalyst (e.g. iron complexes, copper sulphate, or vanadium complexes) is used to catalyse the reaction. The catalyst is homogeneous and is difficult to separate as some catalysts form complexes with carboxylated starch (Achremowicz, Gumul, Bala-Piasek, Tomasik, & Haberko, 2000). As a result, traces of the catalyst appear in the side streams and in the final product.

Heterogeneously catalysed starch oxidation, i.e., by using a solid catalyst, is currently under development. Therefore, the described process is hypothetical, but based on realistic parameters published by Verreast et al. (Verraest et al., 1998). Since solid starch granules do not interact with solid catalyst particles, the starch needs to be gelatinised before oxidation. Starch gelatinisation is achieved in twin screw extruders or jet cookers, where the granules are broken and solubilised by a combination of shear stress and temperature (Grommers & van der Krogt, 2009). The gelatinised starch is then oxidised using molecular oxygen, a supported Pt catalyst, and sodium hydroxide to keep the pH of the reaction constant (Verraest et al., 1998). The energy use in this oxidation with oxygen from air is estimated based on the energy used in aerated reactors in wastewater treatment (Drewnowski, Remiszewska-Skwarek, Duda, & Łagód, 2019; Sandberg, 2010). Similarly, the required oxygen for this reaction is expressed as chemical oxygen demand (COD), and the activity of the catalyst is expressed in terms of oxygen uptake rates (OUR). Energy use for separation of the catalyst is excluded since the catalyst can be fixed in the reactor in either a fixed bed or trickle bed configuration. Impact for the production of the catalyst is not considered as catalyst production generally accounts for <1% of the environmental impact (Benavides, Cronauer, Adom, Wang, & Dunn, 2017).

After oxidation with air over a heterogeneous catalyst, the oxidised starch is drum dried or spray dried (Gharsallaoui, Roudaut, Chambin, Voilley, & Saurel, 2007; Niazi & Broekhuis, 2012), see Figure 3a. After drying, the anionic starch is transported to the

user location for application. As an alternative, the energy intensive spray/drum drying of the anionic starch is circumvented by transporting the native starch to the user location where the native starch is oxidised on-site and then directly applied after further concentration (Figure 3b). Table 2 gives the process conditions for each oxidation method. Oxidised starches are generally applied in a concentration range of 2–10% wt (Maurer, 2009), which overlaps partially with the concentration range of the oxidation reaction.

Table 2. Process conditions for different oxidation methods.

Oxidant	**OCl^-**	**H_2O_2**	**O_2 (from air)**
Starch concentration (w/w)	39%	39%	max. 5%
Granular/gelatinised	granular	granular	gelatinised
Oxidant consumed (g oxidant/g starch)	0.2	0.092	~
Electrical Energy use	0.785 kWh per m^3 starch slurry	0.785 kWh per m^3 starch slurry	3.4 kWh per m^3 starch solution
Oxygen uptake rate	~	~	0.3 mg O_2/L/min

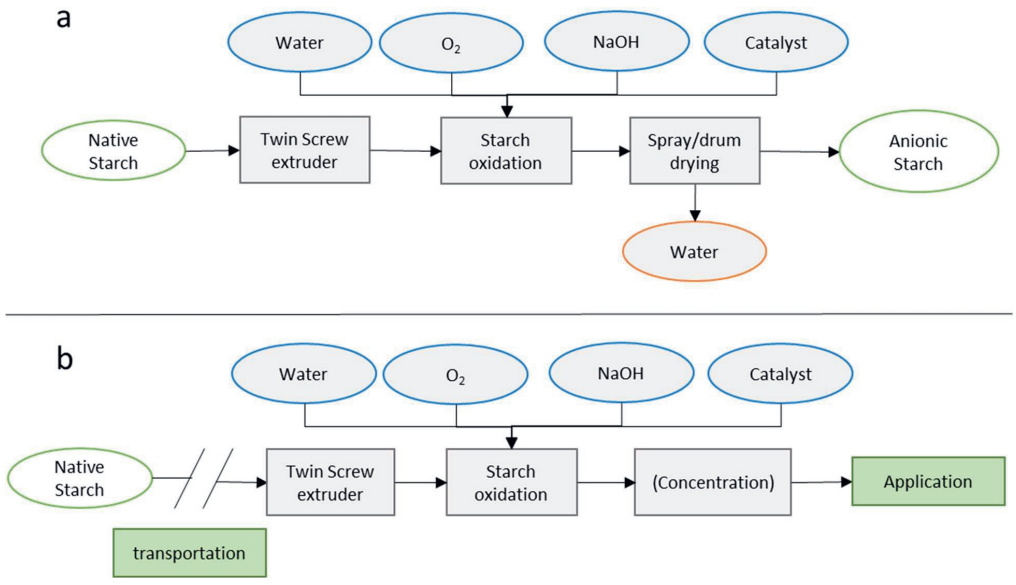

Figure 3. Flowsheets of modules O_2 (a) and O_2DA (b) for the oxidation of native potato starch with molecular oxygen and a heterogeneous catalyst. In the O_2DA scenario, the oxidation is performed on-site the user location to enable direct application of the product and omit the energy-intensive drying step.

2.3 Results and discussion

2.3.1 Identification of environmental hotspots

The contributions of the eight unit operations with the highest impact in each category are shown in Figure 4; the contributions of all remaining unit operations is combined in the 'other' category. Hotspot analysis showed that these eight unit operations were responsible for more than 90% of the total environmental impact in each category for the OCl^- reference case (modules A,B, and OCl^-).

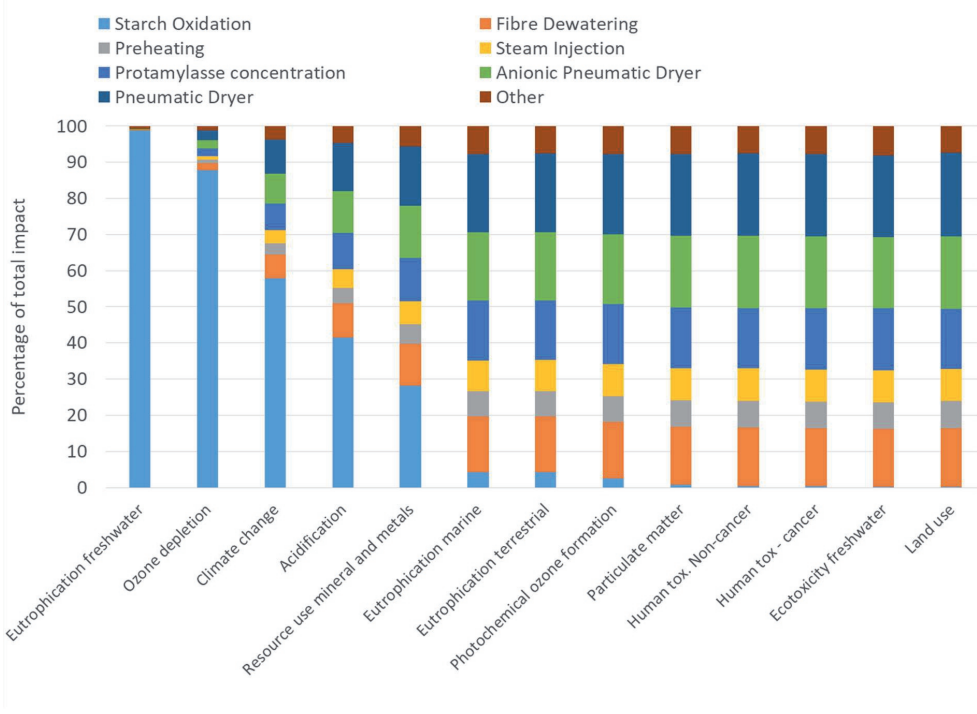

Figure 4. Normalised environmental impacts of the eight highest scoring unit operations that account for more than 90% of the total impact in each category. The contribution of the remaining unit operations is combined in the 'other' category.

Figure 4 shows that the unit operations pneumatic drying of native and of anionic starch, preheating, protamylasse concentration, fiber dewatering, steam injection, and starch oxidation, are the main contributors to the overall environmental impact of the process. Starch oxidation, is the main contributor in the categories of freshwater eutrophication, ozone depletion, climate change, acidification, and resource use. The impacts of the oxidation step are linked to the use of chemicals (NaOCl, NaOH) in the oxidation process (Bay-Smidt, Wischmann, Olsen, & Nielsen, 1994; Chipperfield, 2009; Mellouki et al., 1992). Starch oxidation contributes only marginally to marine and terrestrial eutrophication and photochemical ozone formation. These results show that

the oxidation step is the main hotspot in the production of anionic starch. The other seven highlighted unit operations from Figure 4 are considered secondary hotspots.

The high environmental impact of the preheating, fiber dewatering, pneumatic drying of native and anionic starch, steam injection, and protamylasse concentration units is due to the high energy use for heating and drying in these steps (Celma & Cuadros, 2009; Kudra, 2004). The impact profile of these units, i.e., the ratio of the contributions to a category, is similar across all impact categories because these unit operations use the same type of energy (heat and electricity from a combined heat-power plant utilising natural gas). A full table of the calculated normalised impact indicators for all unit operations is given in Appendix B.

2.3.2 Comparison of oxidation methods

Four different oxidation methods were investigated. It became evident that the O_2-oxidation scenario without direct application of the anionic starch solutions performs poorly compared to the other scenarios (see Fig. SI5 in the SI). In the O_2-oxidation scenario a significant increase in environmental impact is seen for several categories (Climate change +400%, acidification +600%, resource use + 700%; the full data is given in the SI). The high increase in environmental impact is the indirect result of practical limitations. Gelatinised (oxidised) starch cannot feasibly be transported or stored since it is susceptible to microbial decay and retrogradation, which severely reduces the robustness of the supply chain. Moreover, since the concentration of such a solution is low (<5% w/w) the added volume and weight of water substantially increases the cost of transportation. Due to these limitations, the gelatinised starch would need to be dried before transportation and/or storage. In the O_2-oxidation scenario, the starch is in solution and highly viscous after oxidation so that mechanical dewatering or pre-concentration before drying is technologically unfeasible. To dry the oxidised starch solution from the 5% (w/w) to a powder, approximately 9 tonnes of water need to be evaporated per tonne of starch. At a theoretical minimum of 2.3 GJ of energy used per tonne of water evaporated, the energy use for spray or drum drying the anionic starch solution thus becomes infeasibly high (Baker & McKenzie, 2005). For these reasons, the O_2-oxidation scenario is deemed not viable and is omitted from further analysis and graphical representations to increase readability of the viable alternatives. Since the O_2DA scenario performs the oxidation directly before application, no transport, storage or drying of the oxidised starch is required and as a result these limitations of the O_2 scenario do not apply to the O_2DA scenario. For the remaining oxidation methods (H_2O_2 and O_2DA) two comparisons were made. First, the achievable reduction in environmental impact was investigated relative to OCl^- oxidation itself (without including the pre-processing modules A and B). Second, the achievable reductions in environmental impact were placed in context of the complete process chain (including the pre-processing modules A and B).

Figure 5 shows the relative reductions of environmental impact of anionic starch production by employing H_2O_2 oxidation or molecular oxygen oxidation with direct application of the gelatinised anionic starch (O_2DA).

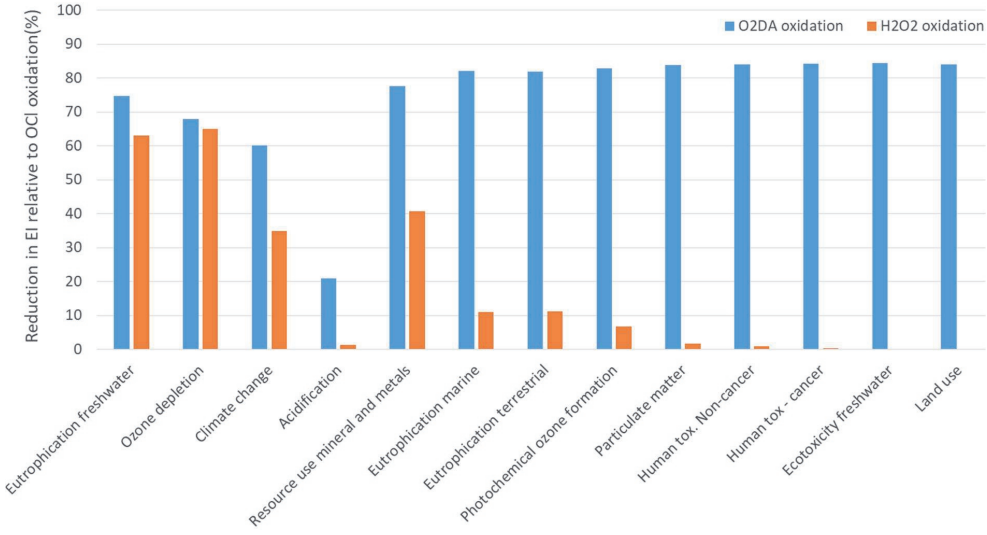

Figure 5. Achievable reduction in environmental impact (EI) by H_2O_2 oxidation or molecular oxygen oxidation with direct application (O_2DA) relative to the OCl^- reference case. Higher values indicate a higher reduction and thus lower environmental impact.

The H_2O_2 and O_2DA scenarios reduce the environmental impact of starch oxidation step compared to hypochlorite oxidation for most categories and increase it in none of the categories (Figure 5). Both the H_2O_2 and O_2DA scenario strongly reduce the impact in the freshwater eutrophication (63% and 75% respectively) and ozone depletion category (65% and 68% respectively). Eutrophication in this process is caused mainly by the chemicals NaOH and NaOCl. Since NaOH use is equal in all processes, the difference in the environmental impact reduction between the H_2O_2 and O_2DA scenario represents the impact of the H_2O_2 itself. The reduction in ozone depletion is a result of the elimination of the use and production of chlorinated compounds (NaOCl) from the process. Chlorine and chlorinated compounds are strong contributors to ozone depletion (Chipperfield, 2009; Mellouki et al., 1992). The H_2O_2 scenario further reduces impact in the categories climate change (35%), resource use (41%), and leads to small improvements (5-10%) in marine and terrestrial eutrophication, and photochemical ozone formation. In comparison to the H_2O_2 scenario, the O_2DA scenario overall shows a higher reduction of environmental impact. In addition to the reduction in freshwater eutrophication (75%), ozone depletion (68%), climate change (60%), and resource use (78%), which is also observed in the H_2O_2 scenario to a slightly lower extend, the O_2DA scenario reduces the environmental impact across all the remaining categories by 75% to 85%. This reduction is attributable to reduction in energy demand through the elimination of the

drying step for the oxidised potato starch. In both, the O_2DA scenario and the H_2O_2, the impact reduction for the category acidification is the lowest. The impact in this category is mainly caused by the usage of NaOH (Corona et al., 2018), which is required to compensate the pH drop of oxidising starch, regardless of oxidation method.

Variations in water use between the OCl^-, H_2O_2, O_2, and O_2DA scenarios were minimal with the initial washing step being the main contributor for all scenarios. Water used in the oxidation step is recovered during the subsequent drying of the oxidised starches and recycled. For this reason the differences in water use between the analysed scenarios do not significantly impact the results.

2.3.3 Overall reduction of environmental impact

Plotting the relative reductions in environmental impact of the investigated oxidation methods provides a good comparative tool, but this comparison alone lacks a broader context since it gives no information on the absolute orders of magnitude of the environmental impacts of the process. To put the results into a broader perspective the environmental impacts of the different oxidation methods were expressed as a contribution to the total system impact as defined by the system boundaries. Hereby, the significance of the reduction of environmental impact of each category can be estimated without the pitfalls of using external normalisation for internally normalised LCA (Pizzol et al., 2017).

The environmental impact reduction of the H_2O_2 and O_2DA scenarios expressed in reduction to the environmental impact of the entire processing chain is given in Figure 6.

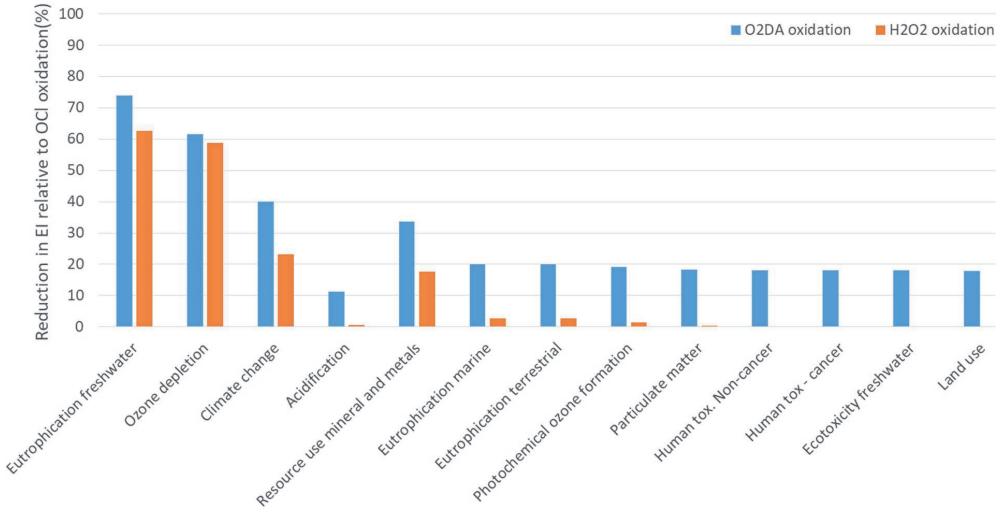

Figure 6. Comparison of the reduction in environmental impact (EI) of the H_2O_2 and O_2DA scenarios expressed in reduction of environmental impact of the overall process

The reduction in freshwater eutrophication (~65%) and ozone depletion (~69%), present in both the H_2O_2 and O_2DA scenarios, remains high in the overall process chain. The reduction in environmental impact in the categories resource use and climate change became moderately more relevant compared to others. In the categories marine and terrestrial eutrophication, land use, acidification, and photochemical ozone formation, the O_2DA scenario still provides relevant reductions in environmental impact of 10%–20%. The significance of the reduced environmental impact of H_2O_2 oxidation compared to OCl^- oxidation, however, seems to be limited to freshwater eutrophication, ozone depletion, climate change, and resource use.

From an environmental perspective, both homogeneously catalysed H_2O_2 oxidation and heterogeneously catalysed O_2 oxidation (O_2DA) are preferred over OCl^- oxidation. The O_2DA scenario provides substantially higher reductions in environmental impact over a broader range of categories than H_2O_2 oxidation.

2.4.4 Evaluation of assumptions in the heterogeneously catalysed oxidation

The analysis showed that the heterogeneously catalysed oxidation of starch using molecular oxygen with direct application (O_2DA) has the potential to significantly reduce the environmental impact of anionic starch production. However, since the data is based on the estimated performance of a conceptual process, the robustness of these findings needs to be evaluated. The most influential assumptions that affect the results for the O_2DA scenario are: 1) the yield of the reaction, and 2) the energy use for aeration.

First, the OCl^- oxidation has a yield of approximately 97% in the currently employed industrial process (Grommers & van der Krogt, 2009). The losses during this reaction are mainly due to oxidative depolymerisation through C2-C3 diol cleavage (Rutenberg & Solarek, 1984; Sangseethong et al., 2010; Whistler & Schweiger, 1957). Heterogeneous catalysts for polysaccharide oxidation that are selective towards C6 oxidation have been developed on lab scale (Verraest et al., 1998). Because of the selectivity towards C6 oxidation, the effect of oxidative depolymerisation is attenuated (Chen et al., 2015; de Nooy et al., 1994; Verraest et al., 1998). It is thus reasonable to assume that the yield of a well-developed heterogeneous catalyst for starch oxidation is at least equal to or greater than that of OCl^- oxidation.

Second, the uncertainty in energy use for aeration, which has two causes: First, the energy use for aeration of the reactor is influenced by varying oxygen transfer rates based on the viscosity of the reaction mixture (García-Ochoa, Castro, & Santos, 2000; Kang, Cho, Woo, & Kim, 1999; Kováts, Thévenin, & Zähringer, 2020; Labík et al., 2018). Second, variances in catalyst activity would result in different reactor size and/or residence time, thus increasing or decreasing energy use for aeration (Drewnowski et al., 2019).

To evaluate the effect of the energy use for aeration on the results, several scenarios with multiples of the estimated energy consumption (0.5x, 5x, and 10x) for the reactor have been computed (Figure 7) to estimate the critical point where the O_2DA method no longer provides substantial benefits over the OCl^- scenario.

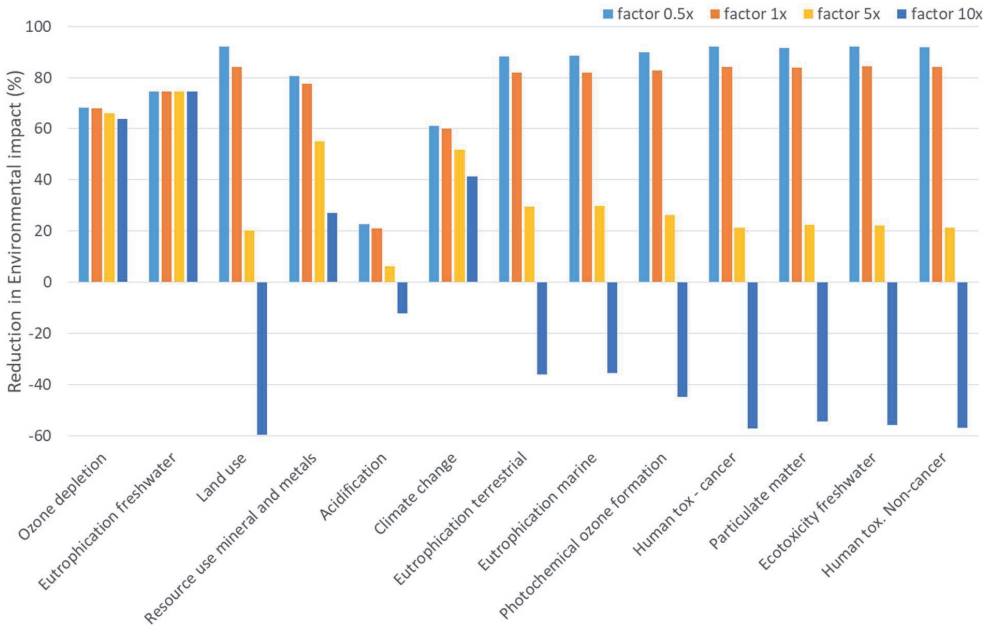

Figure 7. Reduction in environmental impact (oxidation step only) for multiples of estimated energy use (0.5x, 1x, 5x, 10x) for heterogeneously catalysed starch oxidation (O_2DA) compared to the OCl^- reference. Negative values indicate an increase in environmental impact rather than a reduction.

Figure 7 shows that the potential for impact reduction in all categories apart from ozone depletion, freshwater eutrophication, and climate change, decrease significantly with increasing energy use. In most of the categories in which the reduction of impact decreases with increased energy use, the threshold for exceeding the environmental impact of the reference case is between a five-fold and ten-fold increase in energy use. However, for the categories climate change and mineral and metal resource use, the threshold is higher than a factor 10.

From this data, we conclude that even at a five-fold increase of the estimated energy consumption, the heterogeneously catalysed oxidation of starch with oxygen with direct application (O_2DA) will still reduce the overall environmental impact compared to OCl^- oxidation. This shows that the technology change remains viable, from an environmental impact perspective, for energy requirements up to 17 kWh per m^3. Which provides an estimation for the required performance of heterogeneously catalysed oxygen oxidation reactions. At higher energy consumption levels (>17kWh per m^3) a tradeoff needs to be

made between the different impact categories, and the benefit of the O_2DA scenario compared to the OCl^- oxidation is debatable.

2.4 Conclusions

Hotspot analysis showed that the oxidation step in the production chain of anionic starch as a renewable alternative for polyacrylates is the main contributor to environmental impact in the categories freshwater eutrophication, ozone depletion potential, climate change, acidification, and resource use. In addition, unit operations to concentrate or dry products have high energy use and contribute as secondary hotspots in the remaining categories.

Homogeneously catalysed hydrogen peroxide oxidation and heterogeneously catalysed oxidation with molecular oxygen and direct, on-site product application both reduce the environmental impact of the process due to the elimination of OCl^- as an oxidising agent. The greatest reduction is found in the category freshwater eutrophication (~67%), and ozone depletion (~66%). In the categories climate change and resource use, both methods reduce the environmental impact, but homogeneously catalysed hydrogen peroxide oxidation achieved less reduction (35% and 41% respectively) than heterogeneously catalysed oxygen oxidation with direct, on-site product application (60% and 81% respectively).

Since the heterogeneously catalysed oxidation of starch requires the starch to be gelatinised before oxidation, this method is only viable if the starch can be applied directly after oxidation without intermediate drying. As a result of the omission of the drying step, heterogeneously catalysed starch oxidation with direct product application has the potential to further reduce impact in the categories marine and terrestrial eutrophication, photochemical ozone formation, particulate matter emission, human toxicity (cancer and non-cancer effects), freshwater ecotoxicity, and land use by approximately 80%.

As demonstrated, heterogeneously catalysed starch oxidation with molecular oxygen has the potential to substantially reduce the environmental impact of anionic potato starch production. Additionally a performance requirement for the energy use in this process has been estimated at a maximum of 17 kWh per m^3 for a 5% starch solution to maintain improvements over the current process from an environmental perspective. However, further research into the process and into developing a catalyst with sufficient activity, selectivity, and stability is required to eventually phase out the chlorine chemistry.

2.5 Acknowledgements

This work was supported by the Dutch Research Council (NWO) [grant number 870.15.120]. Special thanks to Ellen Slegers for her insights in LCA methodology.

2.6 References

Achremowicz, B., Gumul, D., Bala-Piasek, A., Tomasik, P., & Haberko, K. (2000). Air oxidation of potato starch over Cu(II) catalyst. *Carbohydrate Polymers, 42*(1), 45-50. doi:https://doi.org/10.1016/S0144-8617(99)00128-9

Baker, C. G. J., & McKenzie, K. A. (2005). Energy Consumption of Industrial Spray Dryers. *Drying Technology, 23*(1-2), 365-386. doi:10.1081/DRT-200047665

Bay-Smidt, A. M., Wischmann, B., Olsen, C., & Nielsen, T. H. (1994). *Starch bound phosphate in potato as studied by a simple method for determination of organic phosphate and 31P-NMR*.

Benavides, P. T., Cronauer, D. C., Adom, F., Wang, Z., & Dunn, J. B. (2017). The influence of catalysts on biofuel life cycle analysis (LCA). *Sustainable Materials and Technologies, 11*, 53-59. doi:https://doi.org/10.1016/j.susmat.2017.01.002

Celma, A. R., & Cuadros, F. (2009). Energy and exergy analyses of OMW solar drying process. *Renewable Energy, 34*(3), 660-666. doi:https://doi.org/10.1016/j.renene.2008.05.019

Chen, X., Yan, S., Wang, H., Hu, Z., Wang, X., & Huo, M. (2015). Aerobic oxidation of starch catalyzed by isopolyoxovanadate Na4Co(H2O)6V10O28. *Carbohydrate Polymers, 117*, 673-680. doi:https://doi.org/10.1016/j.carbpol.2014.10.066

Chipperfield, M. (2009). Nitrous oxide delays ozone recovery. *Nature Geoscience, 2*(11), 742-743. doi:10.1038/ngeo678

Ciroth, A. (2007). ICT for environment in life cycle applications openLCA — A new open source software for life cycle assessment. *The International Journal of Life Cycle Assessment, 12*(4), 209. doi:10.1065/lca2007.06.337

Collinson, S. R., & Thielemans, W. (2010). The catalytic oxidation of biomass to new materials focusing on starch, cellulose and lignin. *Coordination Chemistry Reviews, 254*(15), 1854-1870. doi:https://doi.org/10.1016/j.ccr.2010.04.007

Corona, A., Biddy, M. J., Vardon, D. R., Birkved, M., Hauschild, M. Z., & Beckham, G. T. (2018). Life cycle assessment of adipic acid production from lignin. *Green Chemistry, 20*(16), 3857-3866. doi:10.1039/C8GC00868J

de Nooy, A. E. J., Besemer, A. C., & van Bekkum, H. (1994). Highly selective tempo mediated oxidation of primary alcohol groups in polysaccharides. *Recueil des Travaux Chimiques des Pays-Bas, 113*(3), 165-166. doi:10.1002/recl.19941130307

Drewnowski, J., Remiszewska-Skwarek, A., Duda, S., & Łagód, G. (2019). Aeration Process in Bioreactors as the Main Energy Consumer in a Wastewater Treatment Plant. Review of Solutions and Methods of Process Optimization. *Processes, 7*(5). doi:10.3390/pr7050311

European Commission, J. R. C., Institute for Environment and Sustainability. (2012). Characterisation factors of the ILCDRecommended Life Cycle Impact Assessment methods.Database and Supporting Information. *Publications Office of the European Union, EUR 25167*.

Fiedorowicz, M., Tomasik, P., You, S., & Lim, S.-T. (1999). Molecular Distribution and Pasting Properties of UV-Irradiated Corn Starches. *Starch - Stärke, 51*(4), 126-131. doi:10.1002/(SICI)1521-379X(199904)51:4<126::AID-STAR126>3.0.CO;2-N

Forssell, P., Hamunen, A., Autio, K., Suortti, P., & Poutanen, K. (1995). Hypochlorite Oxidation of Barley and Potato Starch. *Starch - Stärke, 47*(10), 371-377. doi:10.1002/star.19950471002

García-Ochoa, F., Castro, E. G., & Santos, V. E. (2000). Oxygen transfer and uptake rates during xanthan gum production. *Enzyme and Microbial Technology, 27*(9), 680-690. doi:https://doi.org/10.1016/S0141-0229(00)00272-6

Gharsallaoui, A., Roudaut, G., Chambin, O., Voilley, A., & Saurel, R. (2007). Applications of spray-drying in microencapsulation of food ingredients: An overview. *Food Research International, 40*(9), 1107-1121. doi:https://doi.org/10.1016/j.foodres.2007.07.004

Grommers, H. E., & van der Krogt, D. A. (2009). Chapter 11 - Potato Starch: Production, Modifications and Uses. In J. BeMiller & R. Whistler (Eds.), *Starch (Third Edition)* (pp. 511-539). San Diego: Academic Press.

Heyns, K., & Paulsen, H. (1963). Selective Catalytic Oxidation of Carbohydrates, Employing Platinum Catalysts. In M. L. Wolfrom & R. S. Tipson (Eds.), *Advances in Carbohydrate Chemistry* (Vol. 17, pp. 169-221): Academic Press.

Holman, P. A., Shonnard, D. R., & Holles, J. H. (2009). Using Life Cycle Assessment to Guide Catalysis Research. *Industrial & Engineering Chemistry Research, 48*(14), 6668-6674. doi:10.1021/ie801934s

Jane, J., Chen, Y. Y., Lee, L. F., McPherson, A. E., Wong, K. S., Radosavljevic, M., & Kasemsuwan, T. (1999). Effects of Amylopectin Branch Chain Length and Amylose Content on the Gelatinization and Pasting Properties of Starch. *Cereal Chemistry, 76*(5), 629-637. doi:10.1094/CCHEM.1999.76.5.629

Kang, Y., Cho, Y. J., Woo, K. J., & Kim, S. D. (1999). Diagnosis of bubble distribution and mass transfer in pressurized bubble columns with viscous liquid medium. *Chemical Engineering Science, 54*(21), 4887-4893. doi:https://doi.org/10.1016/S0009-2509(99)00209-2

Ketola, H. H., FI), Hagberg, Peggy (Maidstone, GB). (2003). United States Patent No.

Kováts, P., Thévenin, D., & Zähringer, K. (2020). Influence of viscosity and surface tension on bubble dynamics and mass transfer in a model bubble column. *International Journal of Multiphase Flow, 123*, 103174. doi:https://doi.org/10.1016/j.ijmultiphaseflow.2019.103174

Kudra, T. (2004). Energy Aspects in Drying. *Drying Technology, 22*(5), 917-932. doi:10.1081/DRT-120038572

Labík, L., Petričříček, R., Moucha, T., Brucato, A., Caputo, G., Grisafi, F., & Scargiali, F. (2018). Scale-up and viscosity effects on gas–liquid mass transfer rates in unbaffled stirred tanks. *Chemical Engineering Research and Design, 132*, 584-592. doi:https://doi.org/10.1016/j.cherd.2018.01.051

Laurent, A., & Hauschild, M. Z. (2015). Normalisation. In M. Z. Hauschild & M. A. J. Huijbregts (Eds.), *Life Cycle Impact Assessment* (pp. 271-300). Dordrecht: Springer Netherlands.

Masina, N., Choonara, Y. E., Kumar, P., du Toit, L. C., Govender, M., Indermun, S., & Pillay, V. (2017). A review of the chemical modification techniques of starch. *Carbohydrate Polymers, 157*, 1226-1236. doi:https://doi.org/10.1016/j.carbpol.2016.09.094

Maurer, H. W. (2009). Chapter 18 - Starch in the Paper Industry. In J. BeMiller & R. Whistler (Eds.), *Starch (Third Edition)* (pp. 657-713). San Diego: Academic Press.

Mellouki, A., Talukdar, R. K., Schmoltner, A.-M., Gierczak, T., Mills, M. J., Solomon, S., & Ravishankara, A. R. (1992). Atmospheric lifetimes and ozone depletion potentials of methyl bromide (CH3Br) and dibromomethane (CH2Br2). *Geophysical Research Letters, 19*(20), 2059-2062. doi:10.1029/92GL01612

Niazi, M. B. K., & Broekhuis, A. A. (2012). Production of amorphous starch powders by solution spray drying. *Journal of Applied Polymer Science, 126*(S1), E143-E153. doi:10.1002/app.36551

Norris, G. A. (2001). The requirement for congruence in normalization. *The International Journal of Life Cycle Assessment, 6*(2), 85. doi:10.1007/BF02977843

Parovuori, P., Hamunen, A., Forssell, P., Autio, K., & Poutanen, K. (1995). Oxidation of Potato Starch by Hydrogen Peroxide. *Starch - Stärke, 47*(1), 19-23. doi:10.1002/star.19950470106

Pizzol, M., Laurent, A., Sala, S., Weidema, B., Verones, F., & Koffler, C. (2017). Normalisation and weighting in life cycle assessment: quo vadis? *The International Journal of Life Cycle Assessment, 22*(6), 853-866. doi:10.1007/s11367-016-1199-1

Recchioni, M., Mathieux, F., Goralczyk, M., & Schau, E. M. (2013). ILCD Data Network and ELCD Database: current use and further needs for supporting Environmental Footprint and Life Cycle Indicator Projects. *Publications Office of the European Union, EUR 25744*.

Rutenberg, M. W., & Solarek, D. (1984). CHAPTER X - STARCH DERIVATIVES: PRODUCTION AND USES. In R. L. Whistler, J. N. Bemiller, & E. F. Paschall (Eds.), *Starch: Chemistry and Technology (Second Edition)* (pp. 311-388). San Diego: Academic Press.

Salemis, P., & Rinaudo, M. (1984). Molecular weight-viscosity relationship for amylopectin, a highly branched polymer. *Polymer Bulletin, 12*(4), 283-285. doi:10.1007/BF00263139

Sandberg, M. (2010). Energy efficient aeration of wastewaters from the pulp and paper industry. *Water Science and Technology, 62*(10), 2364-2371. doi:10.2166/wst.2010.946

Sangseethong, K., Termvejsayanon, N., & Sriroth, K. (2010). Characterization of physicochemical properties of hypochlorite- and peroxide-oxidized cassava starches. *Carbohydrate Polymers, 82*(2), 446-453. doi:https://doi.org/10.1016/j.carbpol.2010.05.003

Tolvanen, P., Mäki-Arvela, P., Sorokin, A. B., Salmi, T., & Murzin, D. Y. (2009). Kinetics of starch oxidation using hydrogen peroxide as an environmentally friendly oxidant and an iron complex as a catalyst. *Chemical Engineering Journal, 154*(1), 52-59. doi:https://doi.org/10.1016/j.cej.2009.02.001

Vanier, N. L., El Halal, S. L. M., Dias, A. R. G., & da Rosa Zavareze, E. (2017). Molecular structure, functionality and applications of oxidized starches: A review. *Food Chemistry, 221*, 1546-1559. doi:https://doi.org/10.1016/j.foodchem.2016.10.138

Verraest, D. L., Peters, J. A., & van Bekkum, H. (1998). The platinum-catalyzed oxidation of inulin. *Carbohydrate Research, 306*(1), 197-203. doi:https://doi.org/10.1016/S0008-6215(97)10055-6

Wang, H., Poya, Y., Chen, X., Jia, T., Wang, X., & Shi, J. (2015). Hydrogen peroxide as an oxidant in starch oxidation using molybdovanadophosphate for producing a high carboxylic content. *RSC Advances, 5*(57), 45725-45730. doi:10.1039/C5RA07747H

Wei, B., Qi, H., Wang, Z., Bi, Y., Zou, J., Xu, B., . . . Ma, H. (2020). The ex-situ and in-situ ultrasonic assisted oxidation of corn starch: A comparative study. *Ultrasonics Sonochemistry, 61*, 104854. doi:https://doi.org/10.1016/j.ultsonch.2019.104854

Whistler, R. L., & Schweiger, R. (1957). Oxidation of Amylopectin with Hypochlorite at Different Hydrogen Ion Concentrations1,2. *Journal of the American Chemical Society, 79*(24), 6460-6464. doi:10.1021/ja01581a027

Zhou, D.-N., Zhang, B., Chen, B., & Chen, H.-Q. (2017). Effects of oligosaccharides on pasting, thermal and rheological properties of sweet potato starch. *Food Chemistry, 230*, 516-523. doi:https://doi.org/10.1016/j.foodchem.2017.03.088

2.7 Appendices

Appendix A: the LCI

Table 3 Life cycle inventory

Category	Unit	Heat from gas (MJ)	Water (kg)	Sodium hydrogen sulphite (Kg)	Sodium hypochlorite (Kg)	Sodium hydroxide (Kg)	Electricity (kwh)	Hydrogen peroxide (Kg)
Acidification	mol H+eq	3.7E-04	1.6E-06	6.4E-05	1.4E-04	8.5E-03	2.8E-03	1.3E-05
Climate change	Kg CO2 eq	7.0E-02	5.8E-04	1.2E+00	1.8E+00	1.4E+00	2.4E-01	1.1E+00
Ecotoxicity freshwater	CTUe	9.1E-03	7.0E-05	9.2E-06	1.9E-05	8.9E-06	7.6E-06	4.4E-06
eutrophication freshwater	kg P eq	4.3E-08	4.5E-10	1.8E-04	2.9E-04	1.0E-04	4.0E-05	9.7E-05
Human tox - cancer	CTUh	7.5E-10	3.1E-12	7.6E-11	2.0E-11	7.7E-12	2.9E-12	8.9E-12
Human tox. Non-cancer	CTUh	1.6E-09	3.6E-12	7.3E-11	9.9E-11	3.5E-11	4.3E-13	3.2E-11
Land use	kg C deficit	1.2E-02	0.0E+00	5.1E-05	3.5E-05	0.0E+00	5.1E-05	9.9E-06
Marine eutrophication	kg N eq	8.1E-05	5.9E-07	3.4E-05	7.5E-05	3.4E-05	5.8E-05	7.1E-06
Resource use (mineral and metals)	kg Sb eq	3.4E-06	1.7E-09	1.9E-05	3.1E-05	1.1E-05	1.1E-06	1.0E-05
Ozone depletion	kg CFC11 eq	8.4E-09	7.2E-12	2.7E-07	1.3E-06	6.6E-07	1.4E-12	2.4E-08
Particulate matter emission	kg PM2,5 eq	1.2E-05	5.0E-08	6.4E-07	1.4E-06	6.4E-07	1.1E-06	1.4E-07
Photochemical ozone formation	kg NMVOC eq	2.5E-04	1.2E-06	5.7E-05	1.3E-04	5.7E-05	9.8E-05	1.2E-05
Terrestrial eutrophication	mol N eq	8.7E-04	4.8E-06	3.7E-04	8.2E-04	3.7E-04	6.4E-04	7.8E-05
Water depletion	m^3	3.7E-04	1.6E-04	0.0E+00	0.0E+00	1.6E-03	0.0E+00	0.0E+00

Appendix B: overview of calculated impact indicators

Table 4 overview of calculated impact indicators, darker shades indicate higher values

Impact categories	Acidification	Climate change	Ecotoxicity	Eutroph. freshw.	Human tox - cancer	Human tox. Non-cancer	Land use	Eutroph. marine	Resource use minerals	Ozone depletion	Particulate matter	Photochem. ozone for.	Eutroph. terr.
units	mol H+eq	Kg CO2 eq	CTUe	kg P eq	CTUh	CTUh	kg C deficit	kg N eq	kg Sb eq	kg CFC11 eq	kg PM2,5 eq	kg NMVOC ec	mol N eq
Washing	0,9	0,7	1,7	0,0	1,6	1,5	1,5	1,6	1,1	0,2	1,6	1,6	1,5
Grinding	1,0	1,0	1,6	0,7	1,6	1,6	1,6	1,6	1,4	0,4	1,6	1,6	1,6
Juice Extraction	0,4	0,3	0,7	0,0	0,7	0,7	0,8	0,7	0,5	0,1	0,7	0,7	0,7
Fibre Sieving	0,4	0,3	0,7	0,0	0,7	0,7	0,7	0,7	0,5	0,1	0,7	0,7	0,7
Classification	0,4	0,2	0,6	0,0	0,6	0,6	0,6	0,6	0,4	0,1	0,6	0,6	0,6
Sideline sieving	0,1	0,0	0,1	0,0	0,1	0,1	0,1	0,1	0,1	0,0	0,1	0,1	0,1
Hydrocyclones	0,1	0,0	0,1	0,0	0,1	0,1	0,1	0,1	0,1	0,0	0,1	0,1	0,1
Drumfilter	0,3	0,2	0,5	0,0	0,4	0,4	0,3	0,5	0,2	0,0	0,4	0,4	0,4
Pneumatic Dryer	13,4	9,4	22,5	0,1	22,7	22,8	23,0	21,7	16,5	2,7	22,6	22,2	21,8
Starch Cyclones	0,0	0,0	0,0	0,0	0,0	0,0	0,0	0,0	0,0	0,0	0,0	0,0	0,0
Fibre Dewatering	9,5	6,7	16,0	0,1	16,1	16,2	16,3	15,4	11,7	1,9	16,0	15,7	15,4
Hyper Filtration	0,1	0,1	0,2	0,0	0,2	0,2	0,2	0,2	0,2	0,0	0,2	0,2	0,2
Preheating	4,3	3,0	7,3	0,0	7,3	7,3	7,4	7,0	5,3	0,9	7,3	7,1	7,0
Steam Injection	5,3	3,7	8,9	0,0	8,9	9,0	9,1	8,5	6,5	1,1	8,9	8,7	8,6
Protein Decanting	0,2	0,1	0,3	0,0	0,3	0,3	0,3	0,3	0,2	0,0	0,3	0,3	0,3
Pneumatic Protein Dryer	0,1	0,1	0,1	0,0	0,1	0,1	0,1	0,1	0,1	0,0	0,1	0,1	0,1
Protein Cyclones	0,0	0,0	0,0	0,0	0,0	0,0	0,0	0,0	0,0	0,0	0,0	0,0	0,0
Protamylasse concentration	10,0	7,3	17,3	0,1	16,9	16,7	16,6	16,5	11,9	2,0	16,9	16,6	16,4
Starch Oxidation	41,4	57,8	0,3	98,9	0,3	0,4	0,1	4,3	28,1	87,9	0,7	2,5	4,3
Anionic Hydrocyclones	0,0	0,0	0,1	0,0	0,1	0,1	0,1	0,1	0,0	0,0	0,1	0,1	0,1
Anionic Sieve	0,3	0,2	0,4	0,0	0,4	0,4	0,4	0,4	0,3	0,1	0,4	0,4	0,4
Anionic Drumfilter	0,4	0,4	0,9	0,0	0,7	0,7	0,6	0,9	0,4	0,1	0,7	0,8	0,8
Anionic Pneumatic Dryer	11,7	8,2	19,7	0,1	19,9	19,9	20,1	18,9	14,4	2,4	19,8	19,4	19,0
Anionic Starch Cyclones	0,0	0,0	0,0	0,0	0,0	0,0	0,0	0,0	0,0	0,0	0,0	0,0	0,0

3.

3. The effect of polydispersity on the conversion kinetics of starch oxidation and depolymerisation

This chapter is published as: Hoogstad, T. M., Konings, G., Buwalda, P. L., Boxtel, A. J. B., Kiewidt, L., & Bitter, J. H. (2019). The effect of polydispersity on the conversion kinetics of starch oxidation and depolymerisation. Chemical Engineering Science: X, 4, 100044.

Abstract

Biobased feedstocks offer a potent source of building blocks for biobased products. However, these feedstocks (e.g. starch, cellulose) are generally highly polydisperse in molecular weight. To study the effect of polydispersity on conversion kinetics, the influence of molecular size on the oxidation and depolymerisation rates of starch was investigated. Kinetic experiments for the homogeneous TEMPO/hypochlorite catalysed oxidation of amylopectins with different molecular sizes showed that large starch molecules oxidise and depolymerise at a higher rate than small molecules. In addition, increasing degrees of oxidation inhibit the rate of further oxidation exponentially. These results demonstrate that polydispersity is an important factor in the conversion of these feedstocks. A model was formulated that assigns individual kinetic parameters to starch fractions of different molecular weight and degree of oxidation. The model predicts 2-D product distributions over molecular weight and degree of oxidation, and predicts asymmetrical distribution shifts as a result of substrate polydispersity.

Keywords: Starch, polydispersity, oxidation, depolymerisation, kinetics, product distribution

3.1 Introduction

Macromolecules from biobased feedstocks i.e., polymers such as starch, cellulose and lignin are excellent building blocks for biobased materials, chemicals and fuels. These biomacromolecules can be used in three ways i.e. 1) by converting them to monomers after which these building blocks can be used to produce the desired material (Aeschelmann & Carus, 2015; Laurichesse & Avérous, 2014) 2) by using them in their native or partially depolymerised form e.g. use of starch or maltodextrins as a food additive (Chronakis, 1998) or 3) by using them in their polymeric form after adding new properties by introducing or modifying functional groups (Laurichesse & Avérous, 2014; Masina et al., 2017).

In general, chemical or biological modifications to modify macromolecules with the desired functionalities are accompanied by undesired side reactions such as the depolymerisation of the native macromolecular structure, which reduces product functionality, value and yield (Forssell, Hamunen, Autio, Suortti, & Poutanen, 1995; Parovuori, Hamunen, Forssell, Autio, & Poutanen, 1995). In addition, the size of the initial macromolecules and those that are produced during depolymerisation affect the kinetics of further conversion of the formed molecules (Floor, Schenk, Kieboom, & van Bekkum, 1989). One case where this is relevant is the oxidation of starch (Floor et al., 1989). Oxidised starches, i.e. starches where part of the OH groups are converted to C=O (carbonyl) or COOH (carboxyl) groups, are applied in, among others, the paper, textile and food industry (Chiu & Solarek, 2009; Masina et al., 2017; Vanier, El Halal, Dias, & da Rosa Zavareze, 2017). Oxidised starches can be produced by various methods, e.g., hypochlorite oxidation, hydrogen peroxide oxidation and ozone oxidation (Masina et al., 2017; Vanier et al., 2017). Depending on the oxidation method, the (physio)chemical properties e.g. gelatinisation, retrogradation, and pasting properties of the product vary (Sangseethong, Termvejsayanon, & Sriroth, 2010; Zhou, Zhang, Chen, & Chen, 2017). Hypochlorite oxidation results in a high carboxyl content compared to carbonyl content (0.6% vs 0.05%). In contrast, hydrogen peroxide oxidation results in mainly carbonyl moieties compared to carboxyl moieties (0.65% vs 0.1%) (Sangseethong et al., 2010). Currently, oxidation with hypochlorite is the most common process on industrial scale (Masina et al., 2017; Vanier et al., 2017).

During either hydrogen peroxide and hypochlorite oxidation, depolymerisation takes place as a side reaction (Parovuori et al., 1995; Vanier et al., 2017) thereby changing the molecular weight distribution of the starch over time. The initial molecular weight distribution of native starch is broad, with a polydispersity index of >100 (Bertoft, 2017; Stacy & Foster, 1957) and polydispersity increases further during depolymerisation. The exact mechanism of depolymerisation, that is, at which location the molecule breaks,

plays a fundamental role in how the molecular weight distributions change during the oxidation reaction. Macromolecules which are cut at its edges retains most of its functionality while the smaller broken parts contribute less to the functional properties. In earlier works Veelaert, de Wit, and Tournois (1994), described the kinetics of periodate oxidation of starch and Tolvanen, Mäki-Arvela, Sorokin, Salmi, and Murzin (2009), described the kinetics of the iron complex catalysed hydrogen peroxide oxidation of starch. More recent works of Kumoro, Ratnawati, and Retnowati (2015), and Salmi et al. (2016), described models for the oxidation of granular starch with hydrogenperoxide. However, these works did not consider the influence of the polydispersity of the substrate nor the correlation between molecular weight, time-dependent molecular weight distributions due to depolymerisation, and oxidation rate.

Nevertheless, Verraest, Peters, and van Bekkum (1998) showed that the degree of polymerisation and the oxidation rate are related in inulin oxidation over Pt/C. The rate and degree of oxidation decreased with increasing molecular weight. Moreover, Floor et al. (1989) showed that the oxidation rate of starch and maltodextrins increased with increasing chain length for tungstate-hydrogen peroxide oxidation. We hypothesise that for the hypochlorite oxidation of solubilised starch, the rate of oxidation also depends on the degree of polymerisation of the starch and that, as a result of these varying rates, not all fractions of the starch achieve the same degree of oxidation. To study this, we looked at the rates of oxidation and depolymerisation for the homogeneously catalysed TEMPO/hypochlorite oxidation of branched starches (amylopectins) of different molecular weight (Figure 1). Homogeneous catalysis was chosen as it excludes mass transfer limitations, is selective towards C6 oxidation (Bragd, Besemer, & van Bekkum, 2002; de Nooy, Besemer, & van Bekkum, 1994), and well documented (Bragd, van Bekkum, & Besemer, 2004). A kinetic model that describes combined oxidation and depolymerisation will be developed to predict the distribution of molecular weight and degree of oxidation of the product. The model thereby provides insight in the influence of feedstock polydispersity on conversion kinetics and product distributions.

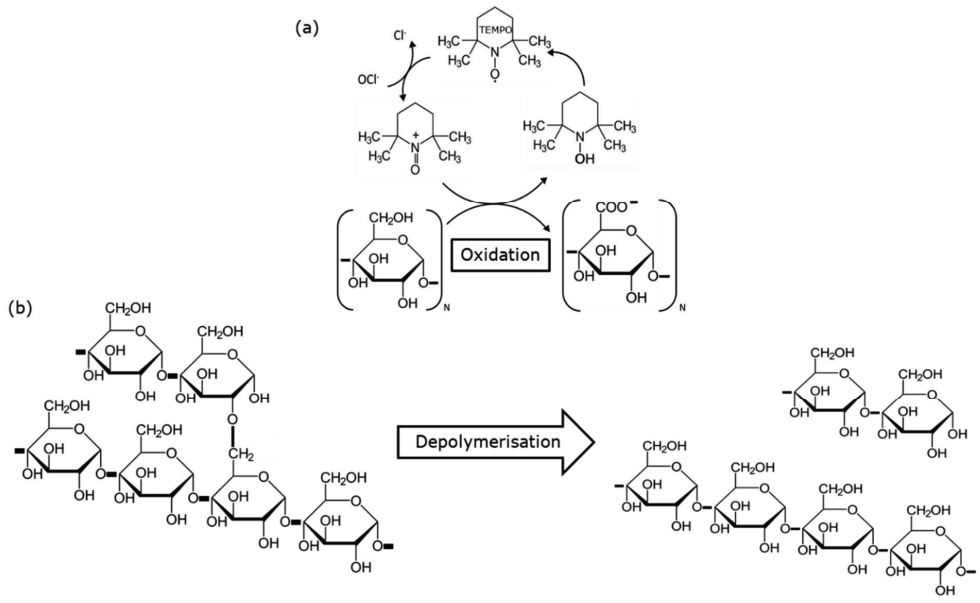

Figure 1 (a) Schematic depiction of the oxidation of starch with OCl^- and TEMPO as proposed in bragd et al. (2000) and (b) simplified starch structure with branching point and depolymerisation product.

3.2 Materials and methods

3.2.1 Experimental

Materials:

Four different commercially available amylopectins (Avebe, The Netherlands) were used to explore the effect of molecular weight and degree of oxidation on the reaction kinetics of oxidation and depolymerisation:

- Eliane™ (DP ~ 250.000 – 500.000), a native waxy potato starch containing >99% amylopectin.
- Eliane™ C200 (DP ~250.000), a cold water-soluble waxy starch made by roller drying.
- Eliane™ MD2 (DP 50) and Eliane™ MD6 (DP 16), maltodextrins made by enzymatic conversion of native waxy potato starch.

These starches contain >99% amylopectin and differ only in their degree of polymerization. Waxy starches, rather than a mixture of amylose and amylopectin, were chosen as amylopectin represents 80 wt% of native potato starch, and to exclude differences in reactivity between amylose and amylopectin from influencing the results. Prior to the oxidation experiment the starches were solubilised to eliminate diffusion limitations within the native starch granules (Huber & BeMiller, 2001; van Warners, Lammers, Stamhuis, & Beenackers, 1990) , and to remove the influence of granule heterogeneity (Fannon, Gray, Gunawan, Huber, & BeMiller, 2004). For Eliane C200, Eliane MD2 and Eliane MD6 Starch solutions of 0.2 wt% were prepared by dissolving the amylopectins in demineralised water at room temperature and stirring for 30 minutes at 700 rpm. An 0.2 wt% solution of Eliane 100 was made by dissolving the starch in an autoclave (Tuttnauer, 2840EL) for 15 minutes at 121 °C, as it is not cold-water soluble.

Experiments:

Oxidation of the starches was performed batch-wise using a 12.5% sodium-hypochlorite solution as oxidant and TEMPO as catalyst. A high concentration NaOCl solution (12.5%) was used to minimise sample dilution during the oxidation experiments. TEMPO was added according to a 4 mg TEMPO to 4g starch ratio (Bragd, Besemer, & van Bekkum, 2000) resulting in a 2 mg L^{-1} final concentration. All experiments were done at 20 °C. During the reaction, the pH was kept constant at 8.5 by titration using a pH-stat (877 titrino plus, Metrohm, Switzerland) and stirred continuously with a magnetic stirrer at 700 rpm. The reaction setup is shown in Figure 2. The amount of added NaOH is a measure for the extend of oxidation (targeted range 0-20%). Therefore, the amount of NaOH added over time during the reaction was taken as a direct measure for the amount of carboxylic acid moieties.

Three sets of experiments were performed:

- To investigate the effect of degree of polymerisation of the starch on the rate of depolymerisation, a large (high M_w) starch (Eliane 100) and a small (low M_w) starch (Eliane MD6) were oxidised stepwise. For each step, a fixed amount of hypochlorite was added to increase the degree of oxidation by 5%. At the different degrees of oxidation, a sample was taken. The molecular weight distributions of these samples and substrates were analysed using HPSEC with RI detection. The complete HPSEC column consisted out of three TosoHaas (Tokyo, Japan) TSK-Gel columns (4000PWXL-3000PWXL-2500PWXL), 6 x 150 mm, with a guard column and was operated at a flow rate of 0.55 ml/min and a temperature of 55°C. 0.2M $NaNO_3$ prepared with MilliQ water and filtered through a 0.45µm millipore filter was used as eluent.
- To investigate the effect of the degree of polymerisation on the rate of oxidation, a large starch (high M_w) (Eliane 100) and a small starch (low M_w) (Eliane MD6) were oxidised using a single dose of sodium hypochlorite to get it to 20% DO. The initial oxidation rates of the two starches were then compared.
- To investigate the effect of degree of oxidation on the rate of oxidation, three starches (C200, MD2 and MD6) were oxidised by adding NaOCl in sequential aliquots to reach 5%, 10%, and 15% degree of oxidation respectively. After each addition, the reaction was continued until the reaction for that step was completed, which is indicated by a stabilised titration curve. The initial rates of each oxidation step for each of the starches were compared.

Figure 2 The reactor setup used for the oxidation experiments. 1) pH-stat, 2) reaction vessel, 3) titrator, 4) pH sensor, 5) stirrer.

3.2.2 Reaction kinetics & modelling

During the reactions of oxidation and depolymerisation, starch molecules break down, which results in a shift of the mean of the size distribution to lower values and increases the variation in molecular size. The initial distribution and the shift in distribution are modelled by discretising the molecular size in classes. Simultaneously to depolymerisation, the starch oxidises, which results in an increasing degree of oxidation. The rate of oxidation is a function of the molecular size and the degree of oxidation and therefore, molecules with different molecular sizes achieve a distinct level of oxidation. To include this effect in the model, the degree of oxidation is also discretized. In the kinetic model the concentrations of starch are expressed in mole anhydroglucose L^{-1} to normalise concentrations to the number of glucose monomers rather than the number of starch molecules. Different states of starch are expressed by $[starch]_{i,j}$ where i refers to the class for the degree of polymerisation, and j to the class of degree of oxidation. Figure 3 schematically expresses the discretisation in polymerisation and degree of oxidation. The crossings in the grid represent the classes of both states. The average reaction vector is the result of many small horizontal and vertical steps over a fine grid (357x20).

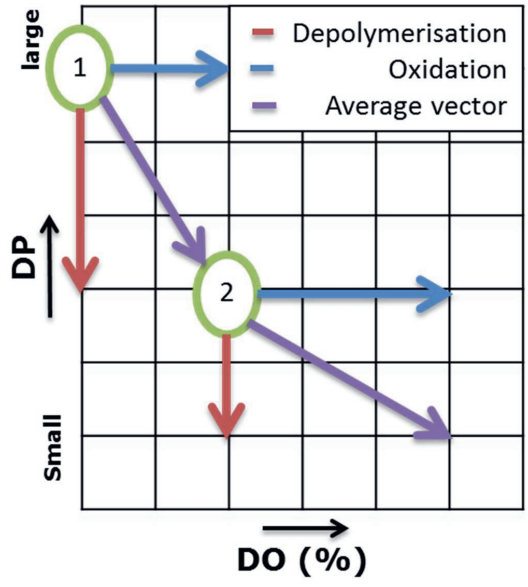

Figure 3 Schematic view on the simultaneous starch oxidation and depolymerisation. Starch classes (green) are affected by two reactions. Degree of oxidation is increased by oxidation (blue) and degree of polymerization is decreased by depolymerisation

Oxidation

The oxidation of hydroxylic starch groups with OCl^- into the carboxylic group takes two steps. Step 1 is oxidation into the aldehyde form, which oxidises in step 2 to the carboxylic form. Although step 1 is the rate limiting step (de Nooy et al., 1994), the response of the system can act as a second order system (Guan et al., 2019). The second order behaviour of the system plays a role when adding aliquots of NaOCl as we did in this research. At the first aliquot, building up the pool of aldehyde groups (ald) plays a role in the response, while for the subsequent aliquots the pool is available. Therefore, the concentration of intermediate aldehyde, [ald], is included in the balances. The mass balances for the oxidation are given by:

$$\frac{d[hyd]}{dt} = -k_{ox}\ [hyd][OCl] \tag{1}$$

$$\frac{d[ald]}{dt} = +k_{ox}\ [hyd] - k_{ox}\ \ [ald][OCl] \tag{2}$$

$$\frac{d[carb]}{dt} = k_{ox2}[ald][OCl] \tag{3}$$

$$\frac{d[OCl]}{dt} = -k_{ox}\ [hyd] - k_{ox}\ \ [ald][OCl] \tag{4}$$

Where hyd, ald and $carb$ refer to hydroxyl, aldehyde and carboxyl (moieties at the C6 carbon), and OCl is the hypochlorite. For the model, selective C6 oxidation is assumed as TEMPO/OCl^- catalysed starch oxidation has a high reported selectivity (Bragd et al., 2000).

With these balances, kinetic parameters for each oxidation class in the grid (Figure 3) can be determined. As the dependency on degree of oxidation is inherent to the location of the grid (j) and the kinetic parameters have been adjusted for the concentration of intermediate, it suffices to use a lumped kinetic parameter for application in the grid. Therefore, for the simulations for starch oxidation the following expression is used:

$$\frac{d[starch]_{i,j}}{dt} = -k_{ox\,i,j}[starch]_{i,j}[OCl]\ +\ k_{ox\,i,j-1}[starch]_{i,j-1}\,[OCl] \tag{5}$$

Where $[starch]_{i,j}$ is the concentration of starch with molecular weight i and degree of oxidation j (mol anhydroglucose L^{-1}). $k_{ox\,i,j}$ is the kinetic parameter for oxidation assigned to the starch fraction of molecular weight i and degree of oxidation j (s^{-1}). The starch concentration with a degree of oxidation j, decreases by oxidation ($-k_{ox\,i,j}[starch]_{i,j}[OCl]$), while it is supplemented by molecules from a lower class ($+\,k_{ox\,i,j-1}[starch]_{i,j-1}\,[OCl]$).

Depolymerisation

The kinetics for depolymerisation is given as:

$$\frac{d[starch]_{i,j}}{dt} = -\,k_{dep\,i,j}[starch]_{i,j} + v_{i,j} \tag{6}$$

Where $[starch]_{i,j}$ represents the concentration of starch in a given molecular weight class i and degree of oxidation class j (mol anhydroglucose monomers per litre). $k_{ox\,i,j}$and $k_{dep\,i,j}$ are the rate constants for oxidation and depolymerisation respectively (s^{-1}), $k_{ox}[starch]_{j-1,i}$ the shift of starch molecules a previous class of degree of oxidation, $v_{i,j}$ represents the production rate of all depolymerised molecules that arrive from higher classes in the current class (i,j).

For the depolymerisation rate constant ($k_{dep\,i,j}$) the following expression was used:

$$k_{dep} = a\,Mw_{class} + b \tag{7}$$

Equation 7 expresses the rate of depolymerisation as a function of molecular weight. If the rate of depolymerisation is independent of molecular size, then $a = 0$.

During depolymerisation starch molecules are cut into two parts. The resulting molecular weight of the fractions is represented by parameter p, ranging between 0 (one low M_w and one high M_w fraction) and 0.5 (equal M_w fractions). The classes in which both parts end are indexed by $i_{dest.}$ and $i'_{dest.}$, the production rate of molecules for each class are given by:

$$i_{dest.} = i\,p\ , \qquad i'_{dest.} = i(1-p)$$

$$v_{i,j} = \sum_{i}^{i_{max}} m\,k_{dep}[starch]_{i,j} \tag{8}$$

$$with\ m = 1 \quad if \quad i_{dest.} = i \quad or \quad i'_{dest.} = i \qquad else\ m = 0$$

Four options for the cutting site parameter p were considered:

1. A fixed value, which represents a preference for a specific cutting site caused by possible limited penetration of catalyst and NaOCl into a solubilised starch molecule:

$$\begin{aligned} p &= d \\ s.t. 0 &< d < 0.5 \end{aligned} \tag{9}$$

2. A linear function of molecular weight describes a scenario where the preference of the cutting site depends on the molecular weight. This option is an extension of model 1, as molecules become smaller, the penetration depth of catalyst and NaOCl changes relative to the molecule, causing p to increase:

$$\begin{aligned} p &= c\, Mw_{class} + d \\ s.t. 0 &< p < 0.5 \\ c &\leq 0 \end{aligned} \tag{10}$$

A random distribution describes a scenario where there is no preference for a specific cutting site:

$$\begin{aligned} p &= uniform\ random\ distributed \\ s.t. 0 &< p < 0.5 \end{aligned} \tag{11}$$

3. A normal distribution as an extension of option 1, with a preference around a specific cutting site, expressed by a normal distribution with mean μ and standard deviation σ:

$$\begin{aligned} p &= normal\ random\ distributed\ (\mu, \sigma) \\ s.t. 0 &< p < 0.5 \end{aligned} \tag{12}$$

The applied grid for the simulations was 357 for the degree of polymerisation (to cover the full range of molecular sizes) and 20 for degree of oxidation which gave a resolution suitable for the experimental data. The simulations and curve fitting were performed with Matlab. Numerical integration was performed using a Runge-kutta 4th order algorithm, and for curve fitting, a multi-start interior point optimisation algorithm was used. Simulations with probabilistic elements were performed using the average of

Monte Carlo runs for each iteration in the optimisation algorithm. The goodness of the fit between models was compared using the sum of squared errors (SSE) over an identical range of Mw_{class} for each model.

3.3 Results and discussion

3.3.1 Basic data from laboratory experiments

The effect of degree of polymerisation on the rate of depolymerisation

Figure 4 presents HPSEC diagrams for Eliane MD6 and Eliane 100. At the right side the full chromatograms are given at different degrees of oxidation. The elution volumes reflect the molecular size distribution, where large molecules appear at lower elution volume and small molecules at higher elution volumes. For Eliane MD6 the distributions at DO= 0, 5, 10, 40% are given. The samples for native Eliane 100 could not pass the column at DO=0% as the starch was not yet sufficiently depolymerised. Therefore, the distribution at DO= 5,10, 40% are given. With increasing DO, the signals in the chromatogram shift to higher elution volumes. This indicates that the molecular weight decreases with increasing DO. By comparing the lines from the 1st and 2nd aliquots (5-10%) it is observed that the molecular size shift for Eliane MD6 is smaller than that of Eliane 100. The large polymer Eliane 100 thus depolymerised faster than the smaller Eliane 6. It has been shown by Zhang and Huber (2018) that at high degrees of oxidation (>30 -40%) and depending on oxidation method, a variety of small oxidised by-products like oxalic acid is formed. Therefore, the focus of this study lies on (low) degrees of oxidation of up to 20% and a C6 selective oxidation method to avoid breakdown of starches into these small by-products.

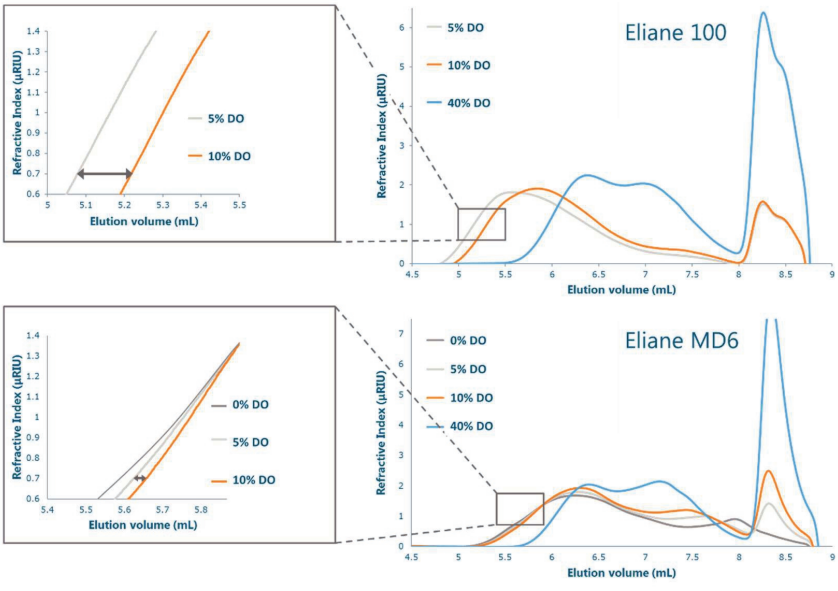

Figure 4 HPSEC diagrams of Eliane 100 and Eliane MD6. Right: the full diagrams. Left: detailed diagram to compare the depolymerisation from 5% to 10% degree of oxidation (DO).

Depolymerisation rates were estimated by fitting the kinetic and depolymerisation models to the HPSEC data (Liu, Castro, & Gilbert, 2011). The HPSEC column itself has a limited resolution for molecular weights. Large molecules can be too big to elute, while the very small molecules (DP<~5) elute all together and cannot be distinguished from each other (Gidley et al., 2010). Therefore, data with elution volume larger than 7.5 ml is ignored for the fit. Figure 5 illustrates a representative fit for the change in molecular weight distribution due to depolymerisation.

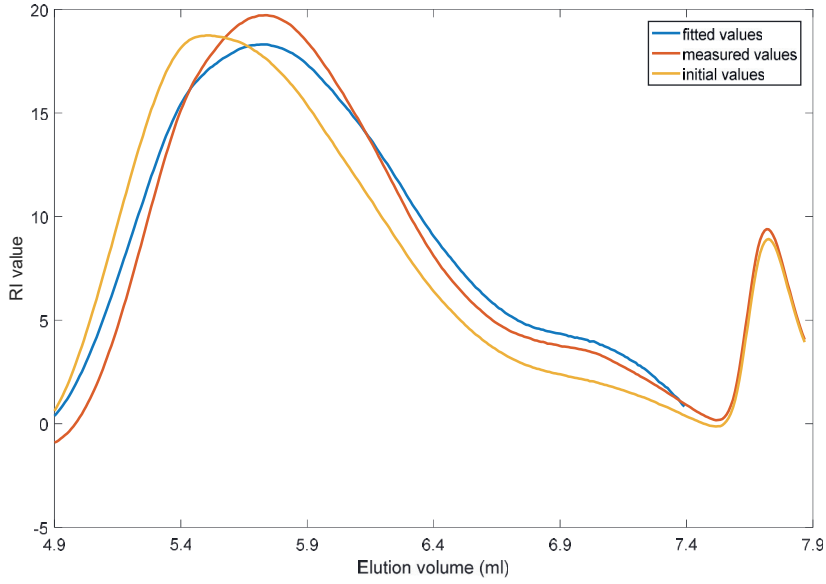

Figure 5 typical fit for the depolymerisation model. Initial values for the fit (Eliane 100, 5% DO), final values for the fit (Eliane 100, 10% DO) and fitted HPSEC chromatogram.

The results of kinetic model fitting showed that the parameters in the expression for k_{dep} (equation 7) are $a = -3.9 \cdot 10^{-7}\ mol\ g^{-1}\ s^{-1}$ and $b = 5.8 \cdot 10^{-5}\ s^{-1}$.

The standard error of estimates for the models with a stochastic value for the cutting parameter p were worse than the expressions for the cutting parameter given by equation 9 and 10 (see Table 1). The best fit for the expressions for the cutting parameter p was obtained with equation 9, where p is expressed as a fixed value. These results imply that the polymer is on average cut so that the resulting fractions weigh 12% and 88% of the original mass. This division of mass fractions could be the result of random cutting of a branched molecule, where molecules with different degrees of branching could have different values for p, as the average distance of a glucose

monomer to the end of a chain is lower in highly branched molecules than low branched molecules.

Table 1 Different expressions for p and best achieved SSE

Cutting parameter expression	**Minimum SSE achieved (μRIU^2)**	p **(-)**
1	356	0.126
2	420	$-4.5 \cdot 10^{-9}$ mol g^{-1} $Mw_{class} + 0.199$
3	1197	Random, 0.001< p <0.499
4	1030	μ = 0.45, σ = 0.1375

The effect of degree of polymerisation on rate of oxidation

During oxidation carboxylic acid moieties are formed (described in equations 1-4), the acid is continuously neutralized by titration with NaOH and therefore the amount of titrate represents the degree of oxidation. The rate of oxidation is obtained by differentiation of the oxidation titration curve (Figure 6). For both Eliane MD6 and Eliane 100 the oxidation rates show an increase directly after the start of the experiment, this behaviour is attributed to the formation of the reaction intermediate (aldehyde). This observation is in line with the findings of (Guan et al., 2019). In the initial phase the oxidation rate for Eliane 100 is far above that of Eliane MD6, while between 2-8 hours the oxidation rate of Eliane MD6 is higher than Eliane 100. As a consequence of the higher initial oxidation rate, Eliane 100 consumes the added NaOCl quickly and the rapidly decreasing concentration NaOCl reduces the conversion rate. The initial oxidation of Eliane MD6 is slower and the concentration NaOCl is higher level for a longer time. This explains the higher titration rate for Eliane MD6 between 2 and 8 hours. After 8 hours, the availability of NaOCl for both systems is low and the reaction rates are similar. The differences in initial maximum oxidation rate demonstrate that the oxidation rate is influenced by the molecular size of the substrate. The initial oxidation rate of large starch molecules (Eliane E100) is approximately a factor two higher than the initial oxidation rate of small molecules (Eliane MD6).

The result that large starch molecules oxidise at a higher rate than small starch molecules is in line with the findings of Floor et al. (1989), who observed the same trend for tungstate-hydrogen peroxide oxidation of maltodextrins. Our data demonstrates that this trend also exists for hypochlorite oxidation of waxy potato starches, and holds for a broader (DP ~16–500.000) range of molecular weights.

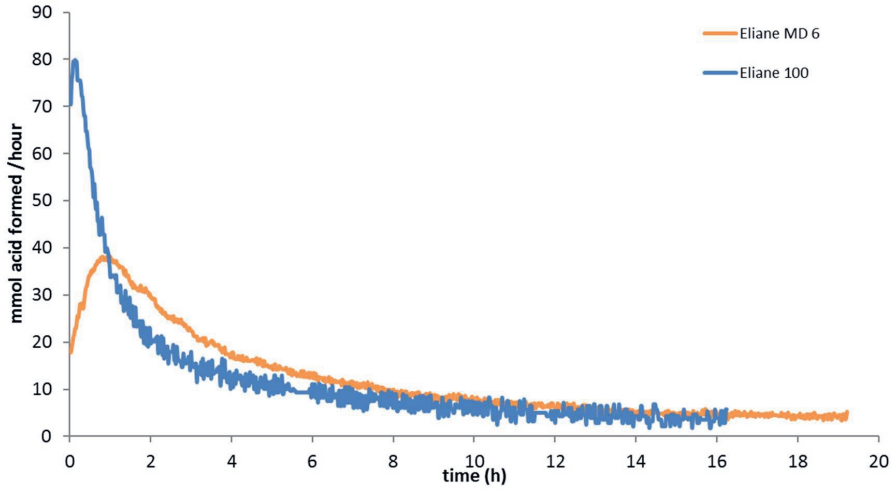

Figure 6 oxidation rate over time for TEMPO/OCL⁻ oxidation of a large starch (DP~ 250.000 -500.000) (blue) and a small starch (DP~16) (orange). Starch concentration 0.2% wt., 20°C . 1mg/gr TEMPO/starch

The effect of degree of oxidation on the rate of oxidation

For determining the rates of oxidation, the reaction conditions for oxidation were chosen to minimise depolymerisation other than oxidative depolymerisation. Thereby reducing the effect of changing molecular weight on the oxidation rates. For this reason, low degree of oxidation (max 20%), mild temperature (20°C) and a dilute system (0.2% wt) were chosen. A typical titration curve of a stepwise oxidation experiment is shown in Figure 7. The figure shows a titration curve over time where the sodium hypochlorite has been added in equal aliquots. The steepness of the slopes in this figure decreases with each new aliquot, indicating that the rate of oxidation decreases with each new aliquot. This effect appears to be greater than can be explained by the decrease in oxidisable groups.

The estimated k-values of the oxidation rates are given in Figure 8, where the rate of oxidation is plotted against the degree of oxidation. If there were no effect of degree of oxidation at the rate of oxidation, then oxidation rates should decrease linearly with the degree of oxidation due to reduced available oxidisable groups. Figure 8, however, shows that the rate of oxidation decreases exponentially with the degree of oxidation of the substrate. The degree of oxidation has thus a negative effect on rate of oxidation. Moreover, the oxidation rate of the larger molecules is the highest in the initial phase of oxidation.

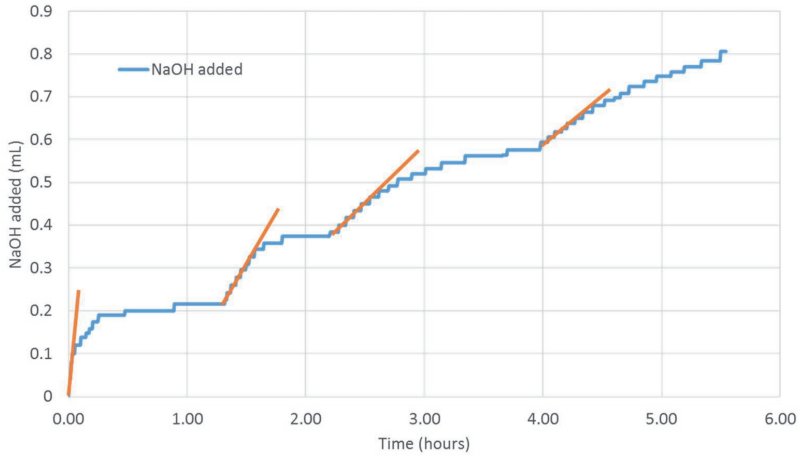

Figure 7 A titration curve for stepwise TEMPO catalysed oxidation of Eliane 100. Aliquots of NaOCl are added to obtain DO of 5, 10 15 and 20%. Orange slopes visualise a decrease in initial oxidation rate for subsequent aliquots. Starch concentration 0.2% wt., 20°C. 1mg/gr TEMPO/starch.

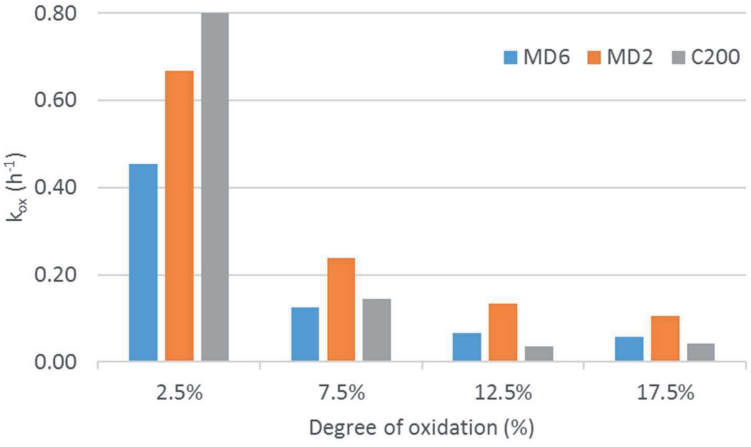

Figure 8 fitted oxidation rates at different degrees of oxidation for different molecular sizes of starch

3.3.2 Application of combined kinetic models

simulating product distributions

The estimated values for the kinetic parameters from the individual depolymerisation and oxidation models were applied in the combined kinetic model for depolymerisation and oxidation (equations 3-10, and Figure 3). The resulting two dimensional

distribution of the starch "population" over 4 points in time is shown in Figure 9. On the horizontal axis of this colour map, degree of oxidation is shown. On the vertical axis the degree of polymerisation is given in the form of a HPSEC diagram with elution volume as unit. Over time the population shifts more to the right, and large molecules (elution volumes <6.4 ml) move faster to the right than small molecules (elution volume >7.9 ml), in accordance with the experimental results. This results in an asymmetrical distribution. The degree of polymerisation of the starch population decreases over time, and a cluster of small molecules forms at high elution volumes (>7.9 ml).

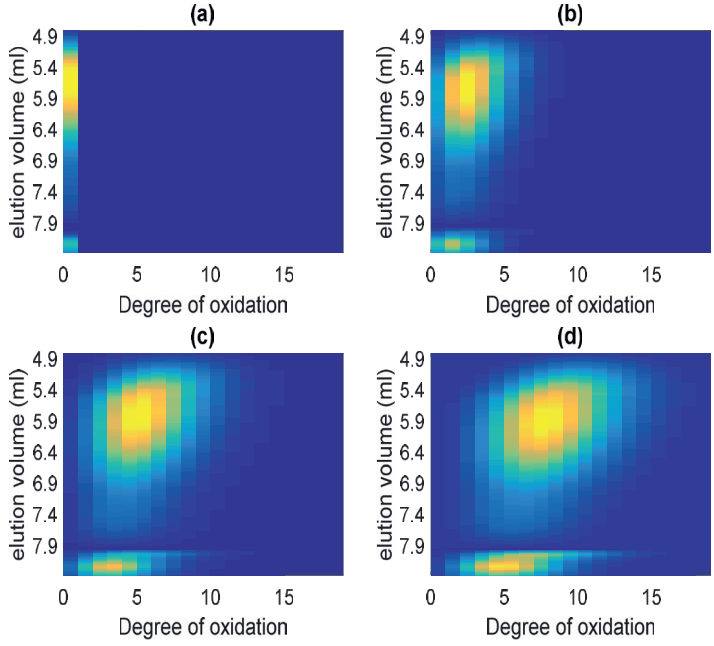

Figure 9 simulated product distributions at four time points (t=0 (a), t = 1/3t_{final} (b), t = 2/3t_{final} (c), t_{final} (d)) during conversion.

Role of kinetic parameters in depolymerisation and oxidation

After the calibration of the model by applying the estimated kinetic parameters, the influence of the parameters a and p on the final predicted starch distribution is assessed. The influence of parameters a and p on the final product distributions becomes more prominent at higher depolymerisation rates. For visualisation, the flat depolymerisation rate b (equation 7) has been doubled to demonstrate the role of the parameters a and p on the final product distribution. Comparison of Figure 9d and Figure 10(middle) shows the effect of doubling b for the standard case. The higher value of b results in stronger depolymerisation and as a result, the intensity of the bulk

products (elution volumes between 5.4 ml and 6.4 ml) is lower and more small molecules (elution volumes > 7.9 ml) are present.

Figure 10 shows the influence of the cutting site parameter p on the final product distribution for 3 cases $p = 0.05$, $p = 0.126$, and $p = 0.5$. The figure shows that for low values of p (cutting close to the edge of the molecules), the number of small molecules increases significantly compared to the number of large molecules when compared to other values for p. The major fraction of the large molecules does not significantly decrease in size. For high values of p (cutting closer to the centre of the molecules), the bulk of the large molecules decreases in size and the shape of the distribution changes significantly by the formation of a second cluster of molecules at 6.9 ml elution volume. The product formed with $p = 0.05$ will retain most of its function as the large molecules do not decrease in size much. The overall yield of functional molecules is, however, lower as the fraction of the small molecules, that do not contribute to product functionality, is larger. In addition to p, parameter a may also play an important role.

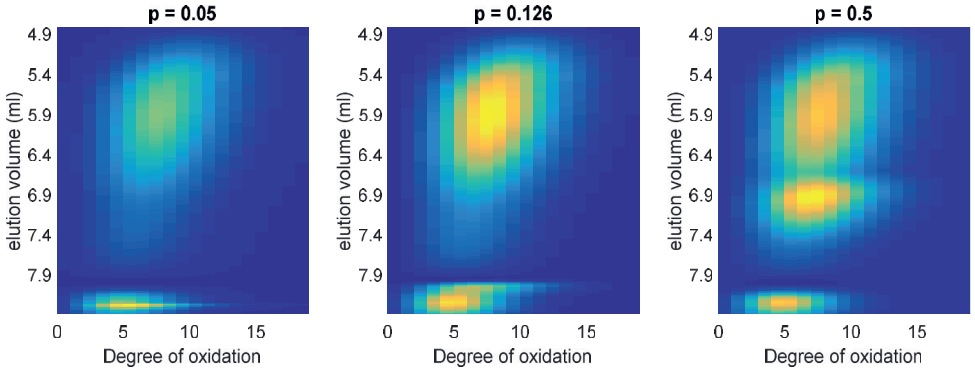

Figure 10 Final product distributions for different cutting site parameter values. p = 0.05 (left), p = 0.126 (middle), p = 0.5 (right).

Figure 11 shows the influence of the molecular weight dependent depolymerisation term a from equation 7. The figure shows that halving the value of a increases overall depolymerisation (more molecules at elution volumes >7.9 ml). Increasing a decreases overall depolymerisation and the final mixture is less polydisperse, with a tight cluster of molecules at 5.8 ml elution volume. The differences between the product distributions when varying parameter a indicate that, in addition to p, a is an essential parameter for the final product distribution.

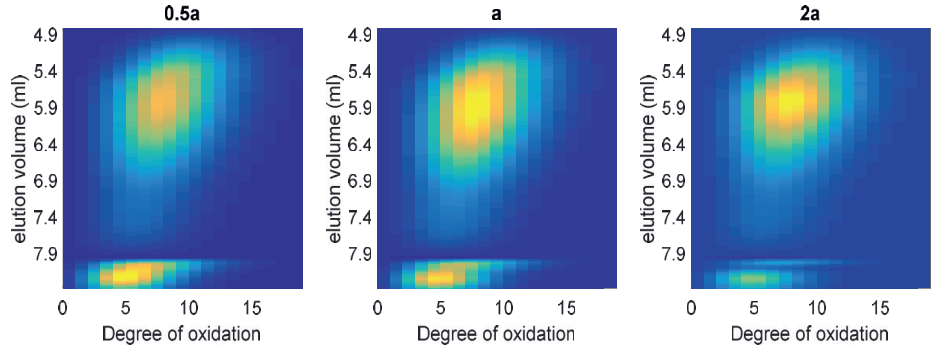

*Figure 11 Predicted final product distributions for varying values of the molecular weight dependent depolymerisation term. a=0.5 * estimated value (left) a = estimated value (middle), a = 2* estimated value (right)*

Figure 12 shows the influence of size dependent and DO (degree of oxidation) dependent oxidation rates on the final product distribution by comparing the presented model (right) and calculations in which the contribution of size-dependent kinetics is cancelled (left). The size dependent term in the kinetics introduces an asymmetric distribution over DO in the product, where large molecules are further oxidised than small ones. The inclusion of an inhibiting effect by the DO on the rate of oxidation, results in a narrower distribution over degree of oxidation. It is important to account for this asymmetry and inhibition, as the combination of molecular weight and degree of oxidation determines product functionality. Models including a size and DO dependent oxidation term will therefore more accurately predict product functionality while traditional models systematically overestimate the obtained degree of oxidation.

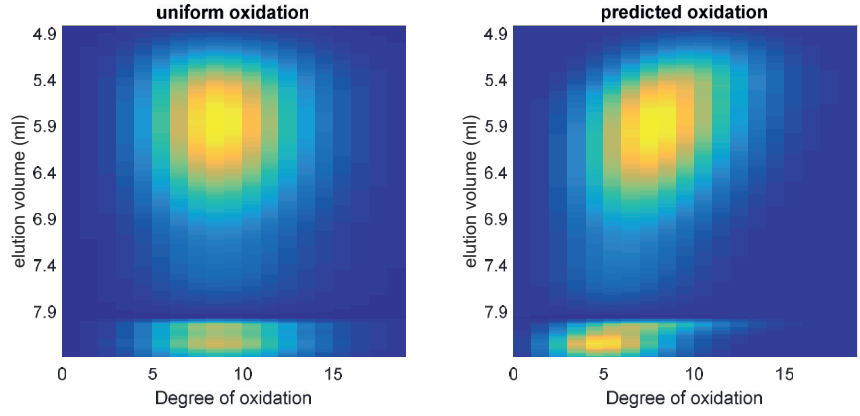

Figure 12 predicted product distributions by a traditional model (left) and the proposed model (right) that includes size-dependent oxidation and decreasing rates of oxidation with increasing degree of oxidation

3.4 Conclusions

The experimental work showed that degree of polymerisation of starches influences the rate of depolymerisation, where large molecules depolymerise at a higher rate than small molecules. The degree of polymerisation also influences the rate of oxidation for starches, where large starch molecules (DP ~250.000 – 500.000) oxidise at about double the rate of small starch molecules (DP~16). Furthermore, an inhibiting effect has been found where the rate of oxidation decreases exponentially with the obtained degree of oxidation.

The kinetics of both depolymerisation and oxidation are expressed in a mathematical model. The kinetic parameters pertaining to the effect of molecular size on the rate of depolymerisation and the rate of oxidation were quantified by fitting the experimental data to the model. Additionally, the parameter that describes the molecular weight ratio of the two fractions of the molecule after depolymerisation was estimated. From these kinetic parameters, the molecular weight dependent depolymerisation rate a and the flat depolymerisation rate b are responsible for overall depolymerisation and polydispersity of the product distribution. Parameter p which describes the molecular weight ratio of the two fractions of the molecule after depolymerisation determines the shape of the product distribution.

The interaction between size dependent depolymerisation and size dependent oxidation, in combination with the inhibiting effect in oxidation, results in asymmetrical product distributions. Traditional models do not predict these asymmetrical distributions. Models that do not include a size dependent and degree of oxidation dependent term for the rate of oxidation will systematically overestimate the degree of oxidation obtained.

3.5. Acknowledgements

This work was supported by the Dutch Research Council (NWO) [grant number 870.15.120].

3.6 References

Aeschelmann, F., & Carus, M. (2015). Biobased Building Blocks and Polymers in the World: Capacities, Production, and Applications–Status Quo and Trends Towards 2020. *Industrial biotechnology, 11*(3), 154-159. doi:10.1089/ind.2015.28999.fae

Bertoft, E. (2017). Understanding Starch Structure: Recent Progress. *Agronomy, 7*(3). doi:10.3390/agronomy7030056

Bragd, P. L., Besemer, A. C., & van Bekkum, H. (2000). Bromide-free TEMPO-mediated oxidation of primary alcohol groups in starch and methyl α-d-glucopyranoside. *Carbohydrate Research, 328*(3), 355-363. doi:https://doi.org/10.1016/S0008-6215(00)00109-9

Bragd, P. L., Besemer, A. C., & van Bekkum, H. (2002). Selective oxidation of carbohydrates by 4-AcNH-TEMPO/peracid systems. *Carbohydrate Polymers, 49*(4), 397-406. doi:https://doi.org/10.1016/S0144-8617(01)00344-7

Bragd, P. L., van Bekkum, H., & Besemer, A. C. (2004). TEMPO-Mediated Oxidation of Polysaccharides: Survey of Methods and Applications. *Topics in Catalysis, 27*(1), 49-66. doi:10.1023/B:TOCA.0000013540.69309.46

Chiu, C.-w., & Solarek, D. (2009). Chapter 17 - Modification of Starches. In J. BeMiller & R. Whistler (Eds.), *Starch (Third Edition)* (pp. 629-655). San Diego: Academic Press.

Chronakis, I. S. (1998). On the Molecular Characteristics, Compositional Properties, and Structural-Functional Mechanisms of Maltodextrins: A Review. *Critical Reviews in Food Science and Nutrition, 38*(7), 599-637. doi:10.1080/10408699891274327

de Nooy, A. E. J., Besemer, A. C., & van Bekkum, H. (1994). Highly selective tempo mediated oxidation of primary alcohol groups in polysaccharides. *Recueil des Travaux Chimiques des Pays-Bas, 113*(3), 165-166. doi:10.1002/recl.19941130307

Fannon, J. E., Gray, J. A., Gunawan, N., Huber, K. C., & BeMiller, J. N. (2004). Heterogeneity of starch granules and the effect of granule channelization on starch modification*. *Cellulose, 11*(2), 247-254. doi:10.1023/B:CELL.0000025399.66700.d7

Floor, M., Schenk, K. M., Kieboom, A. P. G., & van Bekkum, H. (1989). Oxidation of Maltodextrins and Starch by the System Tungstate-Hydrogen Peroxide. *Starch - Stärke, 41*(8), 303-309. doi:https://doi.org/10.1002/star.19890410806

Forssell, P., Hamunen, A., Autio, K., Suortti, P., & Poutanen, K. (1995). Hypochlorite Oxidation of Barley and Potato Starch. *Starch - Stärke, 47*(10), 371-377. doi:10.1002/star.19950471002

Gidley, M. J., Hanashiro, I., Hani, N. M., Hill, S. E., Huber, A., Jane, J.-L., . . . Gilbert, R. G. (2010). Reliable measurements of the size distributions of starch molecules in solution: Current dilemmas and recommendations. *Carbohydrate Polymers, 79*(2), 255-261. doi:https://doi.org/10.1016/j.carbpol.2009.07.056

Guan, Q., Chen, J., Chen, D., Chai, X., He, L., Peng, L., . . . Li, J. (2019). A new sight on the catalytic oxidation kinetic behaviors of bamboo cellulose fibers under TEMPO-oxidized system: The fate of carboxyl groups in treated pulps. *Journal of Catalysis, 370*, 304-309. doi:https://doi.org/10.1016/j.jcat.2019.01.003

Huber, K. C., & BeMiller, J. N. (2001). Location of Sites of Reaction Within Starch Granules. *Cereal Chemistry, 78*(2), 173-180. doi:https://doi.org/10.1094/CCHEM.2001.78.2.173

Kumoro, A. C., Ratnawati, R., & Retnowati, D. S. (2015). A simplified kinetics model of natural and iron complex catalysed hydrogen peroxide oxidation of starch. *Asia-Pacific Journal of Chemical Engineering, 10*(5), 648-658. doi:https://doi.org/10.1002/apj.1896

Laurichesse, S., & Avérous, L. (2014). Chemical modification of lignins: Towards biobased polymers. *Progress in Polymer Science, 39*(7), 1266-1290. doi:https://doi.org/10.1016/j.progpolymsci.2013.11.004

Liu, W.-C., Castro, J. V., & Gilbert, R. G. (2011). Rate coefficients for enzyme-catalyzed reactions from molecular weight distributions. *Polymer, 52*(7), 1490-1494. doi:https://doi.org/10.1016/j.polymer.2011.01.063

Masina, N., Choonara, Y. E., Kumar, P., du Toit, L. C., Govender, M., Indermun, S., & Pillay, V. (2017). A review of the chemical modification techniques of starch. *Carbohydrate Polymers, 157*, 1226-1236. doi:https://doi.org/10.1016/j.carbpol.2016.09.094

Parovuori, P., Hamunen, A., Forssell, P., Autio, K., & Poutanen, K. (1995). Oxidation of Potato Starch by Hydrogen Peroxide. *Starch - Stärke, 47*(1), 19-23. doi:10.1002/star.19950470106

Salmi, T., Tolvanen, P., Wärnå, J., Mäki-Arvela, P., Murzin, D., & Sorokin, A. (2016). Mathematical modeling of starch oxidation by hydrogen peroxide in the presence of an iron catalyst complex. *Chemical Engineering Science, 146*, 19-25. doi:https://doi.org/10.1016/j.ces.2016.02.027

Sangseethong, K., Termvejsayanon, N., & Sriroth, K. (2010). Characterization of physicochemical properties of hypochlorite- and peroxide-oxidized cassava starches. *Carbohydrate Polymers, 82*(2), 446-453. doi:https://doi.org/10.1016/j.carbpol.2010.05.003

Stacy, C. J., & Foster, J. F. (1957). Molecular weight heterogeneity in starch amylopectins. *Journal of Polymer Science, 25*(108), 39-50. doi:https://doi.org/10.1002/pol.1957.1202510804

Tolvanen, P., Mäki-Arvela, P., Sorokin, A. B., Salmi, T., & Murzin, D. Y. (2009). Kinetics of starch oxidation using hydrogen peroxide as an environmentally friendly oxidant and an iron complex as a catalyst. *Chemical Engineering Journal, 154*(1), 52-59. doi:https://doi.org/10.1016/j.cej.2009.02.001

van Warners, A., Lammers, G., Stamhuis, E. J., & Beenackers, A. A. C. M. (1990). Kinetics of the Diffusion and Chemical Reaction of Ethylene Oxide in Starch Granules in a Gas Solid System. *Starch - Stärke, 42*(11), 427-431. doi:https://doi.org/10.1002/star.19900421105

Vanier, N. L., El Halal, S. L. M., Dias, A. R. G., & da Rosa Zavareze, E. (2017). Molecular structure, functionality and applications of oxidized starches: A review. *Food Chemistry, 221*, 1546-1559. doi:https://doi.org/10.1016/j.foodchem.2016.10.138

Veelaert, S., de Wit, D., & Tournois, H. (1994). An improved kinetic model for the periodate oxidation of starch. *Polymer, 35*(23), 5091-5097. doi:https://doi.org/10.1016/0032-3861(94)90670-X

Verraest, D. L., Peters, J. A., & van Bekkum, H. (1998). The platinum-catalyzed oxidation of inulin. *Carbohydrate Research, 306*(1), 197-203. doi:https://doi.org/10.1016/S0008-6215(97)10055-6

Zhang, Z., & Huber, G. W. (2018). Catalytic oxidation of carbohydrates into organic acids and furan chemicals. *Chemical Society Reviews, 47*(4), 1351-1390. doi:10.1039/C7CS00213K

Zhou, D.-N., Zhang, B., Chen, B., & Chen, H.-Q. (2017). Effects of oligosaccharides on pasting, thermal and rheological properties of sweet potato starch. *Food Chemistry, 230*, 516-523. doi:https://doi.org/10.1016/j.foodchem.2017.03.088

4.

4. Size selectivity in adsorption of polydisperse starches on activated carbon

This chapter is published as: Hoogstad, T. M., Kiewidt, L., van Haasterecht, T., & Bitter, J. H. (2023). Size selectivity in adsorption of polydisperse starches on activated carbon. Carbohydrate Polymers, 309, 120705.

Abstract

The influence of molecular weight, polydispersity, and degree of branching of four potato starches (Paselli MD10, Eliane MD6, Eliane MD2, and highly branched starch) on the adsorption rates on activated carbon (Norit CA1) was investigated. Changes in starch concentration and size distribution over time were analysed by Total Starch Assay and Size Exclusion Chromatography. Average molecular weight and degree of branching of a starch scaled negatively with average adsorption rate. Within a size-distribution, adsorption rates scaled negatively with increasing molecule size, resulting in an increased average molecular weight in solution of between 25% and 213% and a decreased polydispersity of between 13% and 38%. Simulation with dummy distributions estimated the ratio of adsorption rates for 20^{th} percentile and 80^{th} percentile molecules within a distribution to range between a factor 4 and 8 for the different starches. Competitive adsorption decreased the adsorption rate of molecules above the average size within a sample distribution.

Keywords: Starch; Adsorption; Polydispersity; Dispersity

4.1 Introduction

Biobased materials and chemicals made from biobased feedstocks are potential sustainable alternatives to petrochemical based counterparts. The use of biobased feedstocks often require pre-treatment and/or chemical modification to arrive at the desired functionalities in the molecules of which the targeted materials and chemicals exist. Catalysis is widely applied to achieve these modifications (Hulea, 2018; Schwartz, Shanks, & Dumesic, 2016; Serrano, Melero, Morales, Iglesias, & Pizarro, 2018; Sheldon, 2014). Biobased feedstocks are a challenging class of reactants to process as many biobased feedstocks are polymeric and inhomogeneous in nature, containing multiple large and complex molecules like lignin, cellulose, and hemicellulose. Additionally, within one type of (bio)polymer a wide range of molecular sizes can be present.

Starch is an example of such a complex feedstock/reactant. Starch contains two biopolymers, amylose and amylopectin. Both these biopolymers have a distribution in molecular weights (Bertoft, 2017; Durrani & Donald, 2000). In previous work we have demonstrated that this inhomogeneity in the reactant affects reaction rates, where a higher molecular weight (DP 250.000 vs DP 16) increases the rates of TEMPO mediated hypochlorite oxidation of starch by a factor two (Hoogstad et al., 2019). However, the influence of molecular weight (distributions) in reactants may not be limited to the chemical reaction but may also influence adsorptive properties of adsorbates prepared for wastewater treatment (Dao et al., 2020), and other steps in the catalytic cycle in different catalytic processes such as adsorption.

The relation between (average) adsorbate size, adsorption rate and equilibrium constants has been studied before. Shirazi, van de Ven, and Garnier (2003a), Shirazi, van de Ven, and Garnier (2003b) studied the adsorption of modified starches on porous glass and pulp fibres respectively. The authors concluded that there is a preferential adsorption of amylose on fibres and on porous glass compared to amylopectin, however, due to the formation of large cluster molecules, amylopectin reached a larger equilibrium constant. Lee, Kwon, and Moon (2004) studied the adsorption rates of glucose, maltose, maltotriose, maltotetraose, and maltopentaose on activated carbon, and found that adsorption coefficients for chain lengths >2 decreased with increasing chain length. El'tekov, El'tekova, and Roldughin (2007) showed that the adsorption rate and equilibrium constant of polystyrene macromolecules on carbon black scaled positively with increasing molecular weight, while the adsorption and equilibrium constant of polysaccharides on sibunit scaled inversely with increasing molecular weight. Yamaguchi, Endo, Takagi, and Hukao (1977), demonstrated that a series of oligosaccharides with degrees of polymerisation between 1 and 22 showed varying trends and optima between adsorption rates and molecular weight for different carbon

adsorbents. Fu and Santore (1998) observed in an experimental study that in the adsorption of polyethylene-oxides on silica small molecules adsorb first, but are replaced by larger molecules as the system equilibrates. Similar results were found by Bessaies-Bey et al. (2019) for the adsorption of polydisperse acrylamides on siliceous material. These studies show that molecular weight of the reactant is an important variable for adsorption rates and equilibrium constant, and that adsorption rates and equilibrium constant can scale either positively or negatively with molecular weight of the reactant, depending on the specific sorbent/sorbate combination.

Quantitative descriptions for the adsorption rates and prediction of the composition of the equilibrated adsorbate mixture of complex and polydisperse reactant mixtures that include size distributions in the feedstock and product mixture, are lacking. Analytical expressions of adsorption isotherms for competitive adsorption of multi-component mixtures can only be derived after making simplifying assumptions (Kast, 1989; Koopal, Tan, & Avena, 2020). As a result, it is often assumed that all molecules in a adsorbate distribution behave like their average. However, this assumption introduces an error which increases with increased polydispersity of the adsorbate. Therefore, for (highly) polydisperse feedstocks, the adsorption dynamics and competitive adsorption between species within a distribution need to be evaluated.

Already some ground breaking modelling studies that provide quantitative insights in the adsorption rates and composition of adsorbed species for the adsorption of a reactant distribution have been done though with some limitations which will be indicated later. Ding et al. (2020) studied the adsorption of C_2-C_6 alkanes using density functional theory and found that adsorption energies increased linearly with increasing chain length. Lishchuk, Ettelaie, and Annable (2017) studied the adsorption of theoretical random block copolymers, composed of varying fractions of two monomers, on planar surfaces. The authors found that the distribution of adsorbed species can differ significantly from the distribution in bulk depending on slight changes in polymer composition, where polymers from the tail-end of the distribution are predominantly adsorbed. Hart and Aarão Reis (2016) studied the adsorption of theoretical linear and square particles on planar lattices. The authors showed that the initial distribution of adsorbed molecules closely matched the initial bulk distribution. However, as the system equilibrates the distribution of the adsorbed molecules increasingly deviated from the initial distribution where small molecules from the tail-end of the distribution are predominantly present on the surface.

This effect, i.e., the increasing difference over time between bulk and adsorbed species, scaled positively with increasing polydispersity index of the initial distribution. Though these studies provide quantitative descriptions of the adsorption rates of polydisperse

reactants and change over time in composition of adsorbed molecules their scope is limited to theoretical polymers or very specific sorbent/sorbate combinations. Moreover, detailed data (e.g. adsorption energies, shape factors, structural sites of adsorbent) has to be available for these reactants and materials to create such models.

Models based on measured data that include size dependent kinetics but do not require detailed data on structural sites and adsorption energies could be an effective "middle ground" tool to aid in the design of catalytic processes for the conversion of complex and polydisperse feedstocks. These models, as an improvement over models that use averaged values, can account for the differences in adsorption rates and equilibrium constants within the distribution and thereby predict the subset of the reactant distribution that is converted. As an additional input compared to models that use average values, these models would require the initial, ≥1 intermediary, and equilibrated distribution of the reactant for adsorption on a given sorbate.

In this study we will propose a method to empirically quantify the size selective effects of polydisperse adsorbate. First, we will show that molecular weight plays a role in the adsorption rates of a polydisperse adsorbate. Second, we will evaluate the initial, intermediate, and equilibrated distributions of the adsorbate. Last, we will provide a method to quantify the size selective effects.

To achieve this, four commercially available starches were used as a model feedstock to investigate how molecular weight and degree of branching of the starch influences the adsorption rates of starch on activated carbon. Based on the aforementioned studies, it is expected that bulk and adsorbed molecular weight distributions of starch differ substantially. Figure 1 schematically illustrates size selective adsorption of a starch sample onto activated carbon, which results in different size distributions between the remaining solubilised starch fraction and the adsorbed starch fraction. The total quantity of starch remaining in solution (blue distribution in figure 1) and its size distribution was measured over time by a Total Starch Assay (TSA) and High Pressure Size Exclusion Chromatography (HPSEC). From the TSA results, initial adsorption rates and adsorption capacity were measured per sample. These values represent the average initial adsorption rate and combined capacity of all starch species present in that sample's molecular size distribution. Subsequently, the HPSEC results was used to calculate number average molecular weight, weight average molecular weight, and polydispersity index during adsorption, and their change over time. This data was used as input for a model that estimates the adsorption rates of select species within a starch distribution to provide a metric for the size selectivity of the adsorption.

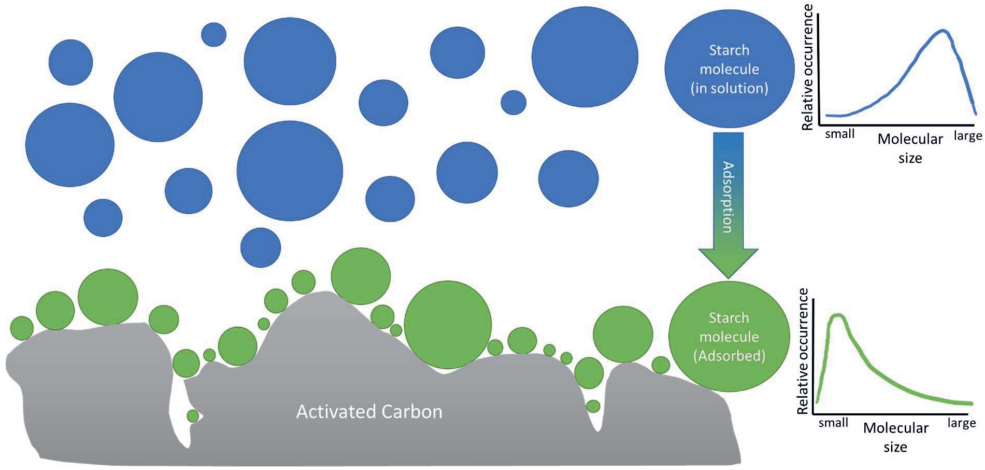

Figure 1 schematic representation of the adsorption of size distributed starch molecules in solution onto activated carbon. The size distribution of starch fraction remaining in solution (blue) has a different size distribution compared to the adsorbed starch fraction (green).

4.2 Materials and methods

4.2.1 Materials

Table 1 provides an overview of the different starches (data as reported by the provider, Avebe, Groningen, the Netherlands) used. The different molecular weights and molecular weight distribution of these starches have been measured and reported in section 3.1. Norit CA1 activated carbon (MilliporeSigma, Germany) was used as adsorbent. Some of the physio-chemical properties of this carbon can be found in Table 2. Some of the data used for obtaining these numbers i.e. nitrogen adsorption and desorption, are shown in Appendix Figure A1.

Table 1 Starches used in this research.

Name:	Origin:	Modification:	Moisture (%)	Branching (%)
Paselli MD10	Potato	Enzymatic, hydrolysis	8	0-5%
Eliane MD6	Waxy potato	Enzymatic, hydrolysis	10	5
Eliane MD2	Waxy potato	Enzymatic, hydrolysis	10	5
HBS	potato	Enzymatic, branching	5.5	7.5

Table 2 Summary of physio-chemical properties of Norit CA1

Surface area	Pore volume		Pore size	
BET surface area ($m^2\ g^{-1}$)	Total pore volume ($m^3\ g^{-1}$)	micropore volume ($m^3\ g^{-1}$)	Average pore diameter (nm)	BJH Desorption average pore width (nm)
1038	0.83	0.27	3.2	8.2

4.2.2 Experimental setup and procedure

Adsorption experiments

Starch solutions of 500 ml containing 2.5 mg starch (dry weight)/ml were made. The dry weight was determined using the moisture content of the starches as provided in manufacturer (Table 2). Starches were solubilized by autoclaving at 120 degrees for 20 minutes.

After cooling to room temperature overnight, starch solutions were mixed with AC in a 4:1 AC to starch ratio (w/w) and stirred with a magnetic stirrer at 500 rpm in an Erlenmeyer at room temperature. Samples of 2 ml were taken before the start of the

experiment i.e., just before adding the AC, after 2 minutes, 10 minutes, 20 minutes, 30 minutes, 1 hour, 2 hours, 4 hours, 8 hours, 24 hours, and 48 hours. Samples were centrifuged at 10.000 x g for 5 minutes to precipitate the activated carbon and starches adsorbed thereupon (figure A4). 1.4ml of supernatant was carefully pipetted into a 1.5ml Eppendorf vial for further treatment and analysis.

4.2.3 Analysis

Total starch assay

the Megazyme total starch assay kit (Megazyme International Ireland Ltd. Bray, Ireland) was used to measure total starch concentration in the samples taken after adsorption according to the manufacturer's protocol (albeit the amounts were decreased with a factor 10) variant for solubilised or suspended starch

HPSEC

The samples taken after reaction (see experimental setup and procedure) were again centrifuged, now at 19000 x g for 10 min to remove any precipitation. The supernatant was analysed with a Dionex Ultimate 3000 system (Sunnyvale, USA) on a column set that consisted of three in series connected TSKgel SuperAW columns (SuperAW4000 6.0 x 150 mm, 6 µm; SuperAW3000 6.0 x 150 mm, 4 µm; SuperAW2500 6.0 x 150 mm, 4 µm) (Tosoh Bioscience, Tokyo, Japan) with a TSKgel guard column (SuperAW-L 4.6 x 35 mm, 7 µm). The injection volume was 10µl and 0.2M $NaNO_3$ was used as eluent with a flowrate of 0.6 mL/min. The column was operated at 55 °C. Refractive Index (RI) was measured by a Shodex RI-101 detector (Showa Denko, K.K., Kawasaki, Japan). Calibration of the column was performed with pullulan standards of 342 Da, 6.3 kDa, 22 kDa, 47 kDa, and 107 kDa (Supelco, Bellefonte, USA). The calibration curve is shown in appendix figure A3. Universal calibration theory is assumed (Gidley et al., 2010).

HPSEC diagrams were baseline corrected, and peak-height normalised according to equations 1 and 2.

$$\eta_{t0} = RI_{max,t0} \tag{1}$$

Where η_{t0} is the normalisation factor for sample $t0$, $RI_{max,t0}$ is the maximum RI response of sample $t0$.

$$\eta_n = \frac{RI_{max,n}}{RI_{\max,\,t0}} \tag{2}$$

Where η_n is the normalisation factor for sample n, $RI_{max,n}$ is the maximum RI response of sample n, and $RI_{max,t0}$ is the maximum RI response of sample $t0$.

Number average molecular weight, weight average molecular weight, and polydispersity index for all samples were calculated from the baseline corrected HPSEC data using formulas 3-5.

$$M_n = \frac{\sum_i N_i M_i}{\sum_i N_i} \quad (3)$$

Where M_n is the number average molecular weight, N_i is the number of molecules in the molecular weight class i. M_i is the molecular weight of the molecule in weight class i.

$$M_w = \frac{\sum_i N_i M_i^2}{\sum_i N_i M_i} \quad (4)$$

Where M_w is the weight average molecular weight. N_i is the number of molecules in the molecular weight class i. M_i is the molecular weight of the molecule in weight class i.

$$Pdi = M_w / M_n \quad (5)$$

Where Pdi is the polydispersity index, M_w is the weight average molecular weight, and M_n is the number average molecular weight.

Modelling

To quantify the size selectivity of the adsorption for each type of evaluated starch, the ratio of adsorption rates between large (represented by an 80th percentile molecule from the distribution) and small molecules (represented by a 20th percentile molecule size from the distribution) within a sample starch distribution was estimated (schematically illustrated in Figure 2). To this end, a bimodal dummy distribution for each type of starch was made comprised of molecules of two sizes, the 20th and 80th percentile value of the sample's initial molecular size distribution. The ratio of 20th percentile and 80th percentile molecules in each dummy distribution was fitted to match the measured initial polydispersity of the corresponding starch sample. Molecules were then removed (representing adsorption) from the dummy distribution following a ratio between the 20^{th} and 80^{th} percentile molecular sizes.

The value for this ratio that resulted in a similar decrease in polydispersity as was measured experimentally was determined. This ratio provides a simplified, quantitative

estimation of the ratio between adsorption rates of large and small molecules (20^{th} and 80^{th} percentile molecular size) within a starch distribution.

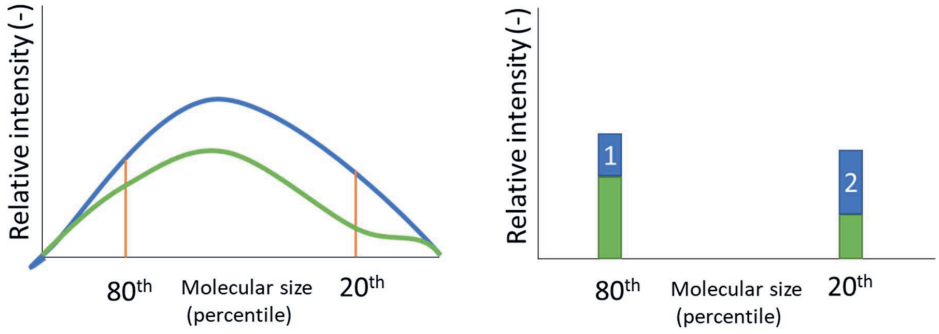

Figure 2 Schematic representation of dummy distribution. Left: continuous distributions of initial (blue) and residual (green) sample distributions. Orange lines indicate the 80^{th} and 20^{th} percentile molecule size. Right: corresponding initial (green plus blue) and residual (green) dummy distributions comprised of only 80^{th} and 20^{th} molecule size starch species. The polydispersity of the dummy distributions are matched to their corresponding continuous distributions. Molecules in box 1 and 2 represent the removed starch molecules. The ratio of the size of box 1 and 2 represents the ratio between adsorption rates for 80^{th} and 20^{th} percentile sized molecules.

4.3 Results & discussion

4.3.1 Characterisation of reactants

Figure 3 shows the HPSEC chromatograms of the four starches after solubilisation. The data has been converted to a Mw calibrated scale and the peak height of the highest Mw peak has been normalised to 1 to highlight the differences in size distributions between the samples.

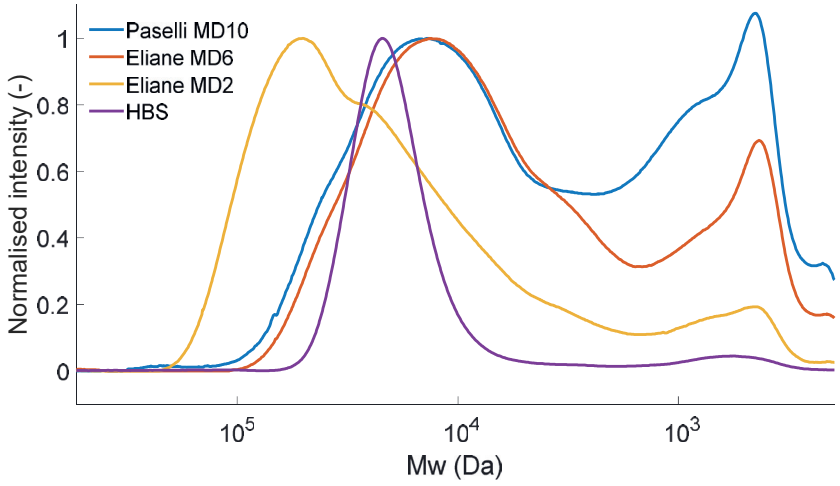

Figure 3 HPSEC chromatogram of all utilised starches after solubilisation. The peak height is normalised to a maximum intensity of 1.

Paselli MD10, Eliane MD6, and Eliane MD2 all have a skewed distribution around their main peak with a long tail containing smaller molecules. In addition, Paselli MD10 and Eliane MD6 show a bimodal profile with a second peak around 0.5 $\times 10^3$ Da which corresponds to the molecular weight of maltose, maltotriose and maltotetraose. Paselli MD10 and Eliane MD6 have a similar distribution width, but Paselli MD10 has a higher content of small (<1 $\times 10^3$Da) molecules than Eliane MD6 resulting in a lower number average molecular weight and higher polydispersity. Ranked by number average molecular weight the order of the starches is: Paselli MD10 (25 $\times 10^3$ Da), Eliane MD6 (26 $\times 10^3$Da), HBS (43 $\times 10^3$Da), and Eliane MD2 (80 $\times 10^3$Da) (Table 3). Paselli MD10, Eliane MD6 and Eliane MD2 have broad distributions with measured polydispersity indices of 2.34, 2.00, and 1.78 respectively; HBS has a lower measured polydispersity index of 1.22 (Table 3).

Table 3 Number average molecular weight and polydispersity index of the evaluated starches

Name:	**Number average molecular weight (kDa)**	**Polydispersity (-)**
Eliane MD2	80	1.78
Eliane MD6	26	2.00
Paselli MD10	25	2.34
HBS	43	1.22

4.3.2 Adsorption

TSA

The evolution of starch concentration in solution during the adsorption experiments for 0 to 48 hours are shown in Figure 4. For clearer visualization of the initial adsorption rate, the data is also shown on a logarithmically scaled time-axis (Figure 4 right).

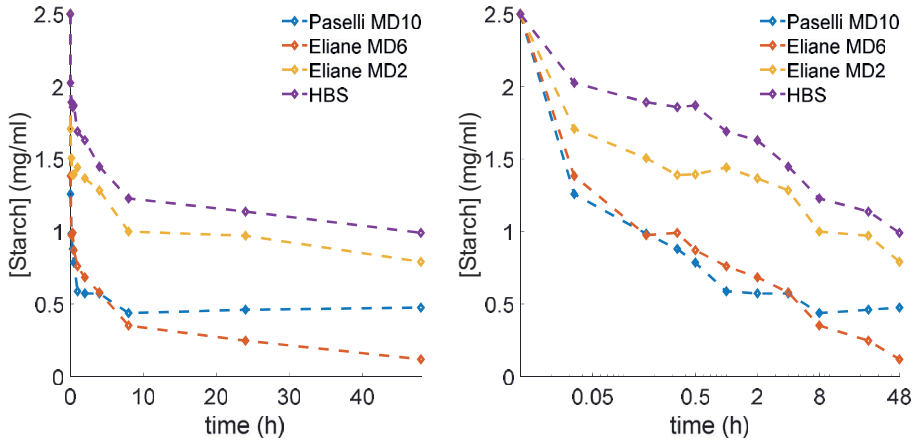

Figure 4 TSA results of the adsorption experiment over time on a linear scale (left) and a logarithmic scale (right). Diamonds show data points, dashed lines are to guide the eye.

The initial starch concentrations, before exposure to activated carbon was 2.5 mg ml^{-1} for all starches. After mixing with activated carbon, starch concentrations in solution decreased over time. This shows that starch was adsorbed onto the activated carbon and removed from the solution. The amount of adsorbed starch after 48 hours was 0.2, 0.24, 0.17 and 0.15 g g^{-1} for Paselli MD10, Eliane MD6, Eliane MD2 and HBS respectively. Paselli MD10 and Eliane MD6 showed similar reduction of solubilised starch concentrations over time up to 8 hours while differences arose in the 8 – 48 hour window. Adsorption continues even after the shown 48 hours of incubation, equilibrium times can be up to 7 days (El'tekov et al., 2007), (Figure A5), however, the rate of adsorption becomes so low, that we consider 48 hours to be a pseudo-equilibrium for practical purposes.

The starches with lower average molecular weight (Paselli MD10 and Eliane MD6) adsorbed at a higher initial rate (0.060 and 0.055 g g^{-1} min^{-1} adsorbed over 2 minutes versus 0.040 g g^{-1} min^{-1} respectively). For Paselli MD10, Eliane MD6, Eliane MD2, and HBS 61%, 47%, 46%, and 31% respectively of the total adsorption over 48 hours takes place in the first two minutes. This shows that the initial rate of adsorption of starches on activated carbon scales negatively with increasing molecular weight. HBS, although lower in average molecular weight than Eliane MD2, showed a lower initial rate of

adsorption (0.025 g g^{-1} min^{-1} after 2 minutes versus 0.040 g g^{-1} min^{-1}). The lower initial rate of adsorption of HBS compared to Eliane MD2 shows that the higher degree of branching of HBS compared to Eliane MD2 (7.5% versus 5%) has a larger influence on initial adsorption rate than difference in molecular weight between these starches alone explains and thus that molecule shape, in addition to molecular size, is a relevant factor.

The starches with lower average molecular weight (Paselli MD10 and Eliane MD6) reached a higher amount of starch adsorbed after 48 hours (0.20 g g^{-1} and 0.24 g g^{-1}) than Eliane MD2 (0.17 g g^{-1}). HBS showed a lower pseudo-equilibrium (0.15 g g^{-1} versus 0.18 g g^{-1} after 48 hours) than Eliane MD2. This shows that, similar to initial adsorption rates, the equilibrium constant of the adsorption of starch on activated carbon also depends on molecular size and degree of branching. Where the equilibrium constant scales negatively with both molecular size and degree of branching.

Durrani and Donald (2000), and Bertoft (2017) suggest that a higher degree of branching decreases flexibility and thus increases rigidity of a starch molecule in solution, leading to the hypothesis that the reduced flexibility leads to less contact area between starch molecule and activated carbon particle causing the lower initial adsorption rate and pseudo-equilibrium. Moreover, the shape of a molecule, in addition to its size, determines whether it can fit and effectively diffuse into a porous material. Flexible linear macromolecules have shown higher effective diffusion coefficients than rigid globular configurations in porous media (Pluen, Netti, Jain, & Berk, 1999; Shirazi et al., 2003a, 2003b). This suggests that equal molecular weight linear starch molecules can access a larger fraction of pores in the activated carbon than the rigid HBS starch molecules. It should be noted that all starch samples, including the waxy potato starch samples (Eliane) and highly branched starch (HBS) contain a fraction of linear molecules. This is a statistical occurrence based on the degree of polymerization of individual molecules within the distribution and the average degree of branching of the sample as a whole. The average degree of branching for Eliane based samples is 5% and for HBS is 7.5%, but for molecules within these distributions with a DP lower than to the inverse of the degree of branching (≤20 and ≤13 glucose units for Eliane and HBS respectively) there is fewer than one expected branching point in the molecule. As a result, there is a chance of these molecules being linear.

Underlaying mechanisms and modelling challenges

The observed size selective adsorption rates and equilibria, and the high initial adsorption rates followed by long equilibrium times indicate a complex adsorption process with an interplay between three likely mechanisms: Differences in structural sites of the adsorbent, size exclusion and pore blocking, and competitive adsorption between different starch species within a distribution. Each of these mechanisms will be

briefly discussed to further explain the results, and the resulting challenges in modelling these mechanisms together will be outlined.

First, different structural sites for adsorption. Between the different structural sites on the adsorbent, there will be a range of affinity values, leading to parallel adsorption processes, each with their own rate constants (Azizian, 2006). In the experimental setup in this study a combination of different structural sites on the adsorbent, and structural differences in adsorbate (varying molecular size and degree of branching) likely results in a broad range of affinity values leading to a broad range of rate constants for adsorption within and between the starch samples.

Second, the pore size distribution of the adsorbent, in combination with a size distribution of the adsorbate can lead to size exclusion, diffusion limitations, and pore blocking, which results in long equilibrium times (Haerifar & Azizian, 2013). Most of the total pore surface area of Norit CA1 is from 1-15 nm pores (Figure A2), only the smallest starches in all distributions fit in these pores. Starch samples with a larger fraction of molecules that can enter the 1-15 nm pores have access to a larger total adsorbent surface area, leading to a higher total adsorption capacity for these samples and thus higher equilibrium values. Since the size of the molecules and the size of the pores are in the same order of magnitude, the effective diffusion rate of starch molecules in these pores is severely reduced (Dechadilok & Deen, 2006; Renkin, 1956), resulting in longer equilibrium times. For starch molecules ≥15nm it is assumed that adsorption takes place at the surface of the AC rather than within the pores because the available pore volume is low (Figure A2) and smaller molecules with higher effective diffusion coefficients will outcompete larger molecules for access to these pores. Moreover, pore blocking likely plays a role since a substantial fraction of the starch molecules in these distributions are larger than the diameter of most pores. Temporary pore blocking reduces adsorption rates and thereby increases equilibrium times while permanent pore blocking decreases total adsorption capacity.

Third, competitive adsorption rates and equilibria. After initial adsorption of small molecules from a distribution, the smaller adsorbed molecules may desorb and be replaced by larger molecules from the distribution, as was observed for the adsorption of polyacrylamides on siliceous material (Bessaies-Bey et al., 2019; Hart & Aarão Reis, 2016) and for partially hydrolyzed polyacrylamides on clay particles (Nakatani, Mohler, & Hughes, 2021). Later data will show that this does not occur in this study. However, we will demonstrate that the rate of adsorption of individual species within a distribution depends on other species within the distribution.

Taken together, these mechanisms result in major challenges in the modelling this adsorption process. Deconvolution of these three mechanisms and quantifying their

individual effects in an adsorption model presents three main challenges: First, the aforementioned possibility of different structural sites, diffusion limitations and pore blocking. No adsorption isotherm describes all these processes (Koopal et al., 2020; Qiu et al., 2009). Second, the adsorption is shown to be size dependent and all samples have a distribution in molecular weight, three of which with a relatively high polydispersity (>1.75). Thus in this process there is no one true rate constant, but rather a range of rate constants depending on the width of the distribution present. Third, the substrate distribution is dynamic since the width of the distribution changes over time as small molecules in the distribution are adsorbed at a higher rate than the large molecules. The quantification of such complex systems is limited to simplified/lumped empirical descriptions, but the observed significant size selective effects underline the added value of including size selectivity into these empirical descriptions. Changes in average molecular weight (both number average and weight average) and polydispersity index during adsorption derived from HPSEC can be used to quantify the size selectivity during adsorption which adds more detail than traditional lumped adsorption models.

HPSEC

HPSEC was used to analyse the (change in) size distributions over time of the starches remaining in solution during adsorption. These size distributions were used to determine the number average molecular weight, weight average molecular weight, and polydispersity index of the starches. Figure 5 shows the peak height normalised and TSA area normalised HPSEC measurements for a subset of samples, the full data is shown in the appendix (Figure A6 and Figure A7).

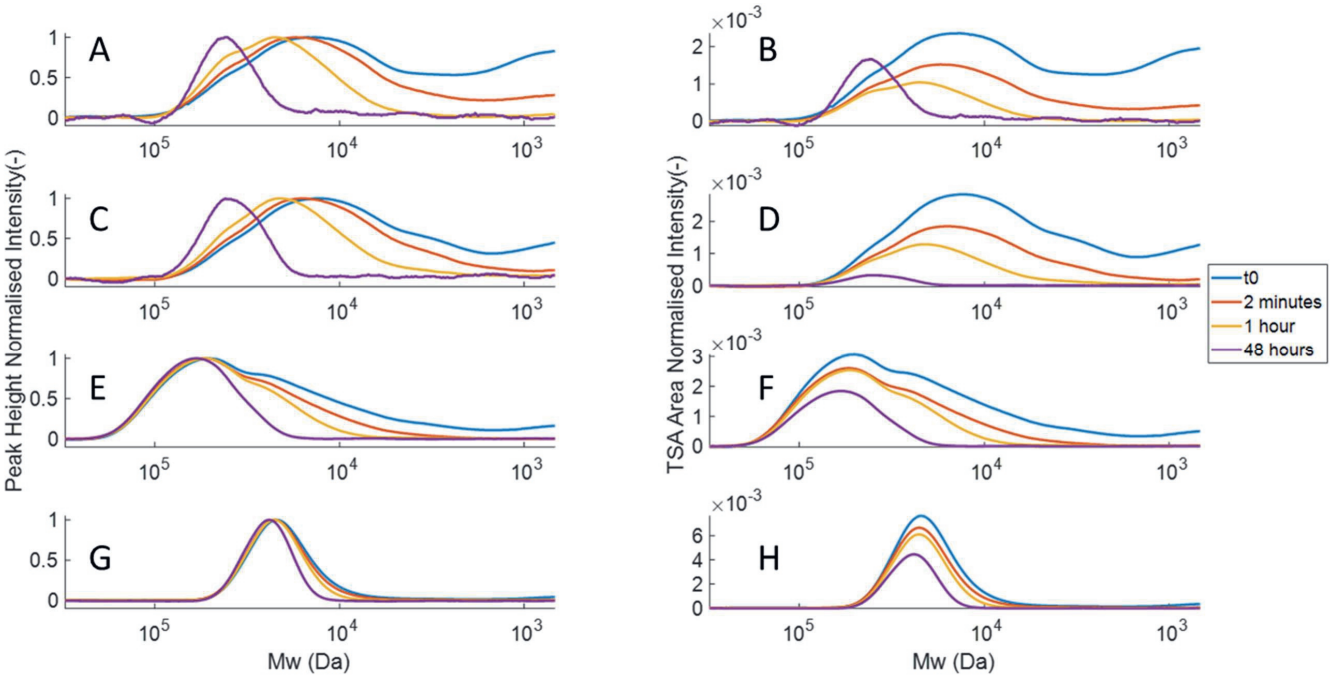

Figure 5 HPSEC measurements of the solubilised fraction of Paselli MD10 (subplots A&B), Eliane MD6 (subplots C&D), Eliane MD2 (subplots E&F), and HBS (subplots G&H) during 4 time points in an adsorption reaction with activated carbon. The chromatograms are normalised to a maximum peak intensity of 1 to best visualise the change in shape of the distribution over time (left column, subplots A, C, E & G) and area normalised to the Total Starch Assay result (right column, subplots B, D, F & H). To improve clarity of the results, only 4 chromatograms are shown per starch. The full data is shown in the Appendix (Figure A6 and Figure A7). Subplots are labelled A through H for future referencing.

Within each subplot, the t0 samples (blue lines) represent the starches before contact with activated carbon. Since the plots were peak height normalized, any change in the shape of the distribution over time indicates size selective effects. After incubation with activated carbon (red, yellow, and purple lines), the chromatograms change over time. In the peak height normalized chromatograms for Paselli MD10 and Eliane MD6 (Figure 5A, C) the peak shifts to the a higher molecular weight with increased incubation times and the peaks become narrower. Figure 5A, C and E show that for Paselli MD10, Eliane MD6 and Eliane MD2 the relative occurrence of starch molecules ≤ 1.1×10^4 Da decreases over time. After 48 hours (purple lines) the signal from these species can no longer be distinguished from the noise. This shows that the low molecular weight fraction of the distribution is removed from solution as these molecules were adsorbed and removed together with the activated carbon. This is in line the observation from the TSA results that small starch molecules show a higher affinity for adsorption on AC than larger starch molecules. In the TSA results size selective effects were observed between different starches, with HPSEC the size selectivity is also observed within the distributions. As a result of the removal of the fraction of small starch molecules, the distribution of molecules remaining in solution becomes narrower with longer incubation times, thus decreasing the polydispersity of the remaining starch in solution. Since there is no visible reoccurrence of starch molecules ≤ 1.1×10^4 Da when reaching the equilibrium, there is no indication that small molecules are desorbed and replaced by large molecules in this adsorption process.

For Paselli MD10 and Eliane MD6 (Figure 5A,C), the peak shifts to higher molecular weights over time. While for Eliane MD2 (Figure 5E), the peak remains at approximately 5×10^4 Da after incubation with AC and thus shows no clear shift over time. This indicates that the relation between molecular weight of a starch molecule and its rate of adsorption is observed only till a certain threshold value (~50 kDa) has been reached. This is in line with the results of (Lishchuk et al., 2017) where for certain polymers an adsorption plateau was reached, at which increased polymer size does not reduce the maximum adsorbed value further.

In addition to peak normalised chromatograms (Figure 5A,C,E,G), which provide insight in the change in shape of chromatograms over time, also TSA area normalised chromatograms are presented (Figure 5B, D,F,H). In general in HPSEC, the area under the chromatogram only provides a limited quantitative measure of the sample (Gidley et al., 2010). However, by normalising the area under the chromatogram to the measured total starch concentration, these areas now allow quantitative interpretation of the HPSEC chromatogram. Although some of the fundamental limitations of HPSEC (assumed universal calibration, nonlinear scaling of RI signal with concentration) are still present, the TSA normalised chromatograms provide a more intuitive interpretation

of the HPSEC chromatograms. The TSA area normalised data (Figure 5B,D,F,H) shows that for all samples, the signal intensity reduces with increasing incubation times for all molecular weights. This shows that adsorption does take place over the whole starch distribution. The Paselli MD10 48 hour sample deviates from this trend due to an unknown experimental error, figure A7 shows that the trend in Paselli MD10 is consistent up to 24 hours. For molecular weights above the ~50 kDa threshold in Eliane MD2, adsorption still takes place as shown in the TSA normalized chromatogram (Figure 5F), but appears to be no longer size selective as indicated by the peak height normalized chromatogram (Figure E).

The peak height normalized chromatogram for HBS (Figure F) shows reduced relative occurrence of molecular weight species in the range of 9×10^3 through 1.1×10^4 Da and a minimal shift of the peak to higher molecular weights with increased incubation times. HBS shows less pronounced size selective effects compared to the change over time in distribution shape in peak normalized chromatograms of Paselli MD10, Eliane MD6, and Eliane MD2 (Figure A,C,E).

From the HPSEC data, the number average molecular weight, weight average molecular weight, and polydispersity index of all the distributions were calculated using equations 3 - 5. The change in these indicators was used as a measure to quantitatively describe the size selectivity of the adsorption. The results of which are shown in Figure 6.

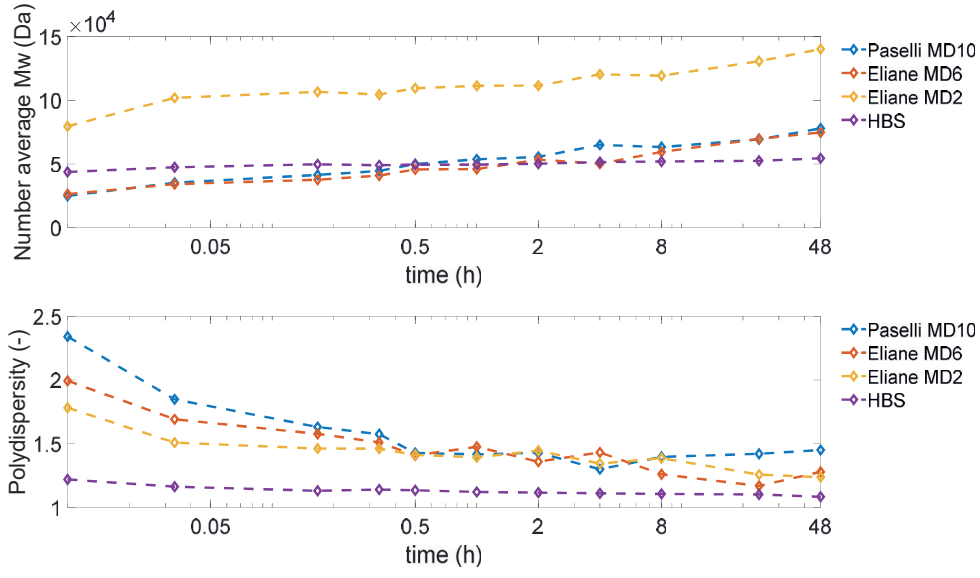

Figure 6 Number average molecular weight (top), and Polydispersity index (bottom) of the different starch distributions left in solution during incubation with activated carbon, calculated from HPSEC data.

Figure 6 (top) shows that all samples follow an upward trend in number average molecular weight with increased incubation times. Figure 6 (bottom) shows a decreasing trend of polydispersity with increased incubation times for all samples. The relative increase in number average molecular weight and relative decrease for polydispersity after 48 hours of incubation with AC (purple lines) compared to the t0 (blue lines) are given in Table 4.

Table 4 relative increase in number average molecular weight and relative decrease in polydispersity after 48 hours of incubation with activated carbon compared to before incubation

Name:	**Relative increase in number average molecular weight (%)**	**Relative decrease in polydispersity (%)**
Paselli MD10	213	38
Eliane MD6	184	36
Eliane MD2	76	31
HBS	25	11

Modelling

Using the dummy distribution method, it was estimated that small molecules (represented by a 20th percentile molecule size) in a distribution adsorb at a 4x, 5.8x, 7x, and 7.9x higher rate for Paselli MD10, Eliane MD6, Eliane MD2, and HBS respectively compared to large molecules in the same distribution (represented by an 80th percentile molecule). In this data, a trend is visible where the ratio of adsorption between large and small species of starch within a distribution increases with increasing average molecular size of the starch sample**.** Counterintuitively, higher relative decrease in polydispersity in starch samples does not lead to a higher difference in adsorption rates over the width of the distribution for these samples. The difference between the 20-80 rate ratio between the Eliane MD6 (5.8x) and Eliane MD2 (7x) starch samples is explained by the wider distribution of Eliane MD2 compared to Eliane MD6, meaning that the 20th and 80th percentile are further apart for Eliane MD2 compared to Eliane MD6. Therefore, a larger difference in adsorption rates between these species is expected. The calculation of polydispersity and decrease thereof during adsorption is sensitive to the width of the distribution, but is also heavily influenced by the bi-modal character of Eliane MD6 and Paselli MD10. A bi-modal character is less present in Eliane MD2 and absent in HBS. This can result in an erroneous interpretation of the data when the decrease in polydispersity over time is used as the sole indicator. Figure 7 shows the adsorption rates of the bulk (indicated by square data markers) and 20th and 80th percentile (indicated by circle data markers) for each of the four starch samples.

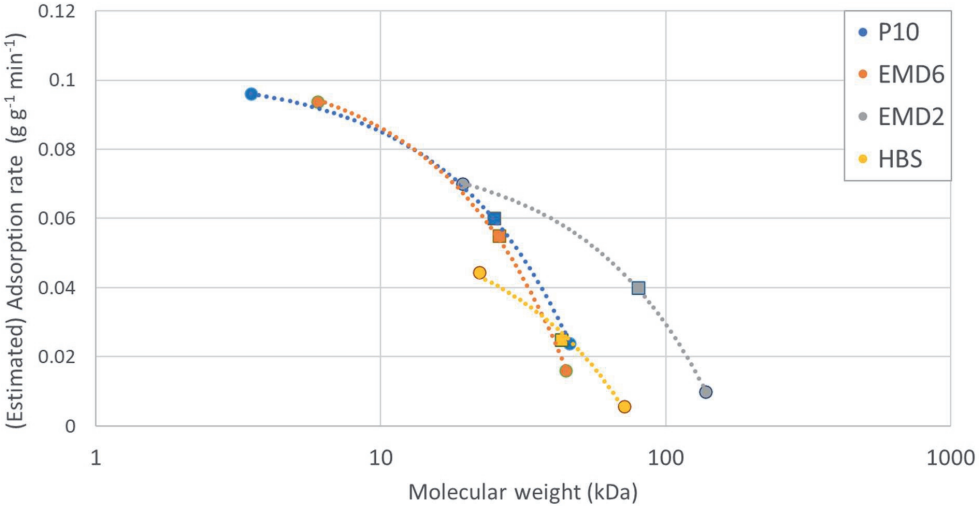

Figure 7 Estimated adsorption rates versus molecular weight for 4 starch samples. The second point in each series (squares) of 3 points represents the average bulk adsorption rate as measured by TSA, while the 1st and 3rd points (circles) in each series represent the adsorption rate of molecules with the 20th and 80th percentile size as estimated with the dummy distribution method. Dotted lines represent linear trendlines fitted on the simulated and measured data.

All samples show a downward trend where the adsorption rate decreases with increasing molecular weight within a sample. Eliane MD6 and Paselli MD10 adsorb at similar rates over the breadth of their molecular weight distribution. The 20th percentile estimated adsorption rates for Eliane MD2, falls on the trendlines for Eliane MD6 and Paselli MD10. However, the average and 80th percentile adsorption rates for Eliane MD2 deviate from the Eliane MD6 and Paselli MD10 trendlines. The average of Eliane MD2 shows a higher adsorption rate than the 80th percentile estimated values for Paselli MD10 and Eliane MD6 (0.04 vs 0.02 g g^{-1} min^{-1}), while the molecular weight average of Eliane MD2 is also higher than the 80th percentile molecular weight of Eliane MD6 and Paselli MD10 (80 kDa vs 14 kDa). This difference in adsorption rate is thus not explained by the molecular weight itself and cannot be explained by differences in structure of the starches since the 80th percentile Mw molecules for Paselli MD10 and Eliane MD6 have the same degree of branching as Eliane MD2. Linear molecules from the amylose fraction in Paselli MD10 or statistical occurrence of linear molecules with 5% degree of branching are not present at the 80th percentile molecular weight of these starches. Rather, the difference in adsorption rates between Paselli MD10 and Eliane MD6, and Eliane MD2 is explained by competitive adsorption of molecules within a distribution. Since Paselli MD10 and Eliane MD6 contain a large fraction of molecules that adsorbs rapidly in the initial stages, there are fewer adsorption sites available for the larger molecules in the distribution. In Eliane MD2, there are relatively fewer molecules in the distribution that rapidly adsorb and occupy adsorption sites. From this data, it can be

concluded that the adsorption rate of a starch species within a sample depends on the smaller starch molecules present within the sample distribution. Considering that smaller molecules within the starch distributions can access pores that the large molecules cannot, the molecules that adsorb within the pores do not contribute to the competition with large molecules. If an equal amount of the adsorbent's surface area was available to all molecule sizes within a distribution, the effects of competition would be greater than what is observed in this study. Therefor it is likely that in adsorption within non-porous materials the competition effect is greater than wat is found in this study.

Considering the difference in degree of branching between Paselli MD10 and Eliane MD6, and HBS, it is expected that a highly branched molecule (7.5% branching) of similar molecular weight as a 5% branched molecule adsorbs at a lower rate. This is observed when comparing the 20th percentile HBS adsorption rates with the average adsorption rates of Paselli MD10 and Eliane MD6. Here, for similar molecular weights, HBS adsorbs at a lower rate than Paselli MD10 and Eliane MD6 (0.045 vs 0.059 g g^{-1} min^{-1}). This trend is no longer present when comparing the adsorption rate of an average size HBS molecule, which is similar to adsorption rates for the 80th percentile molecular weight species in Paselli MD10 and Eliane MD6 at similar molecular weight. Here the effect of structural differences between Paselli MD10 and Eliane MD6, and HBS is no longer represented in adsorption rates. However, adsorption of the 80th percentile molecular weight molecules of Paselli MD10 and Eliane MD6 is likely retarded by internal competition. Differences in adsorption rates due to structural differences between the samples and effects of internal competition have a similar magnitude but in opposite direction, resulting in these influences cancelling out. From this data it can be concluded that competition between different starch species within a distribution, can have as much as an effect on the adsorption rates as differences in structure between starch samples and thus both structure and internal competition are important factors in the adsorption of a starch distribution.

The presence of molecular size distributions, structural differences between or within samples (linear, branched, or highly branched), internal competition on the adsorption of individual species within a sample, and accessibility of pores by a subset of the molecular weight distribution, results in a complex system where measuring adsorption coefficients of individual species within a distribution is not feasible. However, average adsorption rates are insufficient to describe the adsorption in such complex systems since we have demonstrated that adsorption rates within a distribution can vary by a factor 4 to 7.9. Therefore, a three point adsorption model (average, 20th percentile and 80th percentile) is proposed, which is a relatively simple adsorption model that also

includes differences in adsorption rates within a distribution that arise in complex adsorption system with distributed feedstocks.

4.4 Conclusions

In this paper we have demonstrated that the rate of adsorption of starches on activated carbon depends molecular size, degree of branching, and competition within a sample distribution. These effects result in an adsorption rate difference of a factor 4 to 8 between small (20^{th} percentile) and large (80^{th} percentile) molecules within the same distribution. A three-point metric is proposed that includes the measured average adsorption rate for the distribution and an estimation of the adsorption rate of the 20^{th} and 80^{th} percentile molecular weight species within the distribution as a measure of size selectivity in adsorption.

With a similar degree of branching, smaller molecules (Eliane MD6 compared to Eliane MD2) adsorb at an approximately 38% higher initial rate (0.055 g g^{-1} min^{-1} vs 0.04 g g^{-1} min^{-1}) and to an approximately 41% higher maximum (0.24 g g^{-1} vs 0.17 g g^{-1} adsorbed after 48 hours) than large molecules. A threshold molecular mass (~50 kDa), after which molecular mass selectivity disappears, has been observed. For starches of similar size (HBS and Eliane MD6) a higher degree of branching lowered the initial adsorption rate and lowered the maximum adsorbed amount.

By simulating dummy distributions an estimation of the adsorption rates of the 20^{th} and 80^{th} percentile molecular size starch species compared to the average molecular size in the distribution was made. it was estimated that small molecules (20^{th} percentile) within the sample's distributions adsorb at an estimated 4x, 5.8x, 7x, and 7.9x higher rate than large molecules (80^{th} percentile) in the same distribution for Paselli MD10, Eliane MD6 , Eliane MD2, and HBS respectively. Comparing estimated adsorption rates at similar molecular weight for different samples showed that in addition to differences in structure, the internal competition in adsorption between different starch species in the same distribution had a relevant influence on the adsorption rate. The magnitude of the effect of internal competition is roughly in the same order of magnitude as a structure difference between a 5% and 7.5% branched starch, showing that internal competition is a relevant factor in adsorption of feedstocks with a molecular weight distribution.

Models that include size dependent kinetics, as an improvement over models that use averaged values for distributions, can be an effective tool to aid in the design of catalytic processes for the conversion of polydisperse feedstocks. The dummy distribution method used in this paper constitutes one such a model that provides size dependent kinetics based on the average of the distribution, and an estimate for the 20^{th} and 80^{th} percentile molecular sizes of a distribution.

4.5 Acknowledgements

This work was supported by the Dutch Research Council (NWO) [grant number 870.15.120].

4.6 References

Azizian, S. (2006). A novel and simple method for finding the heterogeneity of adsorbents on the basis of adsorption kinetic data. *Journal of Colloid and Interface Science, 302*(1), 76-81. doi:https://doi.org/10.1016/j.jcis.2006.06.034

Bertoft, E. (2017). Understanding Starch Structure: Recent Progress. *Agronomy, 7*(3). doi:10.3390/agronomy7030056

Bessaies-Bey, H., Fusier, J., Hanafi, M., Zhang, S., Destarac, M., Jouenne, S., . . . Sanson, N. (2019). Competitive adsorption of PAM and HPAM on siliceous material. *Colloids and Surfaces A: Physicochemical and Engineering Aspects, 579*, 123673. doi:https://doi.org/10.1016/j.colsurfa.2019.123673

Dao, T.-H., Vu, T.-Q.-M., Nguyen, N.-T., Pham, T.-T., Nguyen, T.-L., Yusa, S.-i., & Pham, T.-D. (2020). Adsorption Characteristics of Synthesized Polyelectrolytes onto Alumina Nanoparticles and their Application in Antibiotic Removal. *Langmuir, 36*(43), 13001-13011. doi:10.1021/acs.langmuir.0c02352

Dechadilok, P., & Deen, W. M. (2006). Hindrance Factors for Diffusion and Convection in Pores. *Industrial & Engineering Chemistry Research, 45*(21), 6953-6959. doi:10.1021/ie051387n

Ding, X., Zhu, H., Ren, H., Liu, D., Yu, Z., Shi, N., & Guo, W. (2020). Adsorption and dehydrogenation of C2–C6n-alkanes over a Pt catalyst: a theoretical study on the size effects of alkane molecules and Pt substrates. *Physical Chemistry Chemical Physics, 22*(38), 21835-21843. doi:10.1039/D0CP03194A

Durrani, C. M., & Donald, A. (2000). Shape, molecular weight distribution and viscosity of amylopectin in dilute solution. *Carbohydrate Polymers, 41*, 207-217. doi:10.1016/S0144-8617(99)00070-3

El'tekov, A. Y., El'tekova, N. A., & Roldughin, V. I. (2007). Kinetic coefficients of the adsorption of polysaccharides from aqueous solutions by Sibunit. *Colloid Journal, 69*(2), 248. doi:10.1134/S1061933X07020160

Fu, Z., & Santore, M. M. (1998). Kinetics of Competitive Adsorption of PEO Chains with Different Molecular Weights. *Macromolecules, 31*(20), 7014-7022. doi:10.1021/ma980042w

Gidley, M. J., Hanashiro, I., Hani, N. M., Hill, S. E., Huber, A., Jane, J.-L., . . . Gilbert, R. G. (2010). Reliable measurements of the size distributions of starch molecules in solution: Current dilemmas and recommendations. *Carbohydrate Polymers, 79*(2), 255-261. doi:https://doi.org/10.1016/j.carbpol.2009.07.056

Haerifar, M., & Azizian, S. (2013). Mixed Surface Reaction and Diffusion-Controlled Kinetic Model for Adsorption at the Solid/Solution Interface. *The Journal of Physical Chemistry C, 117*(16), 8310-8317. doi:10.1021/jp401571m

Hart, R. C., & Aarão Reis, F. D. A. (2016). Random sequential adsorption of polydisperse mixtures on lattices. *Physical Review E, 94*(2), 022802. doi:10.1103/PhysRevE.94.022802

Hoogstad, T. M., Konings, G., Buwalda, P. L., Boxtel, A. J. B., Kiewidt, L., & Bitter, J. H. (2019). The effect of polydispersity on the conversion kinetics of starch oxidation and depolymerisation. *Chemical Engineering Science: X, 4*, 100044. doi:https://doi.org/10.1016/j.cesx.2019.100044

Hulea, V. (2018). Toward Platform Chemicals from Bio-Based Ethylene: Heterogeneous Catalysts and Processes. *ACS Catalysis, 8*(4), 3263-3279. doi:10.1021/acscatal.7b04294

Kast, W. (1989). Physical Adsorption on Heterogeneous Solids. Von M. Jaroniec und R. Madey. Elsevier Science Publishers, Amsterdam – New York 1988. XIV, 353 S., zahlr. Abb. u. Tab., geb., US-$ 131,50. *Chemie Ingenieur Technik, 61*(9), 766-766. doi:https://doi.org/10.1002/cite.330610931

Koopal, L., Tan, W., & Avena, M. (2020). Equilibrium mono- and multicomponent adsorption models: From homogeneous ideal to heterogeneous non-ideal binding. *Advances in Colloid and Interface Science, 280*, 102138. doi:https://doi.org/10.1016/j.cis.2020.102138

Lee, J.-W., Kwon, T.-O., & Moon, I.-S. (2004). Adsorption of monosaccharides, disaccharides, and maltooligosaccharides on activated carbon for separation of maltopentaose. *Carbon, 42*(2), 371-380. doi:https://doi.org/10.1016/j.carbon.2003.11.008

Lishchuk, S. V., Ettelaie, R., & Annable, T. (2017). On the structural polydispersity of random copolymers adsorbed at interfaces: comparison of surface and bulk distributions. *Molecular Physics, 115*(9-12), 1343-1351. doi:10.1080/00268976.2017.1292369

Nakatani, A. I., Mohler, C. E., & Hughes, S. (2021). Chain conformation of polymers adsorbed to clay particles: effects of charge and concentration. *Soft Matter, 17*(28), 6848-6862. doi:10.1039/D1SM00674F

Pluen, A., Netti, P. A., Jain, R. K., & Berk, D. A. (1999). Diffusion of Macromolecules in Agarose Gels: Comparison of Linear and Globular Configurations. *Biophysical Journal, 77*(1), 542-552. doi:https://doi.org/10.1016/S0006-3495(99)76911-0

Qiu, H., Lv, L., Pan, B.-c., Zhang, Q.-j., Zhang, W.-m., & Zhang, Q.-x. (2009). Critical review in adsorption kinetic models. *Journal of Zhejiang University-SCIENCE A, 10*(5), 716-724. doi:10.1631/jzus.A0820524

Renkin, E. M. (1956). filtration, diffusion, and molecular sieving through porous cellulose membranes. *Journal of General Physiology, 39*(5), 820-820. doi:10.1085/jgp.39.5.820

Schwartz, T. J., Shanks, B. H., & Dumesic, J. A. (2016). Coupling chemical and biological catalysis: a flexible paradigm for producing biobased chemicals. *Current Opinion in Biotechnology, 38*, 54-62. doi:https://doi.org/10.1016/j.copbio.2015.12.017

Serrano, D. P., Melero, J. A., Morales, G., Iglesias, J., & Pizarro, P. (2018). Progress in the design of zeolite catalysts for biomass conversion into biofuels and bio-based chemicals. *Catalysis Reviews, 60*(1), 1-70. doi:10.1080/01614940.2017.1389109

Sheldon, R. A. (2014). Green and sustainable manufacture of chemicals from biomass: state of the art. *Green Chemistry, 16*(3), 950-963. doi:10.1039/C3GC41935E

Shirazi, M., van de Ven, T. G. M., & Garnier, G. (2003a). Adsorption of Modified Starches on Porous Glass. *Langmuir, 19*(26), 10829-10834. doi:10.1021/la0350655

Shirazi, M., van de Ven, T. G. M., & Garnier, G. (2003b). Adsorption of Modified Starches on Pulp Fibers. *Langmuir, 19*(26), 10835-10842. doi:10.1021/la035064c

Yamaguchi, T., Endo, K., Takagi, Y., & Hukao, K. (1977). Influence of Pore-size Distribution of Activated Carbons on the Correlation between Adsorptivities of Oligosaccharides and Their Degree of Polymerization. *NIPPON KAGAKU KAISHI, 11*. doi:10.1246/nikkashi.1977.1577

4.7 Appendix

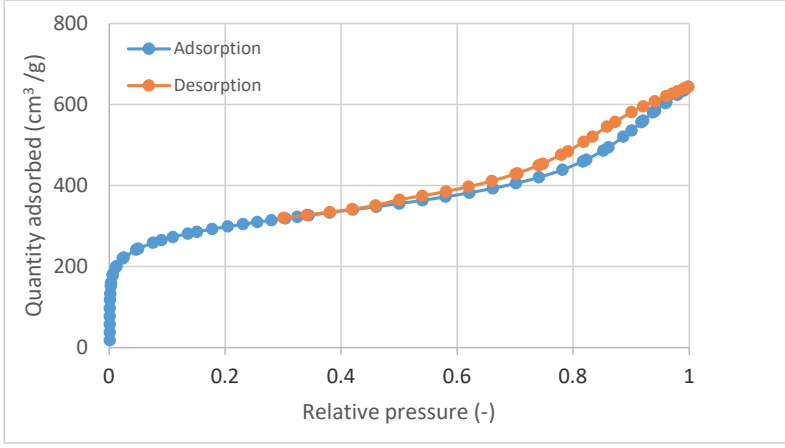

Figure A1 Adsorption and desorption isotherms of nitrogen. Quantity adsorbed is at standard temperature and pressure.

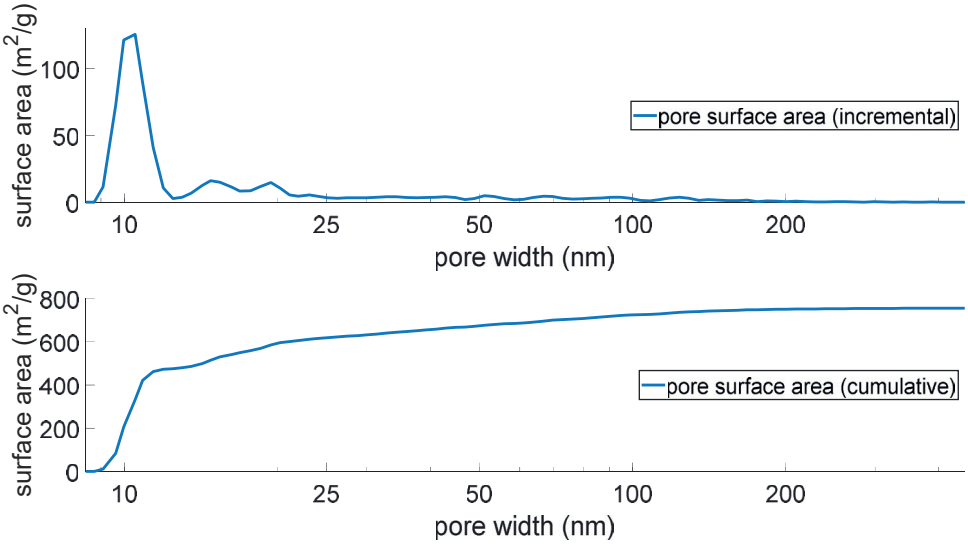

Figure A2 Pore surface area over incremental pore width (top) and cumulative pore area (bottom), as determined by N_2 physisorption.

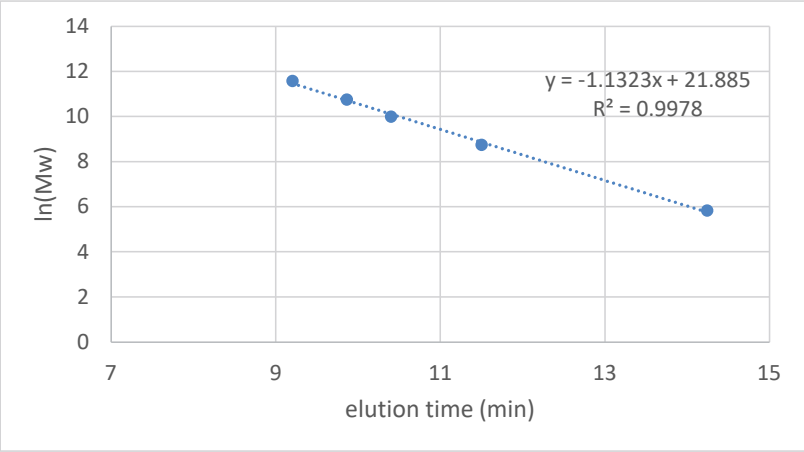

Figure A3 HPSEC calibration curve based on pullulan standards of 342 Da, 6.3 kDa, 22 kDa, 47 kDa, and 107 kDa (Supelco, Bellefonte, USA).

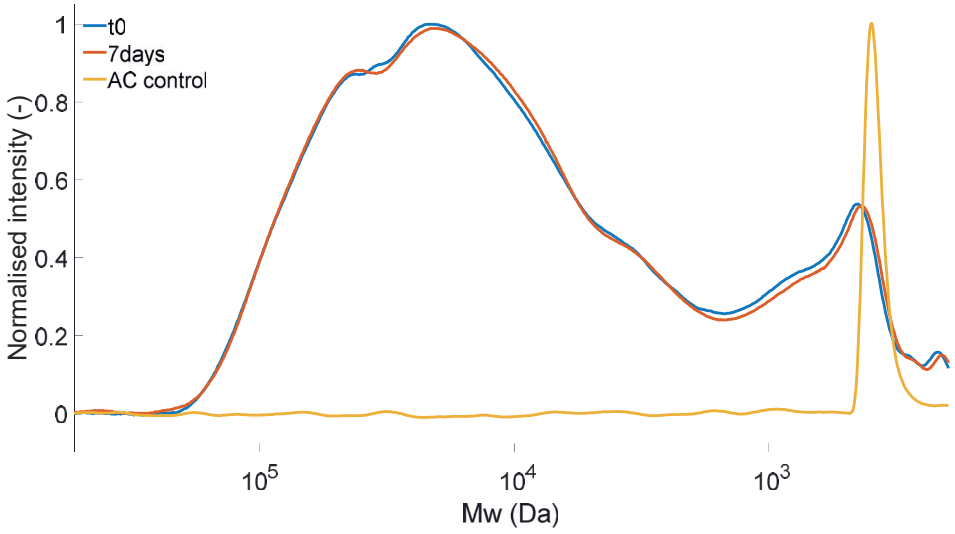

Figure A4 HPSEC chromatogram of the control samples. Negative control after 7 days without addition of AC, and AC blank. Note that a new peak arises at approximately 0.5 kDa for all samples that were treated with AC. This is the result of residues originating from the activated carbon that could not be removed from solution by centrifuging at either 10.000 x g rpm (in the main separation of AC from the solution) or at 19.000 x g rpm (before injecting onto the HPSEC column). This is confirmed by the AC blank samples.

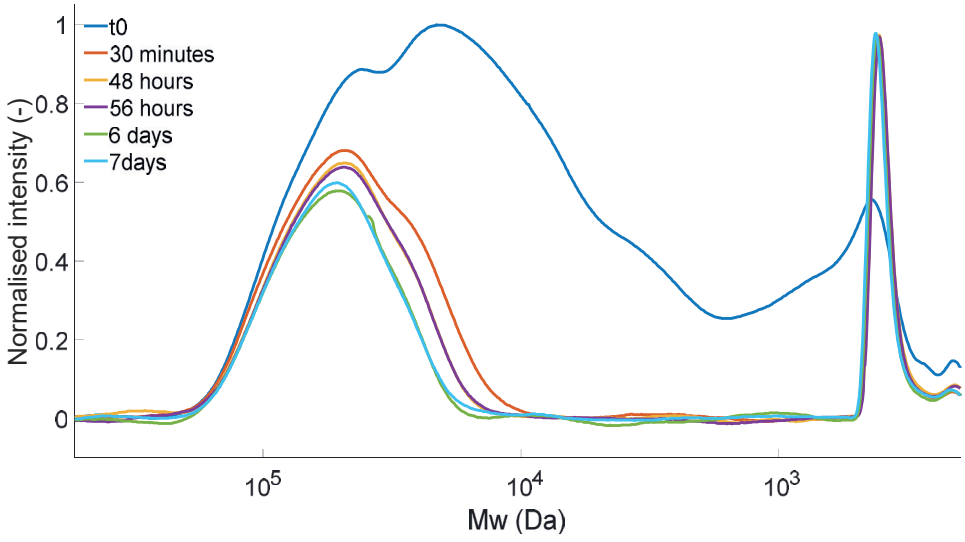

Figure A5 HPSEC diagrams of a mixture of Eliane MD6 and Eliane MD2. Adsorption experiments were performed as described in "Experimental setup and procedure" in the materials and methods but over a longer time period. 48 hours is considered the pseudo-equilibrium in this study, since the 48 hours and the 56 hour samples completely overlap and thus no change is visible within 8 hours. True equilibrium takes up to 6 days.

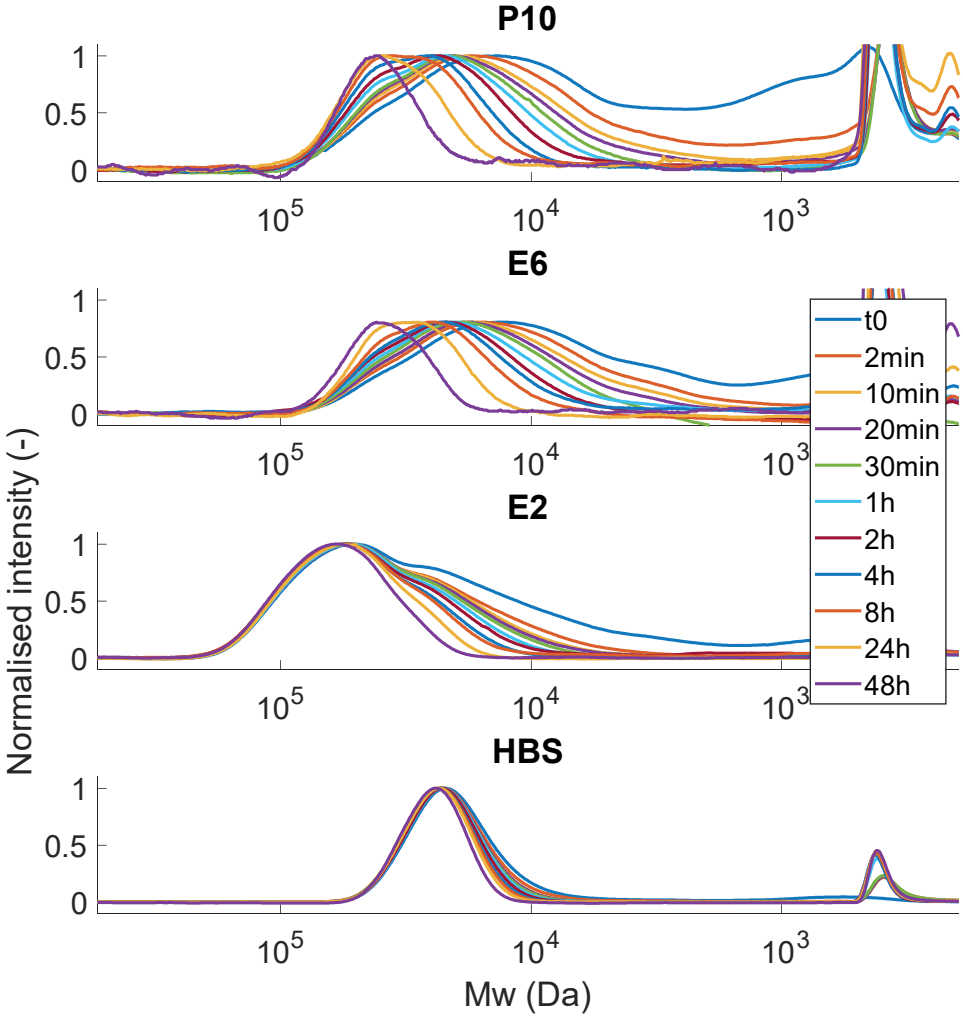

Figure A6 Baseline corrected and peak height normalised HPSEC chromatograms of all time points for the different starches.

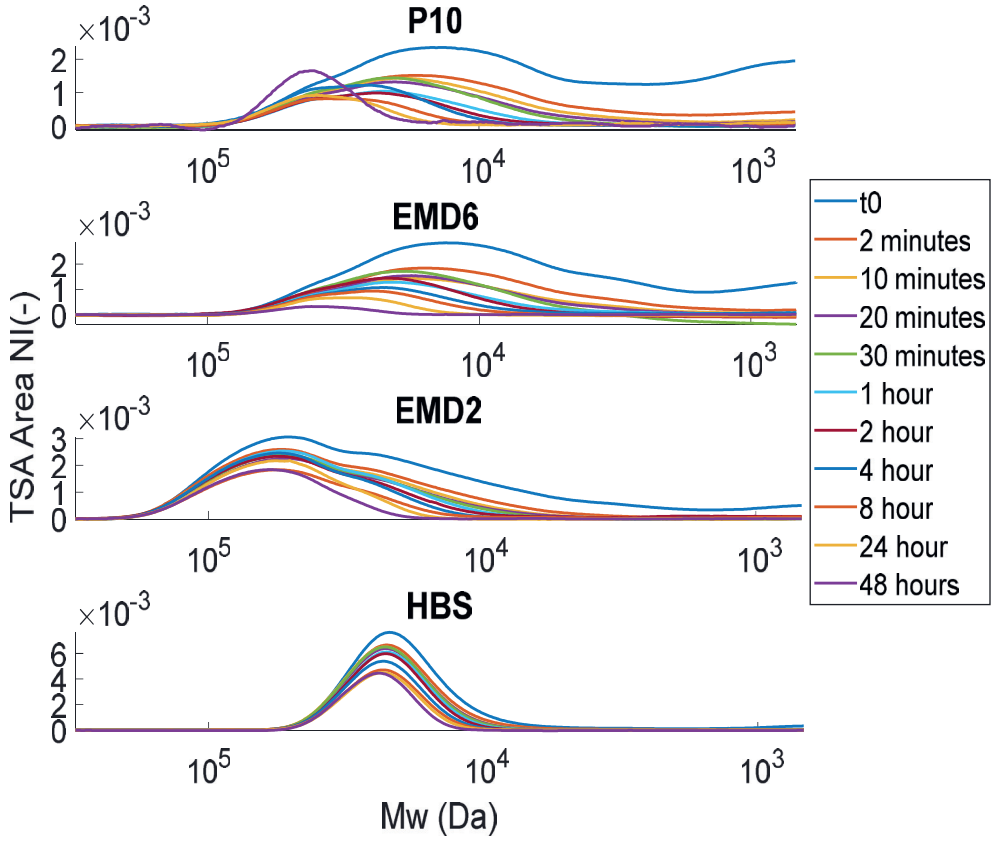

Figure A7 Baseline corrected and TSA area normalised HPSEC chromatograms of all time points for the different starches.

5.

5. Modelling the diffusion of polydisperse macromolecular feedstocks in a porous catalyst support

This chapter is to be submitted: Hoogstad, T. M., van Noord, A., Kiewidt, L., & Bitter, J. H. Modelling the diffusion of polydisperse macromolecular feedstocks in a porous catalyst support

Abstract

Macromolecules from biobased feedstocks are a renewable source for biobased materials, chemicals, and fuels. These macromolecules require catalytic modifications to introduce additional functionalities. However, the size and polydispersity of these substrates introduces a significant mass-transfer challenge in designing heterogeneously catalysed processes for the conversion of these macromolecules. Studies on diffusion of polydisperse biobased macromolecules (r > 10nm) are lacking. In this study, a reaction-diffusion model was used to describe the diffusion and reaction of a polydisperse macromolecular substrate. Normally distributed substrates with varying average size (10 to 100nm) standard deviation σ (20% or 50% of the average), were simulated for conversion in a catalyst with pore sizes ranging from 25 to 250 nm. The results showed that if a system is diffusion limited, the product distribution will consist mostly of tail-end molecules from the substrate distribution, this difference between initial and final distribution was larger for substrate distributions with higher standard deviation. Optimum pore sizes in the trade-off between diffusion limitation versus specific surface area were determined in the range of approximately 2.2 to 2.8 times the molecule size. At optimal pore sizes, difference between the initial and product distribution increased with increasing substrate polydispersity (4% for $\sigma = 0.2\mu$ vs 15% for $\sigma = 0.5\mu$). The overall catalyst activity at optimal pore sizes exponentially with increasing molecular size of the substrate. This trend implies a practical limit to the maximum size of a substrate for heterogeneously catalysed processes. Because of the severe mass transfer limitations in these conversions, a reverse design approach starting at the desired product distribution, and optimising yield within those requirements is advised.

Keywords: hindered diffusion; starch oxidation; modelling; polydispersity; dispersity

5.1 Introduction

Macromolecules from biobased feedstocks, e.g., polymers such as lignocellulose, alginate, and starch, are a source for biobased materials, chemicals, and fuels. These macromolecules often require modifications to their structure and/or chemical composition to introduce additional functionalities. Catalytic conversion of these biomacromolecules is a common strategy to introduce these modifications. However, the size and complexity of these substrates introduces a challenge in designing and optimising catalytic processes for the conversion of these macromolecules (Li, Cui, Wang, & Long, 2023; Sudarsanam, Peeters, Makshina, Parvulescu, & Sels, 2019). Currently in industry, heterogeneous catalysis is applied in approximately 80- 90% of the catalytic processes (Bravo-Suárez, Chaudhari, & Subramaniam, 2013; Copéret, Chabanas, Petroff Saint-Arroman, & Basset, 2003), because of the simple separation and re-use of the catalyst compared to homogeneous catalysis (Glotov & Karakhanov, 2021). With heterogenous catalysis, catalytically active nanoparticles are bound in a porous matrix of a catalyst support material. Porous supports for heterogeneous catalysis can be microporous (pore radius <2 nm), mesoporous (2 nm< pore radius < 50 nm), or macroporous (pore radius >50nm) (Table 1). The pore size and specific surface area are inversely related. In the design of a catalyst support material, a trade-off is made in the selection of the pore sizes between minimising mass transfer limitations in a catalyst by providing pores of a sufficient size, and maximizing the specific surface area of the catalyst.

Table 1 pore sizes of some common catalyst support materials

Pore type	**Material**	**Pore radius (nm)**	**reference**
Meso-macroporous	α –Al_2O_3	1 – 488	(Masuda, Asoh, Haraguchi, & Ono, 2015; Sokolov, Bell, & Stein, 2003)
	Carbon nanotubes and fibres	5 – 250	(De Jong & Geus, 2000; Toebes, Bitter, van Dillen, & de Jong, 2002)
	Macroporous poly (IL) ([VSIM][HSO4] with Fe3O4 particles as hard template)	< 125	(Wu et al., 2016)
Mesoporous	γ –Al_2O_3	1-9	(Huang, Bartholomew, & Woodfield, 2014; Trimm & Stanislaus, 1986)
	SBA-15	1.4-6.4	(Katiyar, Yadav, Smirniotis, & Pinto, 2006)
	IRMOF-74-XI	4.5	(Deng et al., 2012)

	MCM-41	0.9-5	(J. S. Beck et al., 1992)
Microporous	MIL-101(Cr)	0.6-1.7	(Férey et al., 2005)
	Activated carbon	< 1	(Adelhelm & De Jongh, 2011)
	Cloverlite	0.3 – 0.7	(Estermann, McCusker, Baerlocher, Merrouche, & Kessler, 1991)
	ZSM-5	0.3	(van Koningsveld, Jansen, & van Bekkum, 1990)

The largest application fields of heterogeneous catalysis are petroleum refining (e.g. hydroprocessing, cracking, alkylation), chemical processing (e.g. oxidation, hydrogenation, ammonia production) and automotive emission control (Bravo-Suárez et al., 2013). Among the largest substrates in these application fields are asphaltenes with a molecular weight ranging between 500 – 10000 Dalton (Groenzin & Mullins, 2000; Speight, Wernick, Gould, Overfield, & Rao, 1985) and molecular radius ranging between 1.5 and 20 nm (Durand et al., 2010; Eyssautier, Frot, & Barré, 2012; Groenzin & Mullins, 2000). Traditional pore networks in support materials used for heterogeneous catalysts are aimed at conversion of relatively small substrates (roughly <1nm) (Table 1).

However, biopolymers like lignocellulose, alginate, and starch, can have molecular sizes much larger the asphaltene fraction (Table 2). As a result, catalytic modification of biopolymers through heterogeneous catalysis faces additional challenges in the form of reduced bulk diffusion rates as described by the Stokes-Einstein relation, hindered diffusion (when the size of the pore and substrate are in the same order of magnitude), and pore blocking if the pore size is lower than the molecular size (Dechadilok & Deen, 2006; Deen, 1987; Renkin, 1956). Moreover, these biopolymers are often polydisperse meaning they have a wide distribution in their molecular sizes. The width of such a distribution is expressed with the polydispersity index (PI) or dispersity index (D), which is defined as the weight average molecular weight of a sample divided by the number average molecular weight of the sample. The larger the polydispersity index, the wider the distribution of the biopolymer. The differently sized molecules within a biopolymer distribution have different bulk diffusion rates as described by the Stokes-Einstein relation; molecules with a larger radius have a lower bulk diffusion coefficient.

Note that exact molecular sizes of biopolymers are challenging to measure accurately and consistently, as it depends on among other factors, the extraction method, solvent, and variability in substrate source. In addition, experimental and analytical procedures influence the obtained values for the measurements of a single sample across different laboratories (Potthast et al., 2015). As a result, values obtained between different

studies cannot always be directly compared (Zhou et al., 2021). Therefor values given in table 2 are to be used as an estimation rather than precise data.

Table 2 sizes of biobased polymers and asphaltenes

	Hydrodynamic radius (nm)	**PI**
Asphaltenes	5 – 10 (Eyssautier et al., 2012) 1.5 – 2.2 (Durand et al., 2010) 10-20 (Groenzin & Mullins, 2000)	1.8 – 2.1 (Durand et al., 2010)
Cellulose	20-50 (Chang et al., 2016)	2-7 (Emsley, Ali, & Heywood, 2000)
Hemicellulose	34–57 (Shen et al., 2021)	1.37-1.61 (Xie et al., 2020)
Lignin		
	8.4 – 33.5 (Gidh, Decker, See, Himmel, & Williford, 2006) 2-50 (Li et al., 2023)	1.65 – 8.8 (Tolbert, Akinosho, Khunsupat, Naskar, & Ragauskas, 2014)
Amylopecin	110 – 267 (Rolland-Sabaté, Guilois, Jaillais, & Colonna, 2011) 76 – 97 (Zou, Xu, Wen, & Yang, 2020)	1.04 – 1.27 (Mua & Jackson, 1997) >100 (Bertoft, 2017; Stacy & Foster, 1957) 2.22-3.39 (Zou et al., 2020)
Pectin	9 (Gu & Catchmark, 2013) ~ 22 (Masuelli, 2011)	1.15 (Gu & Catchmark, 2013) 3.81-4.38 (Deckers, Olieman, Rombouts, & Pilnik, 1986)
Alginate	43-59 (Nowak et al., 2021)	1.4-6 (Draget, Smidsrød, & Skjåk-Bræk, 2005)

The large molecular size of biopolymers and the resulting diffusion, pore blocking of large molecules are contributing causes that current processing/modification techniques for biopolymers first break them down into platform molecules before further catalytic upgrading. However, maintaining some of the original structure of the biopolymers is beneficial for specific applications. Some examples of this are found in the modification of inulin fibres for colon drug targeting (Giri, Dutta, & Giri, 2021), modification of barley dietary fibres, (Park, Lee, & Lee, 2013), production of aerogel

fibres for insulating materials (Tafreshi et al., 2022), and starch oxidation (Grommers & van der Krogt, 2009).

The catalytic upgrading of biopolymers, without depolymerisation into their respective monomers, requires specialised catalysts with pore sizes that are compatible with the large molecular size and the substrate polydispersity. To guide the design of such catalyst, diffusion models that mathematically describe and simulate the (hindered) diffusion of particles in porous materials can be utilised.

Mathematical approximations for diffusion of macromolecules in porous media date back to early 20th century to understand the permeability of membranes. Researchers found that diffusion rates of molecules through a membrane of a certain pore sizes would result in lower effective diffusion coefficients than expected. The closer the size of the pore to the size of the molecule, the lower the effective diffusion coefficient (Renkin, 1956). The reduced diffusivity of molecules through a membrane was ascribed to hindered diffusion. Around the 1970s the consensus was that hindered diffusion could be ascribed to both a diffusive and convective phenomenon (R. E. Beck & Schultz, 1970). Diffusion of a solute in a pore is lower than in the bulk solution, as the molecule experiences drag imposed by the pore wall. In a similar fashion, the convective transport is impaired by the retarding effect of the pore wall on the solute velocity. In the mathematical models, these phenomena are captured by fitted empirical equations like the Renkin equation (Renkin, 1956) 1956) or a combination of hydrodynamic hindrance factors for enhanced drag and the lag coefficients (Dechadilok & Deen, 2006; Deen, 1987). By implementing these concepts mathematical models can quantify mass transfer (limitations) for varying pore sizes and particle sizes.

Some ground-breaking work has been done with these diffusion models for the diffusion of “large” molecules in catalyst like asphaltenes. (Baltus & Anderson, 1983) confirmed that experimentally diffusion coefficients of asphaltenes through a porous membrane were in “good agreement” with predicted diffusion coefficients from hydrodynamic theory of hindered diffusion. (Tayakout et al., 2010) investigated and described the diffusion of different fractions of asphaltenes in a porous catalyst materials through experiments and modelling. The authors showed that both diffusion limitations as well as adsorption are highly relevant factors to consider in catalyst for heavy oil hydrotreatment. (Parkhomchuk et al., 2021) investigated a multi-scale model for the conversion of macromolecules in a hierarchical alumina catalyst. In this study and in a similar work by (Semeykina, Malkovich, Bazaikin, Lysikov, & Parkhomchuk, 2018) the authors considered theoretical macromolecules of 10nm in size, which is in line with the size of asphaltenes. (Parkhomchuk et al., 2021) recommended pore sizes >70nm for conversion with this substrate.

Although these studies are aimed at macromolecules, studies that investigate macromolecules with sizes in the range of biopolymers are lacking. Moreover, in these studies the effect of molecular weight distributions were not quantified. Molecular weight distributions have been shown to have an effect on processes with polydisperse and macromolecular substrates (Hoogstad, Kiewidt, van Haasterecht, & Bitter, 2023; Hoogstad et al., 2019; Khaleel, Sisco, Tavakkoli, & Vargas, 2022) but is often not considered. The knowledge gap on quantitative diffusion of macromolecules (>10nm) and the effect of molecular weight distributions is also recognized as a major point of improvement for the field in the work of (Li et al., 2023) on the potential of heterogeneously catalysed depolymerisation of lignin.

In this work, we consider a reaction-diffusion model for the oxidation of starch as a case study to represent the catalytic conversion of a generic macromolecular and polydisperse feedstock. This model is used to evaluate the influence of catalyst pore size, average molecular size of the substrate, and the substrate distribution width on overall catalyst activity and the molecular weight distribution of the product. Subsequently, the optimum in the trade-off between high catalyst specific surface area (where smaller pore sizes are beneficial), and mediating diffusion limitations (where larger pore sizes are beneficial) for varying substrate sizes and distributions is evaluated. Finally, implications of these findings on the design process for catalysts for heterogeneous catalysis of polydisperse macromolecular feedstocks are discussed.

5.2 Materials and methods

5.2.1 Reaction diffusion model

A reaction diffusion model was used to describe the diffusion and reaction of a polydisperse macromolecular substrate. Substrates of varying average size (10, 25, 50, 75, 100nm) with two distribution widths (normal distribution with $\sigma = 0.2\mu$, and $\sigma = 0.5\mu$) were simulated for conversion in a catalyst with varying pore sizes (25, 35, 50, 65, 75, 100, 125, 150, 175, 200, 225, and 250 nm), resulting in 120 distinct simulation runs.

The reaction-diffusion model describes the hypothetical diffusion and oxidation of polydisperse starch molecules in a porous catalyst layer of 50 µm length with a porosity of 0.6. Conversion of the starch molecules is assumed to only take place within the pores of the catalyst. The geometries of the starch molecules and the catalyst pores were considered as rigid spheres and uniform cylinders respectively. The bulk liquid was assumed to be ideally mixed. The temperature in both the bulk liquid and the catalyst layer was set to 50 °C. The reaction time was fixed for all reactions at 16 hours. Python (v2.7) was used to carry out all calculations, and the visualizations were done in MatLab (Mathworks).

To capture the behaviour of differently sized starches, the starch molecules were discretised into different classes based on their molecular size. The change in concentration of each class of molecules over the length of the pore and over time was calculated using mass balance equations (eq. 1).

$$\epsilon \frac{\partial C_i}{\partial t} = -\frac{\partial J_i}{\partial x} + r_i \qquad (1)$$

Both the molecular diffusion ($-\frac{\delta J_i}{\delta x}$) and the oxidation rate (r_i) of the starches were considered to contribute to the change in concentration. J_i represents the flux of each class of molecules and ϵ the porosity of the catalyst.

Fick's law was used to describe molecular diffusion in the pores of the catalyst. The diffusion rate was determined for each class of starch molecules (i) over space and time (eq. 2). Based on the planar geometry of the catalyst, the Fickian diffusion was described in the Cartesian coordinate system. Molecules were assumed to only diffuse in the length of the pore. The molecular diffusion was defined according to equation 3.

$$J_i = D_i \frac{\partial C_i}{\partial x} \qquad (2)$$

$$\frac{\partial C_i}{\partial t} = \frac{1}{\epsilon} \cdot \frac{\partial J_i}{\partial r} \qquad (3)$$

The diffusion coefficient (D_i) for each class of starch molecules was determined based on a combination of Stokes-Einstein equations (eq. 4) and the Renkin equation for hindered diffusion (eq. 5). The diffusion in the bulk (D_{b_i}) was calculated with the Stokes-Einstein equation, which describes the diffusion of spherical particles in a liquid with a low Reynolds number (eq. 4).

$$D_{b_i} = \frac{k_b T}{6 \pi \eta r_m} \tag{4}$$

The Renkin equation proposed in Renkin et al. (1956) is used to calculate the total restriction in diffusion of a molecule, given as ratio between the diffusion in the pore (D_i) and bulk (D_{b_i}), based on the pore radius (r_p) and molecule radius (r_m) (eq. 5). The D_i for each class was based on the average r_m in that particular class. If $r_m > r_p$, D_i was reduced to zero to simulate size-exclusion. r_p was a fixed value in each simulation and varied between simulations (no distribution in pore size is assumed).

$$\frac{D_i}{D_{b_i}} = \left(1 - \frac{r_m}{r_p}\right)^2 \left[1 - 2.1\left(\frac{r_m}{r_p}\right) + 2.09\left(\frac{r_m}{r_p}\right)^3 - 0.95\left(\frac{r_m}{r_p}\right)^5\right] \tag{5}$$

Starch sizes are expressed using two metrics, mass based (Mw or DP) or volume based (r_{m_i}). r_{m_i} was converted to Mw though an empirical equation based on Bertoft (2017)(eq. 6). The DP_i was derived from the MW_i, by dividing Mw by the molecular weight of a AHG molecule i.e. 162 g mol^{-1} (eq. 7). The DP was subsequently used to convert the concentration of starch molecules in mol m^{-3} to AHG L^{-1} (eq. 8).

$$\log_{10}(MW_i) = 2.059 \log_{10}(r_{m_i}) + 22.357 \tag{6}$$

$$DP_i = \frac{MW_i}{MW_{AHG}} \tag{7}$$

$$C_{i_{AHG}} = C_i \, DP \tag{8}$$

The initial substrate distribution ($C_{i_{s(0)}}$) was simulated as a normal distribution with an average molecular radius of μ and a standard deviation of σ. A standard deviation (σ) of 20% of μ was chosen to represent narrow distributions and 50% of μ for wider distributions. The distribution was normalized so that the area under the bell-shaped graph, between μ-3σ and μ+3σ, was equal to the total initial starch concentration ($C_{s(0)}$). A limit of 3 standard deviations represent 99.7% of the total area in a normal distribution, which was assumed to give an accurate representation of a polydisperse

substrate distribution. The remaining 0.03% was not considered in this study. $C_{s(0)}$ was chosen to be 0.60 μmol L^{-1}, based on a 5 wt% starch solution and the average molecular weight of $8.9 \cdot 10^7$ g mol^{-1} of a 100 nm starch molecule. The molecules were discretised into 100 classes based on molecular radii between μ-3σ and μ+3σ. The initial concentration of each class was determined by multiplying probability of the average molecule of that class with $C_{s(0)}$.

The classes used for discretising the substrate, based on molecular radii between zero and μ+3σ, were also used to discretise the products. The final product distribution (fPD) was calculated based on the outflux of oxidised molecules per class (J_i) from the pore over the duration of the experiment. Integration of C_i over time was done with the trapezoidal rule to obtain the fPD. Products present in the pore after 16 h were not included in the fPD. The product concentration is the bulk was set to zero, assuming that the product molecules were directly removed from the bulk after exiting the pore.

$$\frac{\delta C_i}{\delta t} = \frac{A}{V} J_i \tag{10}$$

The yield was defined as shown in equation 11.

$$Y_{\frac{P}{S}} = \frac{\sum_{i=n_d}^{2n_d} fPD_i}{\sum_{i=1}^{n_d} (C_{i_{(0)}} + \int_{C_i\,(t=0)}^{C_i(t=t)} \delta C_{i_{(0)}})} \tag{11}$$

The fPD per total surface area in the pores was determined (fPD_{SA}) in relation to the pore surface area in a reference scenario containing pores with a 100 nm radius [EQ].

$$fPD_{SA} = fPD \frac{r_{p_{REF}}}{r_p} \tag{12}$$

The dynamics of diffusion are described by partial derivatives with respect to space and time (eqn 1, 2, 3, 11, 12). The method of lines was used to solve the partial differential equations: the spatial derivatives were discretised using orthogonal collocation, whilst keeping the time variable continuous. Chebyshev roots were used for collocation, so the grid points densified at the boundaries of the grid. The spatial derivative was calculated for each of the grid points with differentiation matrices. The resulting set of ordinary differential equations was subsequently solved by backwards differentiation.

At the beginning of each simulation, only native starch (initial substrate distribution ($C_{i_{s(0)}}$) is present in the bulk (r=R) (eq.13). No starch molecules, either substrates or products are present in the pore (r<R) at that timepoint (eq.14).

$$C_{i_s}(t = 0\,, r = R) = C_{i_{s(0)}} \tag{13}$$

$$C_i(t = 0, r < R) = 0 \tag{14}$$

During the experiment, Dirichlet boundary conditions were applied for both the product and substrate concentrations in the bulk liquid. The substrate concentration in the bulk was thus assumed to be constant over time. The product was assumed to be directly removed from the bulk liquid, its concentration in the bulk was therefore set to zero (eq.15,16)

$$C_{i_s}(t, r = R) = C_{i_{s(0)}} \tag{15}$$

$$C_{i_p}(t, r = R) = 0 \tag{16}$$

At the inner part of the pore (r=0) no flux is present, so a Neumann boundary condition was enforced (eq.17).

$$\frac{\partial C_i}{\partial x}\Big]_{r=0} = 0 \tag{17}$$

5.2.2 Oxidation kinetics

Rather than assuming that the reaction-diffusion system represented in the model is mass-transfer limited instead of reaction-rate limited, the order of magnitude of oxidation rates of starch over a Pt/C catalyst were estimated experimentally to confirm this assumption. Activated carbon was chosen as support material since the pore sizes are smaller than the substrate and reaction was assumed to only take place on the surface of a catalyst particle to isolate the reaction rate as a variable.

A 250 mL batch reaction with at 5% Pt/C catalyst was performed at ambient air pressure, pH 9, and at 50 °C. 25 mmol AHG equivalent substrate and 0.1 mmol Pt was present in each reaction. The pH was kept constant by titration with 0.5M NaOH. The rate constant of the oxidation was determined based on the production of carboxylic acid groups. The amount of NaOH used to retain a constant pH was used as a measure for the amount of carboxylic acid moieties formed in the starch. The specific surface area of the catalyst was estimated to be 366 m^2 m^{-3} based on an average catalyst particle size of 25 µm, a density of 798 kg m^{-3}, and a porosity of 0.6 (as advised by the manufacturer), and 19.5 mg of platinum present in the reaction mixture.

From this data, the rate constant k_r was estimated by fitting first order reaction kinetics. The determined oxidation rate encompasses the rate for absorption to the catalyst, reaction on the catalyst surface, and desorption from the catalyst. After determining the rate constant the oxidation of the starches within the pores of the modelled catalyst was simulated according to first-order reaction kinetics (eq. 18).

$$r_r = \sum_{i=1}^{2n_d} \nu_{i,j} \, (k_r \, C_i) \qquad (18)$$

The oxidation state of the starch molecules was taken as binary value: a molecule was either non-oxidised or oxidised. Varying oxidation states were thereby excluded. The underlaying assumption is that if a molecule has gone through the catalytic cycle once, their degree of oxidation is suitable for applications. This represents a “best case scenario” since if a substrate molecule requires several passes through the catalytic cycle to be sufficiently oxidised, the system would become more mass-transfer limited.

5.3 Results and discussion

5.3.1 Modelling results

The model described in equations 1-18 was run for normally distributed substrates with average molecule sizes of 10, 25, 50, 75, and 100 nm and standard deviations of 20% and 50% of the average molecule size ($\sigma = 0.2\mu$ and $\sigma = 0.5\mu$ respectively) for a total of 10 initial substrate distributions. The diffusion and conversion of these 10 substrate variations were simulated for a catalyst with pore sizes of 25, 35, 50, 65, 75, 100, 125, 150, 175, 200, 225, and 250 nm, resulting in 120 distinct simulation runs.

Figure 1 shows the initial ($C_{s_{(0)}}$) and obtained final distributions (fPD_{SA}, eqn. 12) for all evaluated pore sizes, average molecule sizes, and standard deviations after 16h of simulated reaction time.

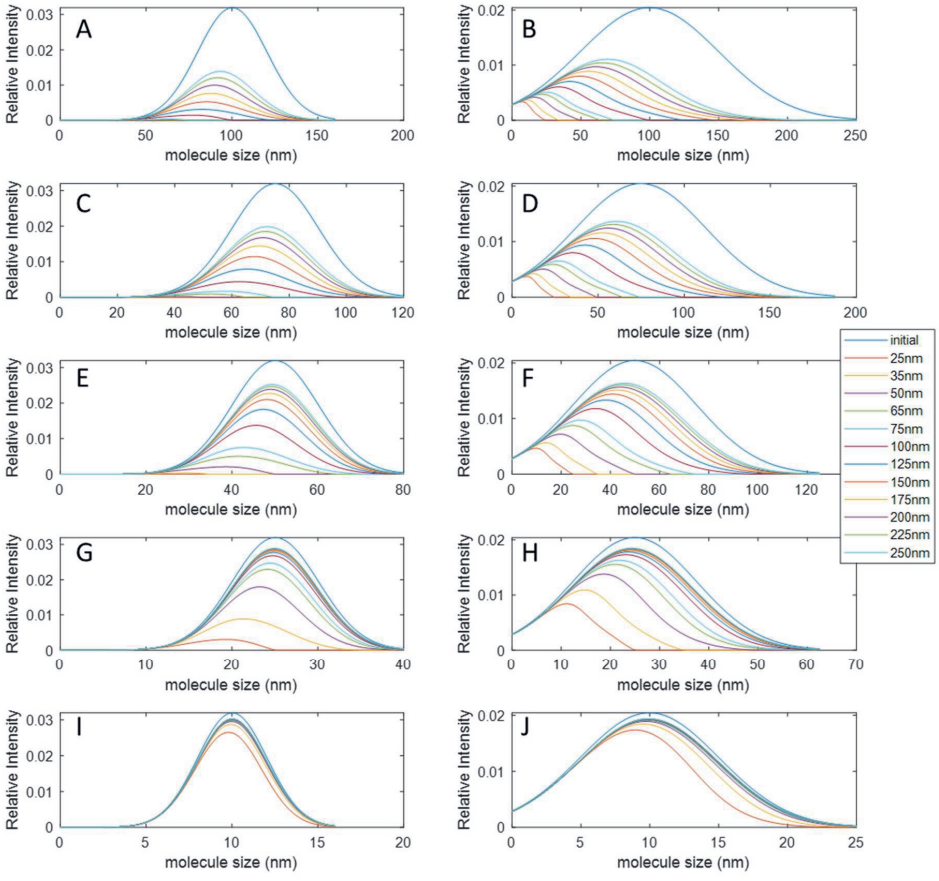

figure 1 substrate and final (t=tf) distributions of oxidised starch molecules for different pore sizes (legend), molecule sizes (ab: 100nm, CD: 75nm, EF: 50nm, GH: 25nm, IJ: 10 nm), and standard deviations (left $\sigma = 0.2\mu$, right $\sigma = 0.5\mu$). the area under the initial distribution is normalised to 1. the area under the curves represent yield.

In figure 1, the shape (average molecular size, peak height, area under the graph) of the product distributions can be compared to the shape of the initial distribution. Since reaction rates were set to an equal value for all starch species, and the total surface area was kept constant for all pore sizes, any differences in shape can be attributed to the differences in diffusion rates between the different starch species and size exclusion effects. For all subplots of figure 1 the yield (area under the graph) increases with increasing catalyst pore size. If the difference in yield (visually determined by the distance between the lines) is large when compared to the yield of one step up in pore size, then the conclusion can be drawn that at those combination of pore size and substrate size there are diffusion limitations. The increased yield at larger pore size is the result of the decreased effects from hindered diffusion with increased pore size. A visual analysis of the yields indicates that the conversion is diffusion limited to some degree for all simulations, although the effects range from insignificant (Figure 1I) where there is severe overlap in the distributions for the range of pore sizes, to highly significant (e.g. figure 1E) where each step increase in pore size increases the yield. The relation between yield and pore size is quantified and further explored in figure 2.

In Figure 1G, the line for pore size of 25nm (orange) drops to a value of 0 at a molecule size of 25 nm. This is an example of size exclusion where the pore size is smaller than a (part) of the starch species in the distribution. The effective diffusion rate is 0 in this regime and no yield can be obtained in this simulation. In practice, a low degree of conversion may still be observed by interaction of the substrate molecule with active sites on the outside of the catalyst particle, however, these effects were not considered in this study.

Figure 1D is an example where the modal molecular size (i.e. the peak) of the product distribution shifts to lower molecular sizes with decreasing pore sizes. This phenomenon is a result of the difference in diffusion rates between different species within the substrate distribution and size exclusion effects. Only a subset of the original substrate distribution can be effectively converted. As a result the conversion will not only have a lower yield as indicated by the area under the graph, but the product will have different characteristics (average molecular weight, and a slightly skewed distribution) than the substrate distribution. Comparing the conversion of an average size of 75nm, but with different standard deviations ($\sigma = 0.2\mu$ and $\sigma = 0.5\mu$) in a 100 nm pore (Figure 1CD, red lines), it can be seen that the shift in modal molecular size of the product distribution in more pronounced for substrate distributions with a higher standard deviation (modal of production distribution ~45 nm) compared to a lower standard deviation (modal of product distribution of ~ 65nm). Thus, with lower ratio of pore size to average molecule size of the initial distribution, the peak of the product distribution shifts towards lower molecular weights. This effect is stronger with higher standard deviations ($\sigma = 0.5\mu$ vs. $\sigma = 0.2\mu$). At higher standard deviations for the initial distribution ($\sigma = 0.5\mu$ vs. $\sigma = 0.2\mu$), and for regions with significant hindered diffusion

the average product size is significantly lower than the average substrate size. This implies that in a conversion of a feedstock with a molecular weight distribution that is limited by (hindered) diffusion, the product distribution will have an lower average molecular size than the original distribution which will also result in suboptimal overall catalyst activity. This is the result of small molecules in a distribution, that are less influenced by hindered diffusion being, converted at an overall higher rate than large molecules in the same distribution. This phenomenon results in asymmetrical product distributions (Hoogstad et al. 2019).

Figure 2 shows the yield of the same set of simulations as shown in figure 1. The area under the curve (i.e. the yield) was expressed as a percentage of the initial substrate quantity. The different pore sizes are displayed on the horizontal axis and the different average substrate sizes are shown in the legend.

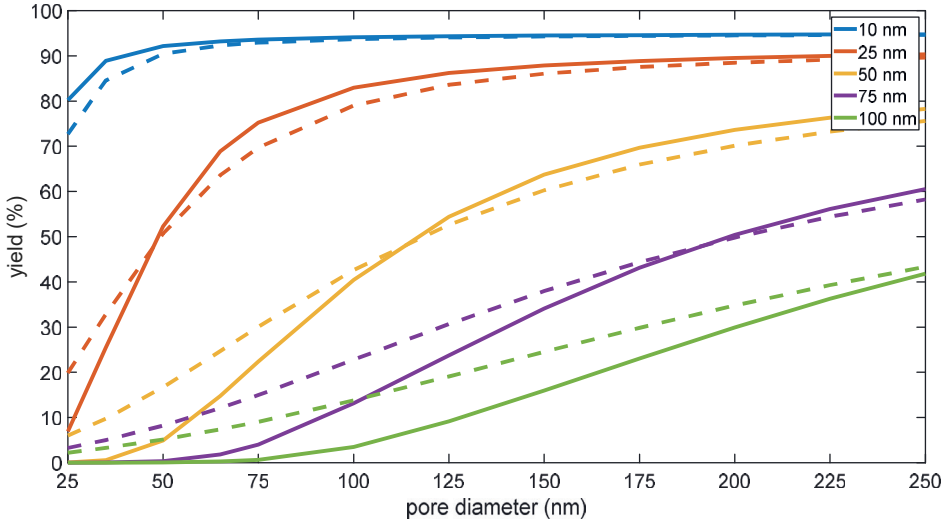

Figure 2 yield of reaction as a function of pore diameter for different initial substrate molecule sizes. Indicated molecule sizes in the legend are averages of a normal distribution, standard deviation was 20% of the average for solid lines, and 50% of the average for dashed lines.

Comparing the yield for different average substrate molecule sizes for a given pore size of e.g. 100nm (Figure 2, height of the solid lines at pore diameter of 100nm) shows that a yield of ~90% is obtained by the 10 nm average substrate size compared to a yield of ~80% for the 25nm substrate, ~40% yield for the 50 nm substrate and 10% and 4% yields for the 75 and 100 nm substrates respectively. Increasing pore sizes increases the yield up to a maximum, this maximum decreases with increasing substrate size as is evidenced by the maximum conversion op 90% for the 10 nm sample, 85% yield for the 25nm size and ~80% yield for the 50nm substrate size. Increasing pore size without a resulting increase in yield indicates that the reaction is no longer limited by (hindered) diffusion, but rather limited by reaction rate or bulk diffusion rate. For the 10nm

substrate, a maximum yield is reached at a pore size of ~50nm, for the 25nm and 50nm substrate the maxima are reached for 175 and >250nm pore sizes respectively. Expressing the pore size after which a maximum yield is obtained as a multiple of the substrate size shows that for the 10nm, 25nm and 50nm substrate sizes this factor is 5x, 7x and >5x respectively. This increase in factor cannot be attributed to hindered diffusion, since the hindrance factor only depends on the ratio of the pore size and the molecule size, instead this increase is explained by the Stokes-Einstein relation, which shows that bulk diffusion of a particle scales non-linearly with increasing particle size.

In Figure 2, a low yield can be observed for substrate distributions with average molecular sizes higher than the pore size. The low percentage of yield is the result of the substrates having a distribution over molecular sizes instead of being monodisperse. In a monodisperse substrate, no yield would be seen for molecule sizes below pore sizes since size exclusion would occur. However, with a standard deviation of 20% of the average substrate size, some formation of product is seen with pore sizes below the average molecule size. The distributions of these products have a lower average molecular size than their initial substrate distribution, as can be seen in Figure 1. For the 100nm substrate (figure 2 green line) there is no increase in yield by increasing pore sizes from 25 to 35 nm. Here the minimum size of molecules in the distribution is the average minus 3 standard deviations, which in this case is a minimum molecular size of 40 nm. Here, the entire substrate distribution is size excluded since the minimum molecule size is larger than the pore size.

Substrates with a higher standard deviation (50% of average, figure 2 dashed lines) have a higher yield at lower pore sizes compared to their lower standard deviation (20% of average, figure 2 solid lines) counterparts (e.g. a 18% yield versus a 8% yield for average molecule size of 100 nm at a pore size of 125 nm). As pore sizes increase, the yields of lower standard deviation substrate will overtake the yields of the higher standard deviation fraction as evidenced by the intersection points of same coloured lines in figure 2. At pore sizes larger than at the intersection point, yield of the lower standard deviation substrate distribution is higher until a regime is reached where the system is no longer limited by diffusion. These results are explained by the fact that a subset in the tail-end (between $\mu - 3\sigma$ and $\mu - 2\sigma$) of the initial high standard deviation substrate distribution contains smaller molecules than the tail-end of the low standard deviation substrate distribution. These molecules in the tail end of the high standard deviation initial distribution can be converted in smaller pores sizes than the tail-end molecules from the low standard deviation initial distribution, resulting in a higher overall yield for the higher standard deviation substrate.

For the 10nm substrate the region where the higher standard deviation variant has a higher yield than the lower standard deviation variant, nor the intersection of the curves is visible in the plotted range. However, it is likely that these behaviours that are

observed in other substrates, do occur for the 10nm substrate and would be visible if the range of pore sizes was expanded.

The 50, 75 and 100nm substrates (figure 2 yellow, purple and green lines) show a sigma shaped curve in yield versus increasing pore size. As is characteristic for sigmoid curves, increasing pore sizes further than the pore size at the infliction point results in diminishing returns on yield, while decreasing specific surface area further. For all samples, the infliction point is found around pore sizes a factor 1.7 – 2 larger than the average molecule size of the substrate. However, this infliction point is not indicative of an optimum pore size of the system as a whole, since the trade-off between pore size and specific surface area is not considered yet.

Figure 3 shows the simulated yields, that have been normalised to correspond with a constant pore volume for all pore diameters, where the normalization factor for each pore size was determined as the ratio of pore volume of the 25nm pores versus pore volume of the other pore sizes. The yields as defined in figure 1 and 2 were multiplied by this ratio for each pore size. Since the porosity of the catalyst particle was kept constant, these values represent the yields achievable for a fixed volume of catalyst and fixed amount of catalyst nanoparticles. The normalisation for pore volume allows the visualisation and determination of an optimum pore size in the trade-off between pore size and specific surface area.

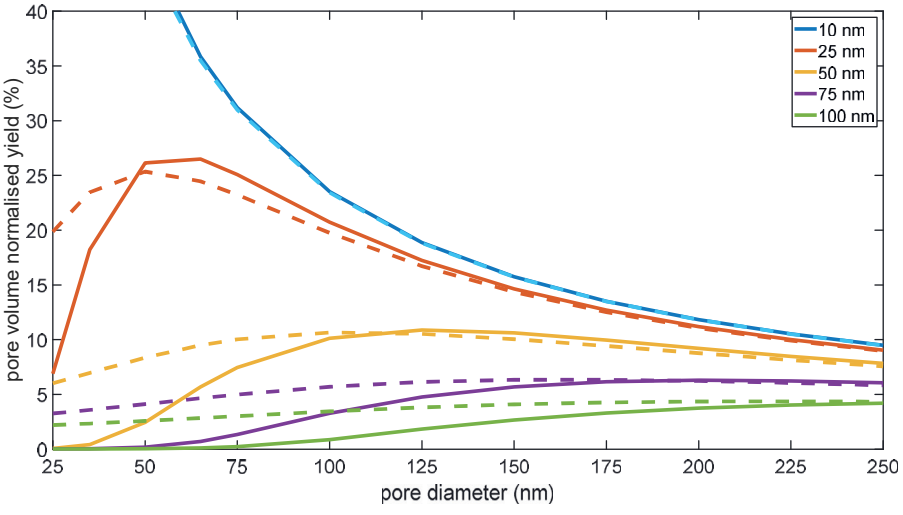

Figure 3 pore volume normalised yield. All pore sizes have the same total pore volume. standard deviation was 20% of the average for solid lines, and 50% of the average for dashed lines. For the 10nm average molecule size the maximum yield was 80% at a pore size of 25 nm (not shown to increase clarity for other substrates).

The data in figure 3 visualises the trade-off between mass transfer limitations at lower pore sizes and reduction of specific surface area for higher pore sizes. The maximum

yield that can be obtained under simulated reaction conditions for the 10, 25, 50, and 75 nm sample sizes are 80, 27, 10, and 6% respectively, showing an exponentially decreasing yields with increasing substrate sizes. This exponential decrease in yield is explained by a combination of larger required pore sizes thus reduced specific surface area, and lower bulk diffusion rates for larger molecule sizes. In practice this would result in exponentially longer reaction times and/or increasing the reactor size to obtain acceptable overall conversion rates and production quantity.

For the 25, 50, and 75 nm substrates an optimum yield is visible at pore sizes of ~60, 125, 210 nm respectively. The 10nm substrate reaches an optimum yield of 80% at a pore size of 22nm (not shown in figure 3 to improve overall figure clarity). When the optimum pore size is expressed as a factor of the average substrate size these factors are 2.2, 2.4, 2.5, and 2.8 for the 10, 25, 50, and 75 nm substrates respectively. The optimum of the 100nm substrate was outside the range of evaluated pore sizes. This trend where the optimum ratio of pore size to substrate size increase with increasing substrate size is again (similar to the ratio of substrate to pore size after which a yield plateau is reached (figure 2)) not attributable to the effects of hindered diffusion, but rather to the non-linear scaling of bulk diffusion rates of particles as described by the Stokes-Einstein relation.

At the calculated optimal pore sizes for the 25, 50, and 75 nm substrates of ~60, 125, 210 nm respectively the average product size for the $\sigma = 0.2\mu$ initial distribution is 24, 47, and 72 nm respectively (obtained from the data shown in figure 1, piecewise linear interpolation was used to estimate values for pore sizes in between simulation steps), thus matching the original substrate distribution closely with only an approximate 4% difference. For the $\sigma = 0.5\mu$ initial distributions, the average size of the product distribution was estimated to be 22nm , 40nm, 66nm respectively for the 25, 50, 75 nm average substrate sizes, this is an average of 15% difference between average initial and average product distribution sizes. A higher standard deviation in the initial distribution ($\sigma = 0.5\mu$ vs $\sigma = 0.2\mu$) thus resulted in a higher difference between average and initial product/substrate distribution of approximately 15% versus 4%.

Integrating the modelling results demonstrates a complex system where diffusion limitations due to hindered diffusion, differences in diffusion rates of substrate species within a distribution, the non-linear scaling of bulk diffusion rates for large molecules as described by the Stokes-Einstein relation, and the effect of distribution width on obtained yields and product distribution, all pose relevant additional challenges in the design of conversions for macromolecular and polydisperse substrates.

5.3.2 Perspective for catalyst design

In the analysis of diffusion limitations it was found that the optimal pore size in the trade-off between specific surface area and attenuating diffusion limitations ranges from 2.2 to 2.8 times the average molecule size. From tables 1 and 2 in the introduction, it can be seen that only highly macroporous support materials like α-alumina, and carbon nanotubes/nanofibres can be made to include these large pore sizes.

This severely limits the choice of catalyst support material for a given process for the conversion of macromolecules with sizes >10nm. Catalyst supports are not only relevant for the porous network that they form, but have additional properties that facilitate chemical conversions such as interaction of substrate molecules with functionalised surface groups on the catalyst support that e.g. influence polarity and charge which in turn influences adsorption, conformation of the adsorbed species, and desorption. The limited selection of catalyst supports with suitable pore sizes provides another challenge in the heterogeneously catalysed conversion of biomacromolecules. Although with research towards the design of macroporous support materials the challenges regarding obtaining the right surface group functionalities may be overcome, other fundamental limitations remain.

The exponentially decreasing overall catalyst activity with increasing molecular size of the substrate, even at optimised pore size, implies that there is a practical limit to the maximum size of a substrate that can be converted by heterogeneously catalysed processes, even if catalyst support materials with suitably large pore sizes can be constructed that sufficiently attenuate (hindered) diffusion limitations and size exclusion. As a result of these limitations, some depolymerising pre-treatment of substrates will likely remain required in practice for processes to be practically and economically feasible. To find the optimal balance between attenuation of the aforementioned mass-transfer limitations and a functionality requirement of a product, the desired molecular size of the product needs to well-understood i.e. property-function relations of the products with respect to their molecular size, polydispersity, and degree of conversion need to be mapped.

Design and optimisation of heterogenous catalysts for the conversion of macromolecular polydisperse feedstocks has additional challenges compared to designing catalysts for the conversion of non-macromolecular substrates. Managing mass-transfer limitations and obtaining the desired product distribution adds extra steps to the design process. And a reverse design approach starting from an ideal product distribution can guide the design of the catalyst. For a given product size the ideal strategy would be to depolymerise the substrate to the required size (while accounting for possible depolymerisation during the conversion), and subsequently perform a trade-off analysis as shown in figure 3 to determine the optimal catalyst material pore size. Figure 4 schematically illustrates a design process for a catalyst for the conversion of a

macromolecular and polydisperse feedstock. The green units in the figure represent new elements or elements that require additional effort compared to design of heterogeneous catalysts for non-macromolecular non-polydisperse substrates. Adsorption and desorption studies are common in catalyst design, however, polydispersity in substrates introduces an additional variable to this testing (Hoogstad et al., 2023). The final step in the flowchart of testing the catalyst and iterating the design includes activity, selectivity, and stability testing among other traditional design elements in this stage.

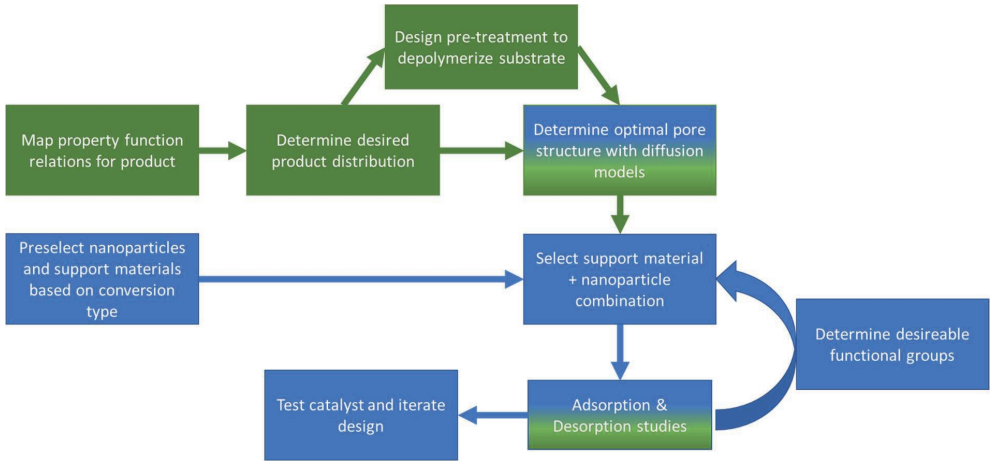

Figure 4 flowchart for heterogeneous catalyst design for macromolecular conversions. Blue elements represent more traditional design elements. Green elements represent design elements that tackle the additional challenges for the conversion of macromolecular substrates.

5.4 Conclusions

In this paper we have considered the diffusion of a polydisperse macromolecular reactant in a porous catalyst material. Diffusion will be a limiting factor in the conversion of macromolecular feedstocks. The Stokes-Einstein relation for diffusion of spherical particles shows that the rate of diffusion of the feedstock scales non-linear and inverse with molecule size. Additionally, in situations where the pore sizes are in the same order of magnitude as the feedstock molecules, effective diffusion rates are further reduced as described by the Renkin equation. Based on the evaluated reaction-diffusion model, for conversion of biomacromolecules >25nm , diffusion will generally be the limiting step.

There is an infliction point in the yield vs pore size curves at pore sizes approximately 1.5-2 times the molecule size for normally distributed substrates with a standard deviation 20% of the average molecular size, and approximately 1.2-1.7 times for substrates with a standard deviation of 50% the average molecular size. Increasing pore size beyond this infliction point results in diminishing returns, although a net benefit is still obtained until the optimum. Optimum pore sizes in the trade-off between diffusion limitation versus specific surface area are approximately 2.2 to 2.8 times the molecule size for average substrate sizes of 10nm to 100nm respectively.

If a system is diffusion limited, a higher polydispersity of the substrate can result in higher yield, however, only a subset of the initial substrate distribution will be converted, thus the size distribution of the product will consist of tail-end molecules of the initial substrate distribution. Therefore, the higher the polydispersity of the sample, the less the product distribution resembles the original reactant distribution if the system is diffusion limited. Also at optimal pore sizes from a diffusion – specific surface area trade-off perspective the difference between the initial and product distribution will increase with increasing substrate polydispersity (4% for $\sigma = 0.2\mu$ vs 15% for $\sigma = 0.5\mu$)

Since processes for the conversion of macromolecular feedstocks are likely to be (severely) mass transfer limited due to their molecular size, and since these feedstocks have the added complexity of naturally occurring size distributions, special attention to pore structures is required for the design of catalysts for the conversions of these feedstocks. Reverse design and optimisation of a process, starting at the desired product i.e. mapping property-function relations, and tuning the process and substrate pre-treatment to obtain optimal yield within those requirements is the advised approach.

5.5 References

Adelhelm, P., & De Jongh, P. E. (2011). The impact of carbon materials on the hydrogen storage properties of light metal hydrides. *Journal of Materials Chemistry, 21*(8), 2417-2427.

Baltus, R. E., & Anderson, J. L. (1983). Hindered diffusion of asphaltenes through microporous membranes. *Chemical Engineering Science, 38*(12), 1959-1969. doi:https://doi.org/10.1016/0009-2509(83)80099-2

Beck, J. S., Vartuli, J. C., Roth, W. J., Leonowicz, M. E., Kresge, C., Schmitt, K., . . . McCullen, S. (1992). A new family of mesoporous molecular sieves prepared with liquid crystal templates. *Journal of the American Chemical Society, 114*(27), 10834-10843.

Beck, R. E., & Schultz, J. S. (1970). Hindered Diffusion in Microporous Membranes with Known Pore Geometry. *Science, 170*(3964), 1302-1305. doi:10.1126/science.170.3964.1302

Bertoft, E. (2017). Understanding Starch Structure: Recent Progress. *Agronomy, 7*(3). doi:10.3390/agronomy7030056

Bravo-Suárez, J. J., Chaudhari, R. V., & Subramaniam, B. (2013). Design of Heterogeneous Catalysts for Fuels and Chemicals Processing: An Overview. In *Novel Materials for Catalysis and Fuels Processing* (Vol. 1132, pp. 3-68): American Chemical Society.

Chang, H., Luo, J., Bakhtiary Davijani, A. A., Chien, A.-T., Wang, P.-H., Liu, H. C., & Kumar, S. (2016). Individually Dispersed Wood-Based Cellulose Nanocrystals. *ACS Applied Materials & Interfaces, 8*(9), 5768-5771. doi:10.1021/acsami.6b00094

Copéret, C., Chabanas, M., Petroff Saint-Arroman, R., & Basset, J.-M. (2003). Homogeneous and Heterogeneous Catalysis: Bridging the Gap through Surface Organometallic Chemistry. *Angewandte Chemie International Edition, 42*(2), 156-181. doi:https://doi.org/10.1002/anie.200390072

De Jong, K. P., & Geus, J. W. (2000). Carbon Nanofibers: Catalytic Synthesis and Applications. *Catalysis Reviews, 42*(4), 481-510. doi:10.1081/CR-100101954

Dechadilok, P., & Deen, W. M. (2006). Hindrance Factors for Diffusion and Convection in Pores. *Industrial & Engineering Chemistry Research, 45*(21), 6953-6959. doi:10.1021/ie051387n

Deckers, H. A., Olieman, C., Rombouts, F. M., & Pilnik, W. (1986). Calibration and application of high-performance size exclusion columns for molecular weight distribution of pectins. *Carbohydrate Polymers, 6*(5), 361-378. doi:https://doi.org/10.1016/0144-8617(86)90026-3

Deen, W. M. (1987). Hindered transport of large molecules in liquid-filled pores. *AIChE Journal, 33*(9), 1409-1425. doi:https://doi.org/10.1002/aic.690330902

Deng, H., Grunder, S., Cordova, K. E., Valente, C., Furukawa, H., Hmadeh, M., . . . Yaghi, O. M. (2012). Large-Pore Apertures in a Series of Metal-Organic Frameworks. *Science, 336*(6084), 1018-1023. doi:10.1126/science.1220131

Draget, K. I., Smidsrød, O., & Skjåk-Bræk, G. (2005). Alginates from algae. *Polysaccharides and polyamides in the food industry: properties, production, and patents*, 1-30.

Durand, E., Clemancey, M., Lancelin, J.-M., Verstraete, J., Espinat, D., & Quoineaud, A.-A. (2010). Effect of Chemical Composition on Asphaltenes Aggregation. *Energy & Fuels, 24*(2), 1051-1062. doi:10.1021/ef900599v

Emsley, A. M., Ali, M., & Heywood, R. J. (2000). A size exclusion chromatography study of cellulose degradation. *Polymer, 41*(24), 8513-8521. doi:https://doi.org/10.1016/S0032-3861(00)00243-3

Estermann, M., McCusker, L. B., Baerlocher, C., Merrouche, A., & Kessler, H. (1991). A synthetic gallophosphate molecular sieve with a 20-tetrahedral-atom pore opening. *Nature, 352*(6333), 320-323. doi:10.1038/352320a0

Eyssautier, J., Frot, D., & Barré, L. (2012). Structure and Dynamic Properties of Colloidal Asphaltene Aggregates. *Langmuir, 28*(33), 11997-12004. doi:10.1021/la301707h

Férey, G., Mellot-Draznieks, C., Serre, C., Millange, F., Dutour, J., Surblé, S., & Margiolaki, I. (2005). A Chromium Terephthalate-Based Solid with Unusually Large Pore Volumes and Surface Area. *Science, 309*(5743), 2040-2042. doi:10.1126/science.1116275

Gidh, A. V., Decker, S. R., See, C. H., Himmel, M. E., & Williford, C. W. (2006). Characterization of lignin using multi-angle laser light scattering and atomic force microscopy. *Analytica Chimica Acta, 555*(2), 250-258. doi:https://doi.org/10.1016/j.aca.2005.09.023

Giri, S., Dutta, P., & Giri, T. K. (2021). Inulin-based carriers for colon drug targeting. *Journal of Drug Delivery Science and Technology, 64*, 102595. doi:https://doi.org/10.1016/j.jddst.2021.102595

Glotov, A., & Karakhanov, E. (2021). Heterogeneous Catalysts for Petrochemical Synthesis and Oil Refining. *Catalysts, 11*(5). doi:10.3390/catal11050602

Groenzin, H., & Mullins, O. C. (2000). Molecular Size and Structure of Asphaltenes from Various Sources. *Energy & Fuels, 14*(3), 677-684. doi:10.1021/ef990225z

Grommers, H. E., & van der Krogt, D. A. (2009). Chapter 11 - Potato Starch: Production, Modifications and Uses. In J. BeMiller & R. Whistler (Eds.), *Starch (Third Edition)* (pp. 511-539). San Diego: Academic Press.

Gu, J., & Catchmark, J. M. (2013). The impact of cellulose structure on binding interactions with hemicellulose and pectin. *Cellulose, 20*(4), 1613-1627. doi:10.1007/s10570-013-9965-8

Hoogstad, T. M., Kiewidt, L., van Haasterecht, T., & Bitter, J. H. (2023). Size selectivity in adsorption of polydisperse starches on activated carbon. *Carbohydrate Polymers, 309*, 120705. doi:https://doi.org/10.1016/j.carbpol.2023.120705

Hoogstad, T. M., Konings, G., Buwalda, P. L., Boxtel, A. J. B., Kiewidt, L., & Bitter, J. H. (2019). The effect of polydispersity on the conversion kinetics of starch oxidation and depolymerisation. *Chemical Engineering Science: X, 4*, 100044. doi:https://doi.org/10.1016/j.cesx.2019.100044

Huang, B., Bartholomew, C. H., & Woodfield, B. F. (2014). Facile synthesis of mesoporous γ-alumina with tunable pore size: The effects of water to aluminum molar ratio in hydrolysis of aluminum alkoxides. *Microporous and Mesoporous Materials, 183*, 37-47. doi:https://doi.org/10.1016/j.micromeso.2013.09.007

Katiyar, A., Yadav, S., Smirniotis, P. G., & Pinto, N. G. (2006). Synthesis of ordered large pore SBA-15 spherical particles for adsorption of biomolecules. *Journal of Chromatography A, 1122*(1), 13-20. doi:https://doi.org/10.1016/j.chroma.2006.04.055

Khaleel, A. T., Sisco, C. J., Tavakkoli, M., & Vargas, F. M. (2022). An Investigation of the Effect of Asphaltene Polydispersity on Asphaltene Precipitation and Deposition Tendencies. *Energy & Fuels, 36*(16), 8799-8808. doi:10.1021/acs.energyfuels.2c01064

Li, L., Cui, M., Wang, X., & Long, J. (2023). Critical Techniques for Overcoming the Diffusion Limitations in Heterogeneously Catalytic Depolymerization of Lignin. *ChemSusChem, n/a*(n/a). doi:https://doi.org/10.1002/cssc.202202325

Masuda, T., Asoh, H., Haraguchi, S., & Ono, S. (2015). Fabrication and Characterization of Single Phase α-Alumina Membranes with Tunable Pore Diameters. *Materials, 8*(3), 1350-1368. doi:10.3390/ma8031350

Masuelli, M. A. (2011). Viscometric study of pectin. Effect of temperature on the hydrodynamic properties. *International Journal of Biological Macromolecules, 48*(2), 286-291. doi:https://doi.org/10.1016/j.ijbiomac.2010.11.014

Mua, J. P., & Jackson, D. S. (1997). Fine Structure of Corn Amylose and Amylopectin Fractions with Various Molecular Weights. *Journal of Agricultural and Food Chemistry, 45*(10), 3840-3847. doi:10.1021/jf960877a

Nowak, N., Grzebieniarz, W., Khachatryan, G., Khachatryan, K., Konieczna-Molenda, A., Krzan, M., & Grzyb, J. (2021). Synthesis of Silver and Gold Nanoparticles in Sodium Alginate Matrix Enriched with Graphene Oxide and Investigation of Properties of the Obtained Thin Films. *Applied Sciences*. doi:10.3390/app11093857

Park, K. H., Lee, K. Y., & Lee, H. G. (2013). Chemical composition and physicochemical properties of barley dietary fiber by chemical modification. *International Journal of Biological Macromolecules, 60*, 360-365. doi:https://doi.org/10.1016/j.ijbiomac.2013.06.024

Parkhomchuk, E. V., Bazaikin, Y. V., Malkovich, E. G., Lysikov, A. I., Vorobieva, E. E., Fedotov, K. V., & Kleymenov, A. V. (2021). 4-Scale model for macromolecule conversion over mesoporous and hierarchical alumina catalysts. *Chemical Engineering Journal, 405*, 126551. doi:https://doi.org/10.1016/j.cej.2020.126551

Potthast, A., Radosta, S., Saake, B., Lebioda, S., Heinze, T., Henniges, U., . . . Wetzel, H. (2015). Comparison testing of methods for gel permeation chromatography of cellulose: coming closer to a standard protocol. *Cellulose, 22*(3), 1591-1613. doi:10.1007/s10570-015-0586-2

Renkin, E. M. (1956). Filtration, diffusion, and molecular sieving through porous cellulose membranes. *Journal of General Physiology, 39*(5), 820-820. doi:10.1085/jgp.39.5.820

Rolland-Sabaté, A., Guilois, S., Jaillais, B., & Colonna, P. (2011). Molecular size and mass distributions of native starches using complementary separation methods: Asymmetrical Flow Field Flow Fractionation (A4F) and Hydrodynamic and Size Exclusion Chromatography (HDC-SEC). *Analytical and Bioanalytical Chemistry, 399*(4), 1493-1505. doi:10.1007/s00216-010-4208-4

Semeykina, V. S., Malkovich, E. G., Bazaikin, Y. V., Lysikov, A. I., & Parkhomchuk, E. V. (2018). Optimal catalyst texture in macromolecule conversion: A computational and experimental study. *Chemical Engineering Science, 188*, 1-10. doi:https://doi.org/10.1016/j.ces.2018.05.005

Shen, F., Ling, H., Ge, W., Yang, Y., Wang, X., Ren, J., & Wang, X. (2021). Self-assembly behavior and conformation of amphiphilic hemicellulose-graft-fatty acid micelles. *Carbohydrate Polymers, 261*, 117886. doi:https://doi.org/10.1016/j.carbpol.2021.117886

Sokolov, S., Bell, D., & Stein, A. (2003). Preparation and Characterization of Macroporous α-Alumina. *Journal of the American Ceramic Society, 86*(9), 1481-1486. doi:https://doi.org/10.1111/j.1151-2916.2003.tb03500.x

Speight, J. G., Wernick, D. L., Gould, K. A., Overfield, R. E., & Rao, B. M. L. (1985). Molecular Weight and Association of Asphaltenes: a Critical Review. *Rev. Inst. Fr. Pét., 40*(1), 51-61. Retrieved from https://doi.org/10.2516/ogst:1985004

Stacy, C. J., & Foster, J. F. (1957). Molecular weight heterogeneity in starch amylopectins. *Journal of Polymer Science, 25*(108), 39-50. doi:https://doi.org/10.1002/pol.1957.1202510804

Sudarsanam, P., Peeters, E., Makshina, E. V., Parvulescu, V. I., & Sels, B. F. (2019). Advances in porous and nanoscale catalysts for viable biomass conversion. *Chemical Society Reviews, 48*(8), 2366-2421. doi:10.1039/C8CS00452H

Tafreshi, O. A., Mosanenzadeh, S. G., Karamikamkar, S., Saadatnia, Z., Park, C. B., & Naguib, H. E. (2022). A review on multifunctional aerogel fibers: processing, fabrication, functionalization, and applications. *Materials Today Chemistry, 23*, 100736. doi:https://doi.org/10.1016/j.mtchem.2021.100736

Tayakout, M., Ferreira, C., Espinat, D., Arribas Picon, S., Sorbier, L., Guillaume, D., & Guibard, I. (2010). Diffusion of asphaltene molecules through the pore structure of hydroconversion catalysts. *Chemical Engineering Science, 65*(5), 1571-1583. doi:https://doi.org/10.1016/j.ces.2009.10.025

Toebes, M. L., Bitter, J. H., van Dillen, A. J., & de Jong, K. P. (2002). Impact of the structure and reactivity of nickel particles on the catalytic growth of carbon nanofibers. *Catalysis Today, 76*(1), 33-42. doi:https://doi.org/10.1016/S0920-5861(02)00209-2

Tolbert, A., Akinosho, H., Khunsupat, R., Naskar, A. K., & Ragauskas, A. J. (2014). Characterization and analysis of the molecular weight of lignin for biorefining studies. *Biofuels, Bioproducts and Biorefining, 8*(6), 836-856. doi:https://doi.org/10.1002/bbb.1500

Trimm, D. L., & Stanislaus, A. (1986). The control of pore size in alumina catalyst supports: A review. *Applied Catalysis, 21*(2), 215-238. doi:https://doi.org/10.1016/S0166-9834(00)81356-1

van Koningsveld, H., Jansen, J. C., & van Bekkum, H. (1990). The monoclinic framework structure of zeolite H-ZSM-5. Comparison with the orthorhombic framework of as-synthesized ZSM-5. *Zeolites, 10*(4), 235-242. doi:https://doi.org/10.1016/0144-2449(94)90134-1

Wu, Z., Chen, C., Guo, Q., Li, B., Que, Y., Wang, L., . . . Guan, G. (2016). Novel approach for preparation of poly (ionic liquid) catalyst with macroporous structure for biodiesel production. *Fuel, 184*, 128-135. doi:https://doi.org/10.1016/j.fuel.2016.07.004

Xie, Y., Guo, X., Ma, Z., Gong, J., Wang, H., & Lv, Y. (2020). Efficient Extraction and Structural Characterization of Hemicellulose from Sugarcane Bagasse Pith. *Polymers, 12*(3). doi:10.3390/polym12030608

Zhou, Y., Zhang, X., Zhang, J., Cheng, Y., Wu, J., Yu, J., & Zhang, J. (2021). Molecular weight characterization of cellulose using ionic liquids. *Polymer Testing, 93*, 106985. doi:https://doi.org/10.1016/j.polymertesting.2020.106985

Zou, J., Xu, M., Wen, L., & Yang, B. (2020). Structure and physicochemical properties of native starch and resistant starch in Chinese yam (Dioscorea opposita Thunb.). *Carbohydrate Polymers, 237*, 116188. doi:https://doi.org/10.1016/j.carbpol.2020.116188

6.

6. General discussion

Scope

The goal of this thesis is to explore challenges in designing catalytic processes for polydisperse feedstocks, using the oxidation of starch as a case study (figure 1). In this chapter knowledge gained from chapters 2-5 is integrated to reflect on that goal. Additionally, the potential for new modelling tools that include the effects of molecular weight (distributions) and the practical implementation of these methods in the design process are discussed.

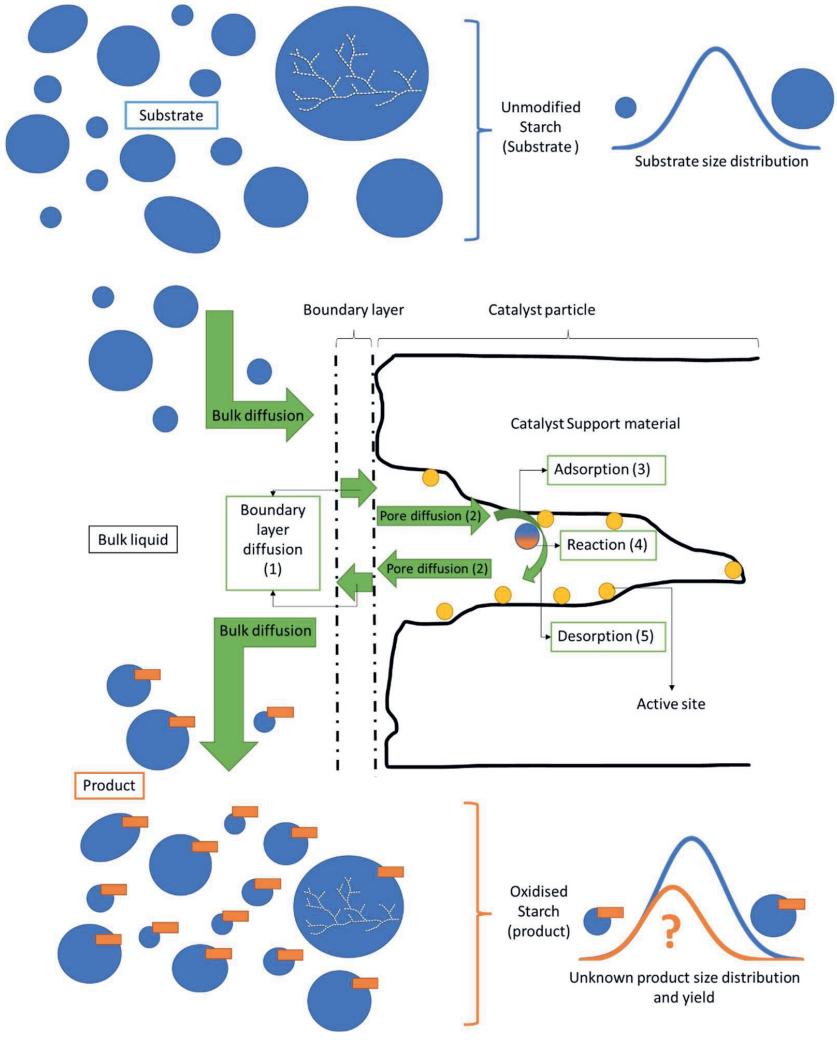

Figure 1 Schematic overview of the overall goal and scope in this thesis as outlined in chapter 1. Starch (blue) is oxidised to anionic starch (blue + orange) by undergoing the catalytic cycle (green) a heterogeneous catalyst (black + yellow). The effect of different steps in the catalytic cycle on the difference between the substrate distribution and product distribution, as well as overall reaction yield is to be investigated. Numbers 1-5 indicate the different steps in the catalytic cycle.

Chapters 1 & 2 – Goal and potential for improvement

A transition towards less fossil dependent materials and production processes is needed (Henrich, Dahmen, Dinjus, & Sauer, 2015; Rama et al., 2022). Biobased materials and chemicals can provide a more sustainable alternative to petrochemical based materials and chemicals (Dahiya, Katakojwala, Ramakrishna, & Mohan, 2020; Vinod, Sanjay, Suchart, & Jyotishkumar, 2020; Weiss et al., 2012). Biobased materials and chemicals are made by processing biobased feedstocks. Biobased feedstocks often require physical and or chemical modification to change, remove, and/or introduce additional functional properties (Nakagawa, Tamura, & Tomishige, 2013). Biobased feedstocks are generally large and complex molecules. In this thesis we explored one such conversion of a biobased feedstock: starch oxidation. Starch oxidation is currently done on industrial scale with sodium hypochlorite as oxidant (Grommers & van der Krogt, 2009; Rutenberg & Solarek, 1984). Hypochlorite is a potent enough oxidant that no catalyst is required. However, as demonstrated in chapter 2, the use of sodium hypochlorite for the oxidation has a high negative environmental impact. Therefore, alternative methods using H_2O_2 and O_2 have been investigated. These alternative oxidants have a lower environmental impact when implemented in the starch oxidation process (chapter 2). However, since these oxidants are less potent, a form of catalysis is needed.

Ninety percent of all industrial processes is catalytic, and eighty percent of catalytic processes are done with a form of heterogeneous catalysis (Bravo-Suárez, Chaudhari, & Subramaniam, 2013; Hegedus et al., 1987). The advantages of heterogeneous catalysts are that they are generally stable at high temperatures, easily recoverable, re-usable, and that the catalyst and substrate being in different phases leads to easier purification of the product. Thus designing a heterogeneous catalysed oxidation process with molecular oxygen provides a seemingly feasible solution to the drawbacks of oxidising starch with hypochlorite i.e. environmental impact, undesired by-products, and depolymerisation (chapter 2). However, designing a catalyst for a conversion using biobased feedstock introduces additional challenges compared to designing more traditional catalytic processes (e.g. for petrochemical feedstocks). Biobased molecules are much larger compared to traditional petrochemical or platform molecules and are polydisperse (Chapter 1, table 1). Oxidation of polysaccharides with heterogeneous catalysts has been performed (Verraest, Peters, & van Bekkum, 1998), where inulin molecules with an average degree of polymerization (DP) of 10 and 30 were oxidised with molecular oxygen over a Pt/C catalyst. Verraest et al. (1998) observed that inulin with longer chain lengths (dp 30 vs dp 10) oxidised at a lower rate. In their research, Verraest et al. (1998) noted several potential explanations for this observation like diffusion limitations, and strong adsorption of polymeric starting materials for the higher molecular weight substrates. Although the findings in their research are very

relevant, some considerations were not included. The effect of polydispersity of the substrate, which has been demonstrated to have a substantial effect on their physiochemical properties (Blecker et al., 2003; Kim, Faqih, & Wang, 2001; Mensink, Frijlink, van der Voort Maarschalk, & Hinrichs, 2015) was not included. Polydispersity of the substrate can lead to internal competition within a distribution as has been demonstrated in chapter 5, thereby affecting the kinetics of the conversion and the resulting distributions in molecular weight and degree of conversion of the product. Moreover, inulin with a DP of 30 (like petrochemical substrates) is a much smaller molecules than other biobased substrates like amylopectins which regularly have DPs in excess of 50.000 (Rolland-Sabaté, Guilois, Jaillais, & Colonna, 2011), which can substantially change the adsorption, diffusion, and reaction kinetics (chapters 3, 4, 5). Moreover, in this work we attempted to gain insight in the individual steps in the catalytic cycle by isolating them, while in previous works only the overall reaction was evaluated.

In this thesis, starch oxidation has been used as a model conversion to explore the effect of feedstock molecular size and size distribution on different steps of the catalytic cycle (figure 1). Three steps in the catalytic cycle have been investigated: reaction (figure 1 step 4) was investigated in chapter 3, adsorption (figure 1 step 3) was investigated in chapter 4, and diffusion (figure 1 step 2) was investigated in chapter 5. In each of these chapters, the respective step in the catalytic cycle has been isolated as much as possible within practical boundaries. In the reaction step (chapter 3), effects of adsorption and diffusion were eliminated by using a homogeneous catalyst. When investigating adsorption (chapter 4), the influence of diffusion as a variable was reduced as much as possible by selecting a sorbent with very small pore sizes, thereby excluding the majority of starch molecules from accessing the pores based on their size. By preventing starch molecules from entering the pores, (hindered) diffusion in pores was excluded as a variable. The diffusion step (chapter 5) was studied through a reaction diffusion model, where effects of size exclusion and pore blocking were excluded, and the system was verified to be mass transfer limited through experiments. By isolating these three steps in the catalytic cycle, a closer investigation of the influence of size, and size distribution was made possible for each of these steps individually.

Chapter 3 - Reaction

In chapter 3 we have shown that in a homogenously catalysed oxidation with TEMPO as catalyst and sodium hypochlorite as oxidant, molecular size of starch affects both the oxidation and depolymerisation rates. Here, both oxidation and depolymerisation rates increased with increasing size of substrate molecule. Since the reaction was isolated as a variable, it shows that size selective effects are present in the reaction step. This serves as a proof of concept that each molecular size in a size distributed feedstock has their

own kinetic parameter. A model that describes the kinetic behavior was created that discretizes the molecular size distribution and assigns individual kinetic parameters for both the oxidation and depolymerisation reactions to the different sized starch species in the distribution. Such a model structure allows to account for size selective effects in reaction rates of polydisperse feedstocks, and is universally applicable for any size influenced process involving a molecular size distribution e.g. adsorption or diffusion. Such a model empirically describes the behavior of a distribution based on experimentally obtained data. The drawback is that the fitting of the parameter values can yield good results for specific conversions with specific feedstocks, but these values require re-calibration when applying such a model to a different feedstock or reaction.

Chapter 4 - Adsorption

In chapter 4, we have demonstrated that the adsorption rates and equilibria of starch on activated carbon depend on molecular size and degree of branching of the sorbate. Here, a lower molecular size increased adsorption rates and shifts the equilibrium towards adsorbed molecules, and a higher degree of branching decreased adsorption rates and shifts the equilibrium towards desorbed molecules. Moreover, the adsorption rate of one specific starch size species in a distribution was reduced by adsorption of smaller molecules from the same distribution since the smaller molecules adsorbed faster and limited the number of available adsorption sites. Thereby showing that the rate of adsorption of a certain starch size species within a distribution depends on the distribution as a whole.

In this chapter it became clear that assigning a unique kinetic parameter to each species or slice in a discretized molecular size distribution can yield a very detailed model for that one specific feedstock and sorbent combination. However, generalizing these parameter values cannot be done, since a change in molecular size distribution of the same feedstock will result in a change in rate constants and requires recalibration of these values. Likewise, these challenges in generalizing such measured values will be present for other steps where internal competition is present (e.g. accessibility to reactive sites for the reaction step). Internal competition for reactive sites may have also played a role in chapter 3. However, in chapter 3 the lack of overlap in molecular weight distributions between the substrates did not provide the level of information that was needed to draw such a conclusion.

Chapter 5 - Diffusion

In chapter 5, a reaction diffusion model was presented for the oxidation of starch. We showed that diffusion will generally be the rate limiting step for the heterogeneously catalysed conversion of polydisperse macromolecules. It was determined that yield and product distribution depend on substrate size, and substrate polydispersity. In contrast

to chapters 3 and 4, these results are not limited by the same caveat of non-generalizability since the diffusion rates of large solutes are already well defined with generalized formula like the Stokes-Einstein relation and the Renkin equation. However, the generalizability still relies on the assumption that the substrate can be approximated as spherical solutes. In chapter 5 we concluded that the optimal pore size of a catalyst support material is approximately 2-3 times the average molecule size of the substrate. Consequently, the limited choice of support materials that can be created with sufficiently large macroporous structures (e.g. α-alumina and carbon nanofibres) limits the design choices for catalysts for macromolecular conversion. Moreover, even at optimal catalyst support pore sizes, a decreasing yield was observed with increasing molecule size due to nonlinear scaling of bulk diffusion rates as described by the Stokes-Einstein relation.

Polydisperse substrates and "the" rate limiting step

In general in the catalytic cycle, one of the steps will be the rate limiting step. When modelling a reaction, the overall reaction rate is often assumed to be determined by the rate limiting step, and the kinetics and dynamics of the other steps can be neglected. However, during the conversion of a polydisperse substrate, one part of the distribution e.g. the smaller quartile of the substrate distribution may be limited by a different step in the catalytic cycle than the rest of the molecules in the distribution. Essentially, since there is a mixture of reactants, not all reactants may share the same rate limiting step. Figure 2 illustrates this concept, where the rates of two processes over a molecular size distribution are shown. One of the rates decreases with increasing molecular size (akin to diffusion), the other is constant over the molecular size distribution. Molecules smaller than the threshold value are limited by a different process than molecules larger than the threshold value. The reaction rate of each individual size species follows the lowest rate, which is the rate limiting step for that size species. Thus, each size species within the distribution still has a single rate limiting step, but when considering the reaction mixture as a whole, two processes can be limiting simultaneously. Therefore, in the conversion of a polydisperse feedstock, one cannot refer to "the" rate limiting step. The wider the molecular size distribution i.e. the higher the polydispersity, the higher the chance of two (or more) rate limiting processes occurring simultaneously within the mixture of reactants. These rate limiting steps can be designated primary and secondary rate-limiting steps, depending on the fraction of the distribution that is limited by the different processes. In the case of figure 2, since a larger part of the distribution is limited by the diffusion rate, the diffusion rate would be the primary rate limiting step, and the reaction rate the secondary rate limiting step.

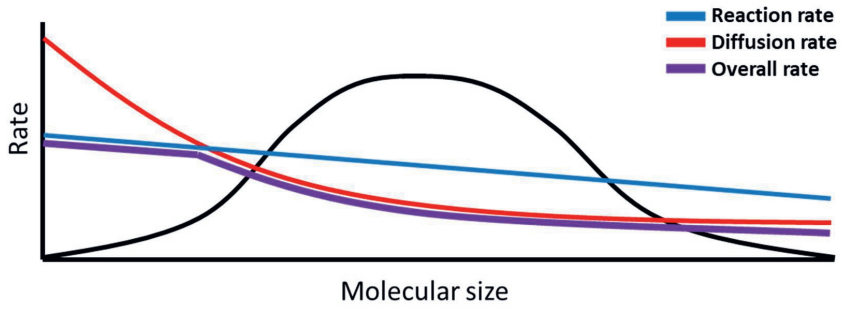

Figure 2 schematic representation of hypothetical rate limiting steps over a distribution. Molecular size distribution of the substrate is shown in black. Diffusion rate is indicated in red, and reaction rate is indicated in blue. The purple line indicates the overall reaction rate of the distribution and follows the lowest value of the different reaction rates for a given molecular size.

Evidence of this for the oxidation of starch was found in chapter 5, where the yield of the smallest substrate distribution did not increase with increasing pore sizes, indicating that the system was no longer mass-transfer limited at these molecule sizes. In chapter 4, a threshold value in adsorption rates was observed, where above a certain molecular size, the adsorption rates no longer decreased by increasing size further. This may have been the result of another molecular process becoming rate limited. However, in chapter 5 the underlaying reasons for the threshold value were not further investigated.

A consequence of the occurrence of multiple rate limiting processes over a (size) distributed feedstock is that all (primary and secondary) rate limiting processes need to be included in models rather than a singular rate limiting step, thereby increasing required efforts for model development and implementation to obtain a model with similar accuracy.

An additional result of the occurrence of multiple rate limiting processes over a (size) distributed feedstock is a more balanced process overall, where the maximum deviation between reaction rates of individual substrate size species and the average reaction rate over the entire width of the distribution is decreased. In cases where a product distribution that closely matches the substrate distribution is needed, secondary rate limiting steps may turn out to be beneficial. Moreover, as is the case with the oxidation of starch the product will not only be distributed in molecular size, but also in degree of oxidation. A very "unbalanced" reaction (i.e. large differences in overall reaction rate between small and large substrate molecules) will result in a wide range of degrees of oxidation for the substrate.

Property-function relations

If a specific value or range of degree of oxidation (or more general, a degree of conversion) is desired, a balanced reaction is beneficial. In the case of starch oxidation,

an hypothetical example is a situation where carbonyl groups instead of carboxyl groups are desired in a product. During oxidation of starch, hydroxyl groups are oxidised to carbonyl groups, after which they are further oxidised to carboxylic acid groups (Bragd, Besemer, & van Bekkum, 2002; Sangseethong, Termvejsayanon, & Sriroth, 2010). If for some application carbonyl groups are desired, but carboxyl groups are not, then "overoxidation" of smaller sized starch species within the distribution can reduce overall product functionality. For such processes, balancing the reaction will be beneficial. However, a good understanding of desired functionalities of the product and how molecular properties, e.g. degree of oxidation, influence these functionalities is needed to optimise product distributions. This relation between product functionalities and molecular properties will be referred to as property-function relations. An analysis of property-function relations will find desired product properties and sensitivity of the application towards changes in product properties, and will thereby reveal the importance of "balancing" reactions.

A rule of thumb for simplification of design

The Stokes-Einstein relation shows a non-linear decrease in bulk diffusion rates with increasing molecule diameter. This diffusion rate is lowered further by drag and lag coefficients when a solute diffuse trough a pore (a.k.a. hindered diffusion). As a result, it is likely that mass transfer limitations will be the main step that limits the overall reaction rate in most heterogeneously catalysed conversion of biomacromolecular feedstocks. This also holds when there are multiple simultaneous rate-limiting steps over the distribution of the substrate, where mass transfer will likely be limiting for the higher molecular size fraction of the substrate molecular size distribution (Gaulier, Barbier, Guichard, Levitz, & Espinat, 2015) (chapter 5). Any secondary rate limiting steps reduces overall reaction rate, but also increases product distribution "balancing". Since mass transfer limitations are expected to be the main limiting process, and models for mass-transfer are generalized, it follows that a general rule of thumb can be derived for the minimum catalyst activity. Where increasing catalyst activity beyond the minimum is unlikely to result in a higher overall reaction rate.

As a result, in the design of catalysts for the conversion of bio-macromolecular feedstocks, less emphasis can be placed on fully optimizing the reaction, adsorption, and desorption rates, since these will be mostly secondary rate limiting steps. Increasing the rates of secondary rate-limiting steps will decrease the balancing of the product distribution and may be undesired depending on the product requirements derived from the property-function relations. Thus in the design of a catalyst for conversion of biobased feedstocks, the priorities likely shift away from optimizing individual reaction steps, and more towards balancing the product distribution and mitigating mass transfer limitations.

The (lack of) generalizability of model results

As stated, the fitted values for the kinetic parameters in both the kinetic model from chapter 3, and chapter 4 lack generalizability across different feedstocks, different processes, and different molecular weight distributions of the same feedstock. As a result the applicability and the relevance of the values of fitted parameters is limited to specific implementations. Consequently, publishing these values is of limited added value to scientific knowledge. However, the provided modelling tools in this thesis provide a method to address the challenges of substrate polydispersity in researching catalysts for macromolecular conversions. Additionally, further development of the modelling tools, and providing proof of concepts for size dependency in processes will have publishable scientific value. The exact values of fitted parameters that are found for each variation of a substrate, although not of academic importance, will allow for optimizing specific reactions, reactors, catalysts, and processes.

The sigmoid curve of technological development

Technological development of a process often follows a sigmoid curve (Andersen, 1999; Campbell, 1983; Dubarić, Giannoccaro, Bengtsson, & Ackermann, 2011; Meng, Dincer, & Yüksel, 2021; Priestley, Sluckin, & Tiropanis, 2020). The proposed methods in this thesis can help in the design of a process for the conversion of macromolecular feedstocks, and can play a role in several phases of the development of new processes. A rough division in two phases can be made, before and after a specific substrate and catalyst (support material + catalytically active nanoparticles) have been chosen. These two phases are here regarded to as the screening phase and the optimizing phase. This section discusses where in this sigmoid curve to strategically employ the methods outlined in this thesis.

Screening in early development

As previously mentioned, the proposed methods from chapters 3 and 4 are empirical, and the calibrated values from these methods are non-generalizable. The lack of generalizability of the determined kinetic parameters will decrease the feasibility of applying such tools in early research states since it requires investment of time and analytic tools to provide the required data as input for models of this complexity. As a result, applying detailed size dependent kinetic models is not worthwhile at an early phase in the research while screening different substrates and/or catalysts for a specific process. However, at this stage a general screening if size dependent steps in the catalytic cycle are present, and their general trends (direct or inverse relation with molecular size) provides useful information for later stages in the development process. Additionally, analysis the property-function relations can reveal sensitivities of the application to changes in molecular weight distributions and/or degree of conversion.

Since mass transfer models are generalizable (chapter 5), early design of required pore sizes and pore structures can be performed, giving additional information for the selection of support materials that can achieve these pore structures.

Optimizing in later development

After the screening phase, the choice of substrate and catalyst (support material + catalytically active particles) will be made. Once this decision is made, size dependent kinetic models can be used to optimize the "balancing" of the reaction if the application is sensitive to changes in molecular weight distributions and/or degree of conversion. If the application is very robust, i.e. insensitive to small changes in product properties, then balancing the product with size selective kinetic models will be of less added value. However, in these cases size dependent kinetic models can be used to optimize the overall reaction rate and yield by evaluating the rate-limiting step(s) and aiding in mitigating these bottlenecks. Figure 3 shows a sigmoidal curve of technological development with key steps for applying the proposed methods in the design process.

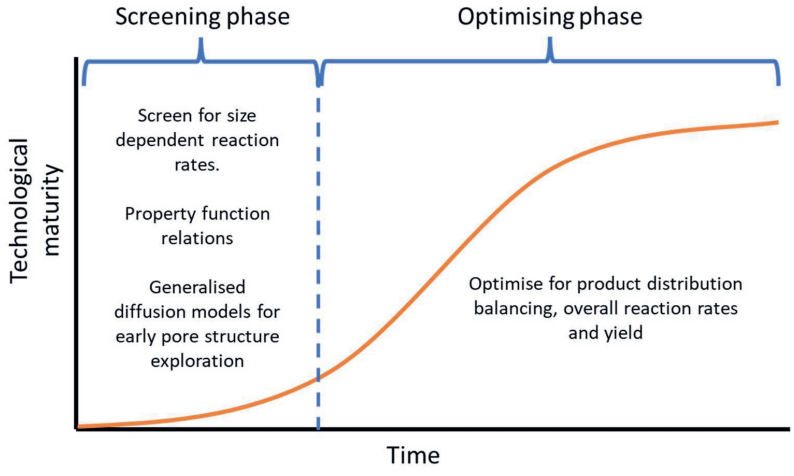

Figure 3 A sigmoid curve representing technological maturity over time applied to catalyst design. Two main phases are defined, the screening phase and optimising phase.

The transition to biobased materials and challenges in conversion

The methods proposed in chapters 3 and 4 aid in the design of catalysts for conversions of polydisperse macromolecular feedstocks, which in turn can aid in the societal transition towards the use of renewable biobased feedstocks to produce biobased materials and chemicals. This section discusses how the methods outlined in chapters 3 and 4 can contribute in the transition towards a biobased economy.

Alternative production methods for existing materials

In this thesis, the oxidation of starch was used as a case study to investigate conversions of biobased macromolecular feedstocks. Oxidised starch is currently already produced on an industrial scale using sodium hypochlorite. However, chapter 2 shows that the environmental impact of the process can be reduced by switching to a heterogeneously catalysed oxidation process with molecular oxygen. In the case of starch oxidation and similar substitutions of conversions in existing production chains, the proposed methods can be aid in the design and optimization of a heterogeneously catalysed conversion. The property-function relations of these products are generally well known since there are established markets. "Balancing" of the product distribution can be done to match the original product closely to be used in the existing markets and production chains. However, external stimuli might be needed to drive innovation in this way since the development of such a process requires investments in R&D, constructing and maintaining the industrial infrastructure, and operational costs. As a result, voluntarily reducing environmental impact by substituting existing production processes often conflicts with financial interests (Fisher-Vanden & Thorburn, 2011). The main driver for commercial parties to reduce the environmental impact of their production processes are reduced energy costs, financial incentives from government instances, or compliance with changing legislation (González-Benito & González-Benito, 2005).

Development of novel biobased materials

Application of size-dependent kinetic models provides a higher level of information in the conversion process, which in turn allows optimisation and fine-tuning of catalysts for the production of specific product distributions. Thereby increasing the controllability of the conversion process and granting access to newly specialised macromolecular materials. These specialised materials can have molecular properties and structures that can be difficult to produce after complete depolymerisation of a biopolymer. Some examples of these type of materials are modified barley dietary fibres (Park, Lee, & Lee, 2013), production of aerogel nanofibres for insulating materials (Tafreshi et al., 2022), modified inulin fibres for colon drug targeting (Giri, Dutta, & Giri, 2021), and carboxymethylcellulose for production of edible coatings (Panahirad et al., 2021; Pinto et al., 2022). With the additional potential for fine-tuning and optimising such products, novel biobased materials and nutritional supplements e.g. specialty fibres can be produced. Herein lies the highest potential for application of these methods, since these novel products can have unique properties that cannot easily be produced through other methods or replicated with other materials.

The current research in finding renewable biobased alternatives to current non-renewable materials, together with the development of new biobased materials with unique properties introduces the challenge of designing conversions for substrates with

high molecular weight and broad molecular weight distributions. Including substrate molecular weight distributions, distributions in degree of conversion, and size dependent reaction steps in kinetic models is a first step in addressing these challenges. With the increasing need for sustainable and renewable products and materials, the line of research in this PhD thesis will increase in relevance as the field of biobased materials and conversions grows.

6.1 References

Andersen, B. (1999). The hunt for S-shaped growth paths in technological innovation: a patent study*. *Journal of Evolutionary Economics, 9*(4), 487-526. doi:10.1007/s001910050093

Blecker, C., Chevalier, J. P., Fougnies, C., Van Herck, J. C., Deroanne, C., & Paquot, M. (2003). Characterisation of different inulin samples by DSC: Influence of polymerisation degree on melting temperature. *Journal of Thermal Analysis and Calorimetry, 71*(1), 215-224. doi:https://doi.org/10.1023/a:1022238905962

Bragd, P. L., Besemer, A. C., & van Bekkum, H. (2002). Selective oxidation of carbohydrates by 4-AcNH-TEMPO/peracid systems. *Carbohydrate Polymers, 49*(4), 397-406. doi:https://doi.org/10.1016/S0144-8617(01)00344-7

Bravo-Suárez, J. J., Chaudhari, R. V., & Subramaniam, B. (2013). Design of Heterogeneous Catalysts for Fuels and Chemicals Processing: An Overview. In *Novel Materials for Catalysis and Fuels Processing* (Vol. 1132, pp. 3-68): American Chemical Society.

Campbell, R. S. (1983). Patent trends as a technological forecasting tool. *World Patent Information, 5*(3), 137-143. doi:https://doi.org/10.1016/0172-2190(83)90134-5

Dahiya, S., Katakojwala, R., Ramakrishna, S., & Mohan, S. V. (2020). Biobased Products and Life Cycle Assessment in the Context of Circular Economy and Sustainability. *Materials Circular Economy, 2*(1), 7. doi:10.1007/s42824-020-00007-x

Dubarić, E., Giannoccaro, D., Bengtsson, R., & Ackermann, T. (2011). Patent data as indicators of wind power technology development. *World Patent Information, 33*(2), 144-149. doi:https://doi.org/10.1016/j.wpi.2010.12.005

Fisher-Vanden, K., & Thorburn, K. S. (2011). Voluntary corporate environmental initiatives and shareholder wealth. *Journal of Environmental Economics and Management, 62*(3), 430-445. doi:https://doi.org/10.1016/j.jeem.2011.04.003

Gaulier, F., Barbier, J., Guichard, B., Levitz, P., & Espinat, D. (2015). Asphaltenes Transport into Catalysts under Hydroprocessing Conditions. *Energy & Fuels, 29*(10), 6250-6258. doi:10.1021/acs.energyfuels.5b01355

Giri, S., Dutta, P., & Giri, T. K. (2021). Inulin-based carriers for colon drug targeting. *Journal of Drug Delivery Science and Technology, 64*, 102595. doi:https://doi.org/10.1016/j.jddst.2021.102595

González-Benito, J., & González-Benito, Ó. (2005). A study of the motivations for the environmental transformation of companies. *Industrial Marketing Management, 34*(5), 462-475. doi:https://doi.org/10.1016/j.indmarman.2004.08.005

Grommers, H. E., & van der Krogt, D. A. (2009). Chapter 11 - Potato Starch: Production, Modifications and Uses. In J. BeMiller & R. Whistler (Eds.), *Starch (Third Edition)* (pp. 511-539). San Diego: Academic Press.

Hegedus, L. L., Aris, R., Bell, A. T., Boudart, M., Chen, N. Y., Gates, B. C., Wei, J. (1987). Catalyst design: progress and perspectives.

Henrich, E., Dahmen, N., Dinjus, E., & Sauer, J. (2015). The Role of Biomass in a Future World without Fossil Fuels. *Chemie Ingenieur Technik, 87*(12), 1667-1685. doi:https://doi.org/10.1002/cite.201500056

Kim, Y., Faqih, M. N., & Wang, S. S. (2001). Factors affecting gel formation of inulin. *Carbohydrate Polymers, 46*(2), 135-145. doi:https://doi.org/10.1016/S0144-8617(00)00296-4

Meng, Y., Dincer, H., & Yüksel, S. (2021). Understanding the innovative developments with two-stage technology S-curve of nuclear energy projects. *Progress in Nuclear Energy, 140*, 103924. doi:https://doi.org/10.1016/j.pnucene.2021.103924

Mensink, M. A., Frijlink, H. W., van der Voort Maarschalk, K., & Hinrichs, W. L. J. (2015). Inulin, a flexible oligosaccharide I: Review of its physicochemical characteristics. *Carbohydrate Polymers, 130*, 405-419. doi:https://doi.org/10.1016/j.carbpol.2015.05.026

Nakagawa, Y., Tamura, M., & Tomishige, K. (2013). Catalytic Reduction of Biomass-Derived Furanic Compounds with Hydrogen. *ACS Catalysis, 3*(12), 2655-2668. doi:10.1021/cs400616p

Panahirad, S., Dadpour, M., Peighambardoust, S. H., Soltanzadeh, M., Gullón, B., Alirezalu, K., & Lorenzo, J. M. (2021). Applications of carboxymethyl cellulose- and pectin-based active edible coatings in preservation of fruits and vegetables: A review. *Trends in Food Science & Technology, 110*, 663-673. doi:https://doi.org/10.1016/j.tifs.2021.02.025

Park, K. H., Lee, K. Y., & Lee, H. G. (2013). Chemical composition and physicochemical properties of barley dietary fiber by chemical modification. *International Journal of Biological Macromolecules, 60*, 360-365. doi:https://doi.org/10.1016/j.ijbiomac.2013.06.024

Pinto, E., Aggrey, W. N., Boakye, P., Amenuvor, G., Sokama-Neuyam, Y. A., Fokuo, M. K., . . . Rockson, M. A. D. (2022). Cellulose processing from biomass and its derivatization into carboxymethylcellulose: A review. *Scientific African, 15*, e01078. doi:https://doi.org/10.1016/j.sciaf.2021.e01078

Priestley, M., Sluckin, T. J., & Tiropanis, T. (2020). Innovation on the web: the end of the S-curve? *Internet Histories, 4*(4), 390-412. doi:10.1080/24701475.2020.1747261

Rama, H. O., Roberts, D., Tignor, M., Poloczanska, E. S., Mintenbeck, K., Alegría, A., . . . Ayanlade, S. (2022). *Climate Change 2022: Impacts, Adaptation and Vulnerability Working Group II Contribution to the Sixth Assessment Report of the Intergovernmental Panel on Climate Change*.

Rolland-Sabaté, A., Guilois, S., Jaillais, B., & Colonna, P. (2011). Molecular size and mass distributions of native starches using complementary separation methods: Asymmetrical Flow Field Flow Fractionation (A4F) and Hydrodynamic and Size Exclusion Chromatography (HDC-SEC). *Analytical and Bioanalytical Chemistry, 399*(4), 1493-1505. doi:10.1007/s00216-010-4208-4

Rutenberg, M. W., & Solarek, D. (1984). CHAPTER X - STARCH DERIVATIVES: PRODUCTION AND USES. In R. L. Whistler, J. N. Bemiller, & E. F. Paschall (Eds.), *Starch: Chemistry and Technology (Second Edition)* (pp. 311-388). San Diego: Academic Press.

Sangseethong, K., Termvejsayanon, N., & Sriroth, K. (2010). Characterization of physicochemical properties of hypochlorite- and peroxide-oxidized cassava starches. *Carbohydrate Polymers, 82*(2), 446-453. doi:https://doi.org/10.1016/j.carbpol.2010.05.003

Tafreshi, O. A., Mosanenzadeh, S. G., Karamikamkar, S., Saadatnia, Z., Park, C. B., & Naguib, H. E. (2022). A review on multifunctional aerogel fibers: processing, fabrication, functionalization, and applications. *Materials Today Chemistry, 23*, 100736. doi:https://doi.org/10.1016/j.mtchem.2021.100736

Verraest, D. L., Peters, J. A., & van Bekkum, H. (1998). The platinum-catalyzed oxidation of inulin. *Carbohydrate Research, 306*(1), 197-203. doi:https://doi.org/10.1016/S0008-6215(97)10055-6

Vinod, A., Sanjay, M. R., Suchart, S., & Jyotishkumar, P. (2020). Renewable and sustainable biobased materials: An assessment on biofibers, biofilms, biopolymers and biocomposites. *Journal of Cleaner Production, 258*, 120978. doi:https://doi.org/10.1016/j.jclepro.2020.120978

Weiss, M., Haufe, J., Carus, M., Brandão, M., Bringezu, S., Hermann, B., & Patel, M. K. (2012). A Review of the Environmental Impacts of Biobased Materials. *Journal of Industrial Ecology, 16*(s1), S169-S181. doi:https://doi.org/10.1111/j.1530-9290.2012.00468.x

Summary

Starch oxidation is currently performed on an industrial scale with sodium hypochlorite as oxidant, however, the use of hypochlorite has undesired side reactions (e.g. depolymerisation, perchlorate formation), and produces stoichiometric amounts of waste (salt). Therefore, a greener solution is sought. Heterogeneous catalysis of starch with oxygen (or air) as oxidant has the potential to improve the sustainability of the current process, but several challenges arise in the design of a heterogenous catalyst for this process. Starch is a large and polydisperse molecule. Within a size distribution, molecules of different sizes may diffuse, adsorb and react at different rates from each other. Studies on diffusion of polydisperse biobased macromolecules ($r > 5nm$) are lacking. The large molecular size and the presence of size distributions, and how this influences several steps in the catalytic process (pore diffusion, adsorption, and reaction) is not well understood. Additionally, current kinetic models do not include the effect of size distributions. As a result, the conversion from substrate size distribution to product size distribution and yield is not well known. In this thesis, the goals are to:

1) Quantitatively validate the premise that heterogeneously catalysed starch oxidation with molecular oxygen is a "greener" solution than the current industrial standard of hypochlorite oxidation.
2) Elucidate effects of substrate size and polydispersity in the different steps of the catalytic cycle (diffusion, adsorption, reaction).
3) Develop kinetic models that predict product distributions and yields for these steps.
4) Evaluate implications of including molecular size and molecular size distributions in kinetic models for the design process of heterogenous catalysts for polydisperse macromolecular feedstocks.

These goals were achieved by a mixed approach including experiments and modelling. The developed kinetic models in this thesis, and part of the results can be generalised to aid in the design of other heterogeneous catalysts for conversions of polydisperse macromolecular feedstocks.

In chapter 2, the premise of "greener" starch oxidation through heterogeneous catalysis is quantitatively verified through process modelling and a life cycle assessment. The potential of two catalysed starch oxidation methods to reduce the environmental impact of oxidised starch production by hypochlorite were assessed. We compared the environmental impact of oxidation with molecular oxygen (heterogeneously catalysed) and hydrogen peroxide (homogeneously catalysed) to hypochlorite oxidation through life cycle assessment. The results confirm that within the overall process from raw material (potato) to oxidised potato starch, the oxidation step with hypochlorite i.e. the

current industrial standard, is the main environmental hotspot in the current process of oxidised starch production, and that both hydroperoxide oxidation and molecular oxygen oxidation with heterogeneous catalyst have the potential to significantly lower the environmental impact of the process. The impact reduction is most significant in the categories of freshwater eutrophication (~67%), ozone depletion (~66%), climate change (35-60%) and resource use (40%-78%) for peroxide and molecular oxygen oxidation respectively.

In chapter 3, the influence of molecular size of starch on the oxidation and depolymerisation rates were investigated. Experiments for the homogeneous TEMPO/hypochlorite catalysed oxidation of amylopectins with different molecular sizes showed that large starch molecules oxidise and depolymerise at a higher rate than small molecules. In addition, increasing degrees of oxidation inhibit the rate of further oxidation exponentially. These results demonstrate that molecular size, and thereby polydispersity of macromolecular feedstocks are important factors for the conversion of polydisperse macromolecular feedstocks. A kinetic model was formulated that assigns individual rate constants to starch species of specific molecular weight and their degree of oxidation. This kinetic model predicts a two dimensional product distribution, with a distribution over molecular weight, and a distribution over degree of oxidation. As a result, the model can predict asymmetrical product distributions where, for example, large starch molecules are more oxidised than small molecules.

In chapter 4, the influence of molecular weight, polydispersity, and degree of branching on the adsorption rates on activated carbon of four potato starches differing in the aforementioned characteristics was investigated. Changes in starch concentration and size distribution over time were analysed by Total Starch Assay and Size Exclusion Chromatography. Average molecular weight and degree of branching of a starch scaled negatively with average adsorption rate. Within a size-distribution, adsorption rates scaled negatively with increasing molecule size, resulting in an increased average molecular weight in solution of between 25% and 213% and a decreased polydispersity of between 13% and 38%. A new quantitative estimation of the influence of size distributions was developed. Here the reduction in polydispersity of sample throughout the adsorption process was used as a measure to estimate the magnitude of the influence of molecular size on the rate constants of adsorption. A dummy distribution containing only the 20^{th} and 80^{th} percentile molecule sizes within the substrate distribution was created. From this dummy distribution molecules were removed to match the measured decrease in polydispersity in the original experimental sample. From this analysis, the ratio of the rate constants of 20^{th} and 80^{th} percentile molecule sizes in the original substrate distribution can be approximated. Simulation with dummy distributions estimated the ratio of adsorption rates for 20^{th} percentile and 80^{th} percentile molecules within a distribution to range between a factor 4 and 8 for the

different starches. Competitive adsorption decreased the adsorption rate of molecules above the average size within a sample distribution.

In chapter 5, a reaction-diffusion model was used to describe the diffusion and reaction of a generalised polydisperse macromolecular substrate. Normally distributed substrates with varying average size (10 to 100nm) and standard deviation σ (20% or 50% of the average), were simulated for conversion in a catalyst with pore sizes ranging from 25 to 250 nm. The results showed that if a system is diffusion limited, the product distribution will consist mostly of tail-end molecules from the substrate distribution, this difference between initial and final distribution was larger for substrate distributions with higher standard deviations. Optimum pore sizes in the trade-off between diffusion limitation versus specific surface area were determined in the range of approximately 2.2 to 2.8 times the molecule size. At optimal pore sizes, difference between the initial and product distribution increased with increasing substrate polydispersity (4% for $\sigma = 0.2\mu$ vs 15% for $\sigma = 0.5\mu$). The overall catalyst activity at optimal pore sizes exponentially with increasing molecular size of the substrate. This trend implies a practical limit to the maximum size of a substrate for heterogeneously catalysed processes. Because of the low diffusivity of macromolecules in solution, severe mass transfer limitations in the conversions of (polydisperse) macromolecular feedstocks is expected. Therefore, a reverse design approach starting at the desired product distribution, and optimising yield within those requirements is advised.

In the discussion we reflect on 1) the concept of a rate limiting step in heterogeneous catalysis, 2) generalisability of the proposed models in the thesis, and 3) applicability of models in the kinetic process.

1) Individual molecules from a polydisperse macromolecular feedstock may be limited by a different step in the catalytic cycle than molecules of another size from the same distribution. Even though each individual molecular size is limited by one step in the catalytic cycle, the distribution as a whole may be limited by more than one step in the catalytic cycle. Therefore, the convention of a single rate limiting step during conversion must be critically evaluated for the conversion of polydisperse macromolecular feedstocks.
2) In chapter 5 it was noted that internal competition in adsorption within a distribution significantly affects the rate constants of adsorption for individual starch size species within that distribution. Moreover, the influence of molecular size (both magnitude and direction) may change between feedstocks (e.g. starch versus cellulose), and different molecular weight distributions within the same feedstock. Therefore, fitted values of rate constants are not generalisable, and need to be empirically determined for each feedstock and process. However, the

modelling tools provide a generalised framework to determine these rate constants.

3) Since fitted values of rate constants are not generalisable across different feedstocks or different molecular weight distributions of the same feedstocks, determining the exact values early in a design process is not beneficial. In early stages of the design process of a catalyst, screening for potential influence of molecular size on steps in the catalytic cycle is advised. In a later phase in the design of a catalyst, kinetic models that include the effect of size distributions can be used to optimise the conversion yield and product distribution.

With the increasing need for renewable biobased alternatives to current non-renewable materials, most of which are based on polydisperse macromolecular feedstocks (e.g. starch), addressing the challenges of designing catalysts for these conversions increases in relevance. Applying kinetic models that include the effect of molecular weight and substrate polydispersity is a first step in addressing these challenges. Thereby aiding in the design of conversions of polydisperse macromolecular feedstocks and contributing to a renewable and biobased economy.

Acknowledgements

I want to thank my promotor, Harry Bitter, for his supervision and support throughout the lengthy process of doing my thesis. Harry, you have heard all the excuses in the book by now. At one point I even considered making an e-mail template: “sorry, I haven’t finished the work yet because {insert generic excuse here}.” Of course, in the end my big book of excuses ran out, and I actually had to buckle down. Thank you for your patience and scientific insights. I think I am now finally able to “guide the reader” and to place “facts before fiction”.

I want to thank all my other supervisors during my PhD. Ton van Boxtel, you helped me get started and helped defining the scope of my first two papers. It’s a good thing you didn’t wait for me to finish before you retired. One of the habits that I copied from you is that I always carry around some blank A4 papers and pencils, for easy visualisation of concepts in meetings, and during teaching. Lars Kiewidt, even though your stay in BCT was short, you have provided valuable input on some of my papers, especially the reaction-diffusion model. I could not have done that without your help. Everyone can take the meticulousness and exactness in your scientific approach as an example. The Scott-scale you made is still there (at the time of writing). Tomas van Haasterecht, your insight and knowledge are on another level. Thanks for the input and asking the difficult questions. A special thanks to Piet Buwalda, who has sadly passed away. Your enthusiasm for starch was contagious. Wednesdays always had a special atmosphere because of your singing and whistling in the hallways. I’m sure you would have loved the results from the adsorption experiments.

I want to “tank” Daniel for being a good friend, colleague, bandmember, drinking buddy, paranymph, and hole-digger. Your antics are always entertaining. You have helped me to grow and diversify as a musician, teacher, and scientist. Thank you for letting me crash at your place after some parties got a little too good.

I want to thank Cynthia for being my paranymph and for your insights on starch and HPSEC. It helped out a lot in the analysis of my samples. But most of all, thank you for all of the good and happy times with you and Bas. The nice walks, lunches, drinks, and amazing music. Your lively spirit can brighten anyone’s day.

To my colleagues from BCT who have since finished, moved on, or hanging on just a little longer than me: Sanne, Piet, Elvira, Farnoosh, Nazila, Roxani, Gerben, Evie, Laura, Marlene, Simha, Eleni, Cynthia, Daniel, Rachel, Ellen, Jurjen, Andrada, Sanne the second, and Umay. I’m sure I’m forgetting some names here, I have always been terrible at that. Thank you all for the good times! Gerben, thanks for some great board game nights and introducing me to D&D! Roxani, it was very cool to be your paranymph, I enjoyed the numerous drinks we had over the years, whether it was at the NCCC, random borrels, or the few occasions you joined for band practice.

I would like to thank Gerda, Danielle, Susan, Annemarie, and Nadine for their support on administrative and lab-work tasks. I'm surprised I didn't break more stuff during my experiments, since there is no Ctrl+Z in real life, but I am not going to push my luck and I will stick to Ctrl+Z territory in the foreseeable future.

I would like to thank my current colleagues in FTE/ABE for the fun coffee breaks, the regularly organised sports, the fatty Fridays, dinners, and many more good times. You are a great group of friends and colleagues. Salma, thank you for being my unofficial third paranymph. I do not yet know what you, Daniel, and Cynthia are preparing, but I am sure it will be something nice and unexpected. Special thanks to Rachel for teaching me the fundamentals of teaching, putting me in front of a class to give a lecture for Modelling Dynamic Systems, and helping me with getting my current position. I have no idea where I would have ended up without you, but I don't think it could have been better than where I am now.

I want to thank my previous and current office mates: Evie, Nazila, Carlos, Haris, Sayed, Congcong, and Rachel. It is/was fun to have you around and distracting each other from work at one moment and providing valuable input for work the next.

I want to thank the former and current members of the Keynote Speakers. Daniel, Kay, Cristina, Tessa, and Sanja. Music on Tuesdays is a weekly highlight and helps me let loose and relax by living in the moment. You are a great bunch of people. Cristina, your jokes occupy a unique and anomalous space in the humour dimension, it's awesome! Sanja, your experience as a PhD coordinator came in handy towards that very stretchy last bit of my PhD, your advice was very useful, thank you! Thanks to the many guests that have joined over the years during our practice sessions, you've made it all the more fun!

I want to thank my family members for supporting me in this journey, asking me what my thesis is about, and hiding their regret for asking that question when I started explaining the various topics.

Of course many thanks to my awesome wife and love of my life, Femke. During my PhD we went from dating, to living together, to engaged, to married. During that time, we have had many great experiences and moments, and our relationship is still getting "more awesomer" every day. I'm proud of how we have grown as people and as a couple, without losing our child-like imagination. Thank you so much for putting up with my shenanigans and PhD stress, supporting and motivating me for the whole 7 years, 9 months and 23 days, and picking up the slack where needed. You are an amazing person, and I couldn't be happier being together with you.

Overview of completed training activities

Discipline specific activities

Netherlands Chemistry and Catalysis Conference	NCCC	2016
Applied Biobased materials conference	AMIBM	2016
Netherlands Chemistry and Catalysis Conference	NCCC	2017
Chemistry as innovating science	CHAINS	2017
Netherlands Chemistry and Catalysis Conference	NCCC	2018
Netherlands Process Technology Symposium	NPS	2018
Netherlands Chemistry and Catalysis Conference	NCCC	2019
Europacat	EFCAT	2019

General courses

VLAG PhD week	VLAG	2016
Competence assessment	WGS	2016
Brain training	WGS	2016
Presenting with Impact	Wageningen in'to Languages	2017
Efficient writing strategies	Wageningen in'to Languages	2018
Scientific writing	Wageningen in'to Languages	2018

Assisting in teaching and supervision activities

Modelling Dynamic Systems	WUR	2016 - 2018
Modelling of Biobased Production Systems	WUR	2016 - 2018

Other activities

Research proposal	BCT	2016
PhD discussion meetings BCT	BCT	2016 - 2019
Meetings with project advisory board	BCT/Avebe	2016 - 2019
PhD trip to Denmark and Sweden	BCT&BNT	2018

The research described in this thesis was financially supported by the Dutch Research Council (NWO) under grant number 870.15.120

Financial support from Wageningen University for printing this thesis is gratefully acknowledged.

Cover design by Tim Hoogstad

Printed by proefschriftmaken.nl on 100% recycled paper.